Towards a Somatosensory Neuroprosthesis: Characterizing Microstimulation of the DRG and Spinal Cord for Sensory Restoration

by

Ameya Chandrashekhar Nanivadekar

MSE in Bioengineering, University of Pennsylvania, 2014

Submitted to the Graduate Faculty of

the Swanson School of Engineering in partial fulfillment

of the requirements for the degree of

Doctor of Philosophy

University of Pittsburgh

2020

UNIVERSITY OF PITTSBURGH

SWANSON SCHOOL OF ENGINEERING

This dissertation was presented

by

Ameya Chandrashekhar Nanivadekar

It was defended on

August 27, 2020

and approved by

L.E. Fisher, Ph.D., Assistant Professor, Department of Physical Medicine and Rehabilitation

S.F. Lempka, Ph.D., Assistant Professor, Department of Biomedical Engineering, University of Michigan

H.R. Koerber, Ph.D., Professor, Department of Neurobiology

T.D.Y. Kozai, Ph.D., Assistant Professor, Department of Bioengineering

D.J. Weber, Ph.D., Associate Professor, Department of Bioengineering

Dissertation Director: L.E. Fisher, Ph.D., Assistant Professor, Department of Physical Medicine and Rehabilitation

Towards a Somatosensory Neuroprosthesis: Characterizing Microstimulation of the DRG and Spinal Cord for Sensory Restoration

Ameya Chandrashekhar Nanivadekar, PhD

University of Pittsburgh, 2020

Restoring sensation is key to making prostheses more functional. While there have been important advances in the design and actuation of prosthetic limbs, these devices lack a means for providing direct sensory feedback. As such, users must infer information about limb state from cues like pressure on the residual limb, resulting in diminished control of prostheses, and reduced adoption and use of these technologies.

The dorsal root ganglia (DRG) are an attractive target for a somatosensory neural interface. The DRG are enlargements of the spinal nerve that house the cell bodies of primary sensory neurons and provide access to a heterogenous population of somatosensory fibers. Importantly, the separation of motor and sensory pathways at the spinal roots allows recruitment of sensory afferents without coactivating motor efferents which may otherwise contaminate a myoelectric control interface.

This dissertation examines a novel way of interfacing with the DRG and dorsal roots using epineural electrodes, that takes us a step closer towards developing a somatosensory neuroprosthesis. I begin with an animal model to compare the recruitment properties of epineural and penetrating electrodes when stimulating afferents in the lumbar DRG. In the next section, I develop a computational model to explain the mechanism of recruitment of afferents. Finally, I describe a series of experiments in human upper-limb amputees to characterize the modality and utility of sensations evoked when the cervical spinal cord and spinal roots were stimulated.

keywords: dorsal root ganglion, epineural electrodes, computational modeling, spinal cord stimulation, somatosensory feedback, amputation, neuroprosthesis.

Table of Contents

List of Tables

List of Figures

Preface

Dedicated to my grandfather, Aaba,
for teaching me that the pursuit of perfection requires patience
and is always worth the effort

आस्ते भगः आसिनस्य उर्ध्वस्तिष्ठति तिष्ठतः।
शेते निपद्यमानस्य चराति चरतो भगः॥

"If I have seen further, it is by standing on the shoulders of giants."

- Isaac Newton

I am both humbled and honored to present the culmination of my research efforts over the past six years. However, I have not been alone and this work would not have been possible without the support, encouragement, guidance and wisdom of several people.

Foremost, I would like to thank my advisor and mentor Dr. Lee Fisher, for giving me the opportunity to work on a variety of different projects throughout my time at the Rehab Neural Engineering labs (RNEL). I acknowledge with deep gratitude his insights, his patience, his support, and his belief in me throughout my journey as a PhD student. In addition to the science and engineering lessons that I have gained, Dr. Fisher has always underscored the importance of clear communication and that has helped me focus as a researcher and become a better presenter, writer and project manager. I would also like to thank Dr. Robert Gaunt, who was my first advisor at RNEL and helped frame my philosophy and early approach to research. Dr. Gaunt emphasized that in addition to focusing on my thesis and research, it was important to use my time as a PhD student to diversify my experiences and 'try to say yes' whenever a new project came along. I've greatly benefited from saying 'yes' to a lot of opportunities that have come my way. Thank you also to Dr. Collinger, Dr. Capogrosso and Dr. Boninger for their guidance, advice and mentorship.

I would also like to thank my dissertation committee for their considerate feedback and helpful suggestions that have helped shape this work. Dr. Weber, thank you for urging me to focus on the broader impact of the work we do and think of how we can address unanswered question that still remain. Dr. Lempka, thank you for allowing me to visit your lab and train on some of the modeling techniques used in chapter 3 of this thesis. Dr. Koerber, thank you for your deep understanding of the neurophysiology of the DRG and insight into how we can improve selective recruitment by sensory modalities. Dr. Kozai, thank you for providing me with detailed feedback on my writing and how to structure research statements.

The best part about working at RNEL has been the friendships and camaraderie that I have developed with my fellow labmates. I would like to thank everyone at the Rehab Neural Engineering labs who has been directly or indirectly involved in making this work possible. Bill Cusack, thank you for being my 'unofficial' mentor and teaching me how to

use the animal lab setup when I joined the lab. I learnt a lot from you when I first started in the lab, and while I do not think I've been able to develop as meticulous a method as yours, the need to focus on the details (and maintain a lab notebook) certainly made an impression. Chris Ayers, thank you for introducing me to desktop composting and almond butter, but also for teaching me how to write good, modular code and the importance of reading user manuals. Matt Bauman, Sharlene Flesher and John Downey, thank you for being role models and senior PhD students that I looked up to, right from the first poster session during interview weekend. Carl Beringer, thank you for the FroYo and Three D's breaks and for my solid theoretical understanding of jiu-jitsu and weightlifting. Monica Liu, thank you for being a great friend and the smartest person I know when it comes to machine learning, statistics and programming, I have learnt a lot from our conversations. More importantly, thank you for the daily break to grab chips. Bailey Petersen and Devapratim Sarma, working with you guys on the lower-limb sensory restoration project has been one of the most fun experiences of my time in RNEL. Thank you for letting me be a part of the team, covering for my occassional grump and introducing me to the world of fluorescent beverages at Starbucks. Santosh Chandrasekaran, thank you for being a great friend, mentor and teammate. I'm eternally grateful for your guidance and support (and for being equally clueless) during those early-HAPTIX all-nighters spent building, testing and debugging our experiment setup. Chaitanya Gopinath, thank you for our insightful discussions ranging from neurophysiology to the future of neuroscience research and your belief that neuroengineers are not real. Special thanks to Robert Graham at the Neuromodulation lab for his crucial guidance and expert advise on the DRG modeling project.

RNEL is blessed with an amazing team of engineers and I'm thankful for their help and support in building, testing, debugging and managing our equipment, and data. I'm personally grateful that they've always been willing to share their knowledge with me and help me learn to use new tools. Thanks to Max Novelli for letting me be a part of the MDF development, always highlighting the latest and shiniest software for data analysis and visualization and for helping me switch away from MATLAB to python. Thanks to Tyler Madonna, and David Weir for their help in setting up the clinical experiment rigs and our discussions ranging from 3d printing and android development to ethics and the use of social

media. Thanks to Tyler Simpson, for being the go-to problem solver and having the answer for every engineering issue in the lab. Thanks to Jeff Weiss, for the framework and code base for our clinical experiment rig and for help with development with the Modular Prosthetic Limb.

A special thanks to our amazing group of research coordinators and lab managers who keep the lab running behind the scenes and make our clinical studies possible. Thanks to Bree Bigelow, Lauren Wilcox, Howard Stein, Kelly Meyers, Holly Jourdan, Marisa Ciora and Debbie Harrington. To our study participants, you are the real pioneers of neurotechnology and neuroprosthesis research, thank you for providing the grounding motivation for this dissertation. Without your amazing cooperation, enthusiasm and insights, none of this would be possible.

To my friends, Nikhil, Prashant, Omkar, Tejas, Shefali, Akhilesh, Kalyan, Turja, who have wondered how I am still stuck in school, thanks for excusing my spotty attendance record at get-togethers and trips. Thanks for believing that I would finish someday, I think I may be kind of almost done soon.

Lastly, I would like to thank my family for all they have done for me. Dad, thank you for the old PalmV, the O2 Xda, the Slingbox and all the gadgets and tools I got to play with growing up. My creativity and near compulsive need to build new gadgets and repurpose old tech comes directly from this experience. More importantly, thanks for pushing me to always get out of my comfort zone and teaching me to always stay humble. Mom, thank you for being the best teacher I have had and always being there for me. I can only try to be as level headed and calm as you are when things are chaotic. To my sister Shruti, your work ethic and determination has always been an inspiration. Thanks for the countless pep talks, words of encouragement and last minute advice and feedback that have kept me going over the years. Lastly, a huge thank you to my wife Shweta, for her unending love and support, for pushing me when I needed to focus, for being the voice of reason when things got tough, for going to sleep with the lights on while I worked, for reminding me to eat lunch everyday and for making sure I kept working towards my goal. I hope I have made you all proud.

1.0 Introduction

1.1 The Importance of Somatosensory Feedback

We experience our world through sensation. The human perceptual system has remarkable adaptations to extract tactile, proprioceptive and nociceptive information from our environment. Specialized receptors transmit this information at a high resolution to the brain where an integration of these sensory inputs creates the perception of our environment. We rely on this percept to inform our interaction with the surroundings, yet we are not always consciously aware of it. The ability to feel or sense objects predicates how we interact with them therefore, any disruption can be disorienting and in several cases debilitating.

The loss of somatosensory feedback has a profound impact on the ability of individuals to interact with their environment and perform activities of daily living. Feedback is required to monitor the physical state of each body segment, maintain stability amidst perturbations, and regulate changes in control, especially for complex tasks such as reaching, standing, and walking. The importance of this feedback is demonstrated in individuals with diabetic neuropathy for example. These patients have shown an increased risk of falling due to a loss of sensation from the foot [1]. Patients with large-fiber sensory neuropathies have also shown severe motor impairments and difficulty maintaining postural stability [2]. Similarly, loss of sensation in the upper extremities affects fine motor control and the ability to coordinate movements at multiple joints [3]. Often individuals have to visually attend to the task being performed in order to supplement the reduced sensory feedback [4].

These issues are mirrored in individuals with amputation. In addition to learning to use an external prosthesis, amputees have to devise ways of compensating for the lack of sensory feedback in current state-of-the-art prosthetic devices. The current repertoire of prostheses ranges from simple cosmetic hands and feet to cable actuated hooks and state-of-the-art dexterous robotic limbs. However none of these devices provide tactile feedback and intuitive control remains elusive. In fact, users prefer to use simpler body powered prostheses because they can infer information about limb state from pressure exerted on the residual

limb. For upper limb amputees, object manipulation and regulating grip force using visual feedback alone is slow and cumbersome. Trans-tibial amputees compensate for a lack of ankle proprioception by increasing reliance on visual feedback, putting them at risk for falls when visual feedback is unreliable [5, 6, 7]. Additionally, reduced sensory feedback makes activities such as climbing stairs or walking on uneven terrain difficult and dangerous with a prosthetic limb [8].

In the United States alone nearly 200,000 people undergo the amputation of a limb for a variety of reasons each year [9]. Of these potential prosthesis users, only 40% continue to use their prosthesis [10]. The rate of adoption of prostheses is limited by poor device functionality, weight, discomfort and a lack of sensory feedback [11, 12, 13, 14]. Without the development of a prosthetic device that can incorporate sensory feedback, amputees continue to experience a severe reduction in their quality of life.

Developing a means to restore sensation after amputation is the primary objective of the work presented in this thesis. This thesis evaluates the dorsal root ganglion and lateral spinal cord as a target for a potential somatosensory neural interface (SSNI). The discussion focuses on the performance and mechanism of recruitment of afferents at the DRG via epineural stimulation. Additionally, the efficacy of lateral spinal cord stimulation to provide focal, stable and graded sensory feedback in upper limb amputees is demonstrated. While DRG and dorsal rootlet stimulation is discussed in the context of a prosthetic device for upper limb amputees the principles and methods of providing sensory feedback should be generalizable to lower limb prosthetics, and distal neuropathies where artifical somatosensory feedback is necessary.

Currently, learning to use a prosthetic devices is considered akin to learning skilled tool use [15]. However, appropriate feedback referred to an artificial hand can to lead to perceptions of embodiment [16]. The ultimate goal of this work would lead to the development of a SSNI that can produce dexterous movements and naturalistic sensations.

1.2 Delivering Artificial Somatosensory Feedback

Several research groups have explored a variety of approaches to provide sensory feedback to amputees and examined the effects of feedback on prosthetic control. Novel solutions for somatosensory feedback include sensory substitution, direct or transcutaneous peripheral nerve stimulation, spinal cord stimulation, and muscle reinnervation.

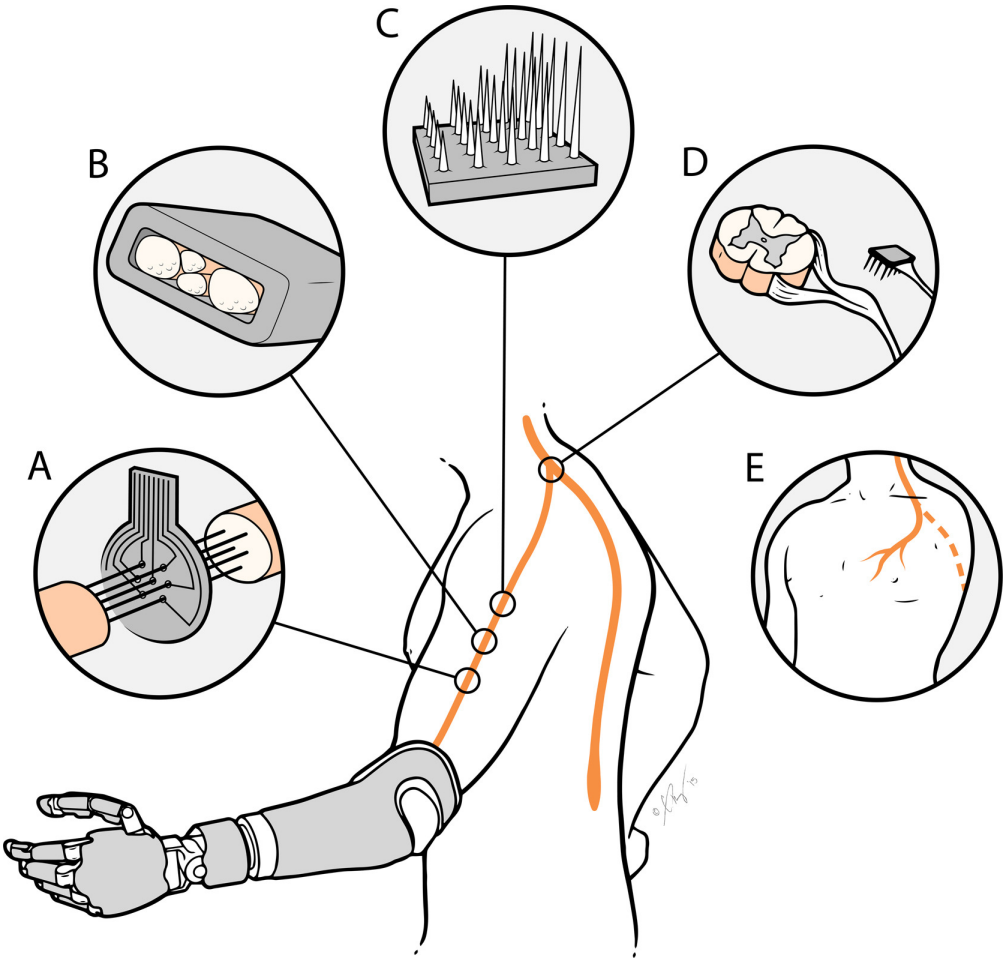

Figure 1.1: Illustration of different approaches to restore the sense of touch through a peripheral nerve interface. A) Regenerative electrodes. B) Extra-fascicular electrodes. C) Intra-fascicular electrodes. D) Dorsal root ganglion implant. E) Targeted sensory reinnervation. Adapted from [17]

1.2.1 Sensory Substitution

Non-invasive devices have been used to provide feedback via sensory substitution wherein an alternative modality replaces the one usually employed by the intact pathway. An early study by Mann et al involved applying vibration on the skin of the residual limb to convey limb position information to the prosthetic user [18]. This study showed that error on a task where the position of the prosthetic had to be matched to a target, was reduced by 50% when feedback was provided in this manner [19]. Other groups have also examined this approach using either vibrotactile, electrotactile or auditory [20, 21, 22, 23, 24] feedback as a means of conveying sensory information. The advent of wearable electronic devices too has renewed the interest in using sensory substitution as a tool for rehabilitation and providing feedback to prosthesis users [25]. However, since the sensations do not appear to emanate from the missing limb, sensory substitution may require significant learning for amputees to become adept in utilizing the feedback [26, 27].

Somatotopically-matched feedback, wherein the user perceives the sensation at the contact location on the prostheses, may provide more intuitive signals [28, 29] for prosthetic control. The current technologies for interfacing with peripheral nerves to restore sensory feedback include intrafascicular electrodes that penetrate into the nerve, epineural electrodes that wrap around the nerve, and anastomosis of nerve stumps to an intact muscle (e.g., the muscles of the chest), in a process known as targeted sensory reinnervation (TSR).

1.2.2 Peripheral Nerve Stimulation

Peripheral nerves have been targeted using a variety of neural interfaces including epineural cuff electrodes like the flat interface nerve electrode (FINE) [30, 31, 32] or microelectrodes that penetrate the epineurium, such as the longitudinal intrafascicular electrode (LIFE) [33], transverse intrafascicular multichannel electrode (TIME) [34, 35], or Utah slant array [36, 37].

1.2.2.1 Intrafasciular electrodes Electrodes such as the longitudinal intrafascicular electrode (LIFE) and transverse intrafascicular multichannel electrode (TIME) are designed to be implanted in peripheral nerves and penetrate through the epineurium, to achieve intimate contact with sensory and motor neurons. Rossini and colleagues implanted LIFEs for 4 weeks in the median and ulnar nerves of a subject with transradial amputation [38]. For this study, stimulation of peripheral nerves provided sensory feedback while using a prosthetic hand controlled by EMG signals from the biceps and triceps. The participant in this study reported sensations in the forearm and movement in the phantom hand.

Dhillon and colleagues achieved discrete tactile and proprioceptive sensations with stimulation through LIFEs implanted in median and/or ulnar nerves in 13 upper limb amputees [39, 40]. In a further study, by Horch et al ., LIFEs were implanted in the median and ulnar nerves of two transradial amputees [33]. These studies were the first demonstrations of direct neural feedback through stimulating individual fascicles of peripheral nerve stumps in amputees to produce graded, discrete sensations of touch or movement, even years after amputation.

Utah slanted electrode arrays have also been implanted into the median or ulnar nerves of 3 upper limb amputees to provide sensory feedback [36, 37]. This study demonstrated that penetrating electrodes could evoke focal cutaneous and proprioceptive percepts in the phantom hand up to 14 months after implantation. Along with long term efficacy, this study also demonstrated improvements in dexterous control of a robotic arm when stimulation mirrored the firing pattern of intact neurons. Similarly, Raspopovic and colleagues explored the use of TIME electrodes to stimulate the median and ulnar nerves in a closed-loop neuroprosthesis [34, 35]. In that study, a participant incorporated sensory feedback in real-time, grasping tasks and object discrimination tasks. More recently, this group has demonstrated that peripheral nerve stimulation of the tibial nerve provided real-time tactile and proprioceptive feedback that promoted improved mobility, fall prevention, and agility, in 3 transfemoral amputees [41, 42].

1.2.2.2 Epineural electrodes Epineural electrodes provide a less invasive approach to interfacing with peripheral nerves. Because they sit outside the epineurium and are more mechanically stable than penetrating microelectrodes, epineural electrodes typically achieve a more stable chronic interface, but with less selective stimulation. A set of studies using a cuff known as the flat interface nerve electrode (FINE) on the median and ulnar nerve demonstrated the ability to elicit focal percepts for up to 80 months in 1 subject and 24 months in another [30, 43, 31]. These devices are designed to maintain the oblong cross-section of peripheral nerves, keeping electrodes closer to those fascicles than can be achieved with cuffs with a circular cross-section. This study also developed a take-home system to understand embodiment of a prosthesis and understand whether subjects could learn to use artificial somatosensory feedback in tasks of daily living [44, 15].

Using a similar epineural cuff electrode, Ortiz-Catalan et al. stimulated the median and/or ulnar nerves in 4 individuals with upper limb amputation and observed improvements in grasping coordination during an object lift-and-hold task for a novel osseointegrated upper limb prosthesis [45, 46, 47]. Additionally, epineural cuff electrodes have been used to restore sensation and study the impact on postural stability, in two individuals with transtibial amputation [32].

These approaches have clearly demonstrated the ability to evoke focal sensations that are perceived to emanate from the upper-limb, even decades after injury. They also demonstrate very stark improvements in how subjects incorporate this feedback to use their prosthesis. However, they involve specialized electrodes and surgeries that are not part of common surgical practice. Further, peripheral nerve approaches often target distal nerves, which could limit their use in people with proximal amputations, such as shoulder disarticulations.

1.2.2.3 Transcutaneous electrical nerve stimulation Non-invasive somatotopic techniques, such as transcutaneous electrical nerve stimulation, have also been used to recruit afferent nerve fibers, that run superficially to the skin surface. A benefit of this method is it does not require surgery and recent studies have shown that it can evoke focal percepts in the phantom limb for upper [48, 49] and lower limb [50] amputees.

1.2.3 Targeted Sensory Reinnervation

Targeted sensory reinnervation is an approach that can allow vibrotactile or electrotactile feedback on the residual limb to be perceived as emanating from the missing limb. This is achieved by surgically redirecting the nerves that formerly innervated the missing limb to innervate patches of skin on the residual limb or trunk. Sensory afferents then innervate the skin and muscles, and tactile stimulation of the reinnervated region produces percepts in the phantom limb [51]. Kuiken et al . surgically transplanted the residual median, ulnar, radial, and musculocutaneous nerves to the pectoral musculature in three participants with transhumeral amputations [52, 53]. After reinnervation, electrical stimulation of the skin evoked percepts, including touch, pain, temperature, and proprioception, in the phantom limb.

1.2.4 Spinal Cord Stimulation

Spinal cord stimulation (SCS) is an FDA-approved, commercially available technology that could potentially be used to restore somatosensation. SCS leads are currently implanted in approximately 50,000 patients every year in the USA to treat chronic back and limb pain [54]. In the week-long trial phase that normally precedes permanent implantation of these devices, the leads are inserted percutaneously into the epidural space on the dorsal side of the spinal cord via a minimally invasive, outpatient procedure [55]. Clinically-effective stimulation parameters typically evoke paresthesias (i.e. sensation of electrical buzzing) that are perceived to be co-located with the region of pain. SCS leads are typically placed over the dorsal columns along the midline of the spinal cord. This placement results in paresthesias that are limited to the proximal areas of the trunk and limbs. However, recent studies have demonstrated that stimulation of lateral structures in the spinal cord and spinal roots can evoke paresthesias that selectively emanate from the distal regions of the body [56, 57, 58, 59]. As such, these devices provide an attractive option for widespread deployment of a neuroprosthesis for providing sensory feedback from distal aspects of the amputated limb, including the hand and fingers.

1.2.5 Early Stage Novel Approaches

Existing somatosensory neural interfaces face a critical trade-off between invasiveness and efficacy in providing sensory feedback. There are a host of safety issues associated with implanting electrodes that penetrate the epineurium, such as LIFEs, TIMEs, and USEAs, that could affect their long term stability. Electrode insertion results in mechanical damage to the tissue followed by glial scarring [60], which isolates the electrode from the neurons, [61] causing changes in the response to stimulation over time [62]. Studies using epineural electrodes, such as nerve cuffs and FINEs, have demonstrated that it is possible to achieve a long-term stable interface with distal peripheral nerves [43]. However, the percepts evoked by these are less focal, which may limit their efficacy in improving control of prosthetic limbs. In addition, the invasive surgery required to implant these electrodes is a major barrier to clinical translation. New approaches targeting peripheral nerve structures continue to be developed in the effort to provide sensory feedback. However, many of these techniques are still in early stages of development and lack substantial quantitative evidence in randomized, controlled trials with a focus on sensory restoration.

1.2.5.1 Regenerative electrodes These electrodes are designed to be implanted at the end of a transected nerve, allowing the nerve to grow through a lumen that contains electrical contacts, providing an intimate contact with the nerve. They provide high selectivity and long-term stability for both recording and stimulation and address the issue of glial scarring and mechanical damage to the neural tissue. MacEwan et al . designed macro-sieve electrodes that were implanted between transected ends of sciatic nerves in adult male rats [63]. Although their study did not directly address sensory feedback, it demonstrated that nerve regeneration was possible through these electrodes and the regenerated nerves had morphology and electrophysiological properties comparable to control fibers. Furthermore, stimulation through macro-sieve electrodes produced comparable muscle forces and allowed selective recruitment of fibers up to 3 months post-implant, providing a promising interface for future neuroprosthetic applications.

Navarro et al. developed a double-aisle electrode that allows selective stimulation and recording of nerve fascicles up to 6 months post-implant [64]. Other non-obstructive regenerative electrodes, such as the regenerative multielectrode interface [65] and the regenerative scaffold electrode [66], have also demonstrated a stable interface with amputated peripheral nerves and may be useful in neuroprosthetic applications for peripheral nerve injury and sensory restoration.

Regenerative peripheral nerve interfaces (RPNIs) are conceptually similar to TSR, but involve surgical placement of a small autologous partial muscle graft onto the peripheral nerve, which reinnervates the graft. RPNIs have been used for the treatment of postamputation neuroma pain [67], and have recently been used for prosthetic control, as the muscle graft acts as a bioamplifier for descending motor commands in the nerve. Chestek et al . demonstrated in rhesus macaques, that RPNIs provide a stable interface for recording high signal-to-noise ratio electromyographic signals for up to 20 months [68]. Long-term survival of these muscle grafts, up to 20 months post-implant, has also been demonstrated in several animal experiments using RPNIs for prosthetic control [69, 70]. Additionally, in a study with two distal transradial amputees, electrical stimulation via RPNIs demonstrated the ability to evoke cutaneous and proprioceptive sensations [71].

1.2.5.2 Optogenetics This technique is based on genetically modifying neurons to express light sensitive ion channels (opsin proteins). This provides an attractive method to activate or inhibit by light, only those neurons that express opsins. Selective recruitment via optical stimulation of sensory neurons has been demonstrated in a mouse model where the level of excitation or inhibition was modulated by the intensity of light [72]. However, the technical feasiblity and ethical and safety concerns related to transgenic approaches to incorporate opsins in neurons is a significant barrier that precludes any research into optogenetic approaches for somatosensory feedback in humans.

1.2.5.3 Focused ultrasound and Infrared nerve stimulation This is another non-invasive method that has been used to modulate neuronal activity and conduction properties of nerves [73]. It has also been used in a rat model to modulate the vagus nerve as a poten-

tial therapy for epilepsy and depression and achieve conduction block for potential analgesic applications [74, 75, 76]. Infrared nerve stimulation is another non-invasive method that provides high spatial resolution without the stimulation artifacts that traditional electrical nerve stimulation produces. Recent studies have shown that infrared stimulation coupled with electrical stimulation of the sciatic nerve can generate sustained plantarflexor muscle contraction in rats [77]. Additionally, infrared stimulation can selectively, rapidly, and reversibly recruit small-diameter sensory fibers in the mammalian vagus nerve [78]. However, while technical feasibility may not be an issue for either of these technologies, it is necessary to characterize the potential for thermally induced damage on nerves and establish safety limits for usage.

1.3 Dorsal Root Ganglia as a Target for a Somatosensory Neural Interface

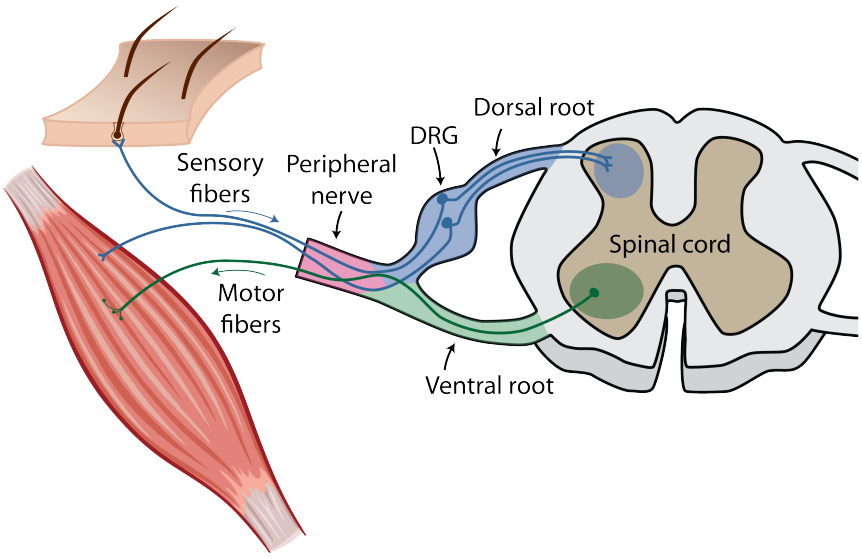

Figure 1.2: Anatomy of the spinal roots and periphery

The dorsal root ganglia (DRG) are enlargements of the spinal nerve located bilaterally in the intraforaminal space at each spinal vertebral level [79]. The DRG contains the cell bodies of primary sensory axons that innervate the periphery thus providing a compact

target for accessing large populations of somatosensory fibers [80]. Primary sensory afferents display a characteristic pseudounipolar morphology and an excitable soma and axon hillock [81, 82]. Histology studies have shown that the cell bodies of these afferents cluster near the periphery of the DRG when viewed in cross section [83]. This might explain recent observations where afferent activity was recorded using non-penetrating epineural arrays on the DRG surface [84]. These anatomical characteristics may also be useful for recruiting afferents using epineural electrical stimulation at the DRG.

Furthermore the DRG are segregated from motor efferents in the ventral root thus allowing for stimulation of afferents without risking uncomfortable contractions in residual muscles in a potential myoelectric control interface for amputees. Several studies have focused on building encoding models for primary afferent activity at the DRG [85, 86, 87, 88, 89, 90, 91, 92, 93, 94, 95, 96, 97]. These encoding models can be used to provide patterned biomimetic stimulation, while preserving the structure of information relayed to downstream sensory processing targets.

The spinal segmental level determines the location at the periphery innervated by these primary afferent neurons such that three to four DRG may provide the sensory representation of the entire limb [98]. However, while dermatomal segregation exists for large regions of the limb across DRG, the lack of a consistent somatotopic organization of sensory fibers within each DRG [99, 100] is a challenge for selective recruitment. Neighboring neurons may convey varied modalities of sensory information making it difficult to target particular afferent types and regions of the limb, at the time of electrode implantation. Therefore broad and diverse electrode coverage is important for a potential SSNI at the DRG.

1.4 Problem Statement and Hypothesis

While there have been important advances in the design and actuation of prosthetic limbs, these devices lack a means for providing direct sensory feedback. As such, users must infer information about limb state from cues like pressure on the residual limb, resulting in diminished control of prostheses, and reduced adoption and use of these technologies. Previous work in the Rehab Neural Engineering lab has focused on restoring sensation by electrically stimulating primary sensory afferents in the dorsal root ganglia (DRG). Recent animal experiments have demonstrated that stimulation through penetrating microelectrodes can achieve activation of small populations of primary afferents (PAs) in the DRG with a high degree of selectivity. These results suggest that the DRG and dorsal spinal cord are promising neural targets for restoring sensation, however significant challenges remain in the development of a somatosensory neuroprosthesis.

Currently available penetrating microelectrode technologies are not suitable for long-term implantation in peripheral nerves or the DRG, as the chronic immune response to their presence causes a high rate of device failure. Instead, multiple recent studies in human subjects have demonstrated that it is possible to achieve a chronic, stable stimulation interface with peripheral nerves by placing electrodes on the epineural surface of those nerves. For clinical translation of a DRG somatosensory neuroprosthesis, epineural electrodes may provide an ideal interface however they have not been tested in the context of selectively recruiting neurons within the DRG. This dissertation examines a novel way of interfacing with the DRG and dorsal roots that can be incorporated into a upper limb prosthesis to restore sensory feedback. A feline model for primary afferent recruitment will be used to compare the selectivity of epineural and penetrating stimulation. Next an anatomically and neurophysiologically accurate computational model of the DRG will be developed to study the mechanism of afferent recruitment. Finally, a series of experiments with upper limb amputees will be described that characterize the locus, modality and utility of percepts evoked when the cervical spinal cord and spinal roots are stimulated. The following specific aims will be pursued:

Aim 1: Compare the selectivity of afferent microstimulation at the DRG using epineural electrodes and penetrating electrode arrays.

Selectivity is extremely important in the development of a somatosensory neuroprosthesis, as it can make the difference between a highly focal evoked sensation (e.g. fingertip pressure) and a diffuse and less useful sensation (e.g whole arm tingle). It is anticipated that the relatively large exposed area and distance from PA targets, will impact recruitment selectivity of epineural electrodes. To test this hypothesis, we will deliver stimulation at the DRG using epineural electrodes and characterize the overall patterns of recruitment.

Hypothesis 1.1: Distribution of distal nerve branches that can be recruited through epineural stimulation is comparable to penetrating electrodes but fewer epineural electrodes are capable of selectively recruiting different nerves.

Hypothesis 1.2: Threshold charge injection is higher while dynamic range is unchanged for selective recruitment using epineural electrodes

Aim 2: Identify the mechanism of PA recruitment in the DRG for epineural stimulation and optimize electrode design for increased selectivity.

Recent experiments, have shown that the selectivity achieved with epineural stimulation at the DRG is nearly as good as that achieved with penetrating microelectrodes. The DRG houses cell bodies for PAs that are concentrated around the circumference and axons concentrated near the center. This unique anatomical structure may impact selectivity achieved by epineural electrodes. To test this hypothesis, we will model the effects of stimulation through epineural electrodes, to determine the locus of action potential generation in response to low amplitude stimulation as well as explore the effects of epineural electrode size and spacing on the selectivity and dynamic range of stimulation.

Hypothesis 2.1: Stimulation of the DRG with epineural electrodes results in generation of action potentials in the axon hillock i.e. where the axon stem exits the neuronal cell body

Hypothesis 2.2: The size and spacing of PA cell bodies (100 μm) near the epineurium enables selective recruitment via epineural stimulation

Aim 3: Characterize the modulation of evoked percepts as a function of electrode location and stimulus parameters via stimulation of dorsal spinal cord rootlets in upper limb amputees.

Selectively activating subpopulations of sensory afferents at the DRG may correspond to anatomical localization of sensory fibers at the periphery. However, modulating stimulation parameters may impact the subjective quality of the percept. To test this hypothesis, we will perform first-in-human experiments to explore the ability to generate sensations via epidural stimulation of the dorsal spinal rootlets in upper limb amputees.

Hypothesis 3.1: The intensity, focality, and modality of evoked percepts is correlated with the stimulation amplitude, location of stimulation cathode and frequency of stimulation respectively.

Hypothesis 3.2: Percepts evoked per electrode are stable in terms of locus and modality for a given set of stimulation parameter.

Hypothesis 3.3: Somatotopically-matched feedback delivered via lateral spinal cord stimulation can be used in a functional object manipulationn task.

2.0 Selectivity of afferent microstimulation at the DRG using epineural and penetrating electrode arrays

The contents of this chapter are published as: *Nanivadekar AC, Ayers CA, Gaunt RA, Weber DJ, Fisher LE. (2019). Selectivity of afferent microstimulation at the DRG using epineural and penetrating electrode arrays. J Neural Eng. 2019 Dec 13;17(1):016011.*

2.1 Introduction

By 2020, over 2.2 million people in the United States will be living with limb loss [101]. Approximately 65% of amputations affect the lower limbs [101]. Lower-limb amputations are commonly associated with mobility issues, decreased balance confidence, and falling [102]. In stark contrast to these statistics, the acceptance rate of prevailing lower-limb prostheses is below 50% [10]. While there have been important advances in the design and actuation of prosthetic limbs, these devices lack a means for providing direct sensory feedback and force the user to rely on visual feedback or infer information about limb state from pressure exerted on the residual limb by the prosthetic socket. This results in longer rehabilitation, diminished control of prostheses, and reduced adoption and use of these technologies [103].

Multiple recent studies have demonstrated that stimulation of peripheral nerves in the residual limbs of amputees can evoke naturalistic sensory percepts, referred to the amputated limb, even decades after amputation [34, 30, 39, 40, 104]. Recent studies using epineural nerve-cuff electrodes, which wrap around peripheral nerves, have demonstrated that it is possible to achieve a long-term stable interface with distal peripheral nerves in people with arm [30], [43] and leg [32] amputation. While the sensations evoked by stimulation through these electrodes were highly stable over multiple years, the selectivity of stimulation (i.e. the ability to evoke sensations in focal areas of the distal limb) was somewhat limited. These limitations become especially obvious when comparing the focality of sensations generated by epineural stimulation to what can be achieved by stimulating peripheral nerves with

penetrating microelectrode arrays, which are inserted into the nerve. For example, microelectrode arrays implanted in the median and ulnar nerves of amputees can generate highly localized sensation in the fingertips and palm [36] of the phantom hand whereas nerve-cuff electrodes evoke sensations across multiple phalanges and larger areas of the palm and dorsum of the phantom hand [31]. Longitudinal intrafascicular electrodes implanted through peripheral nerves in individuals with upper limb amputation have also demonstrated the ability to evoke both focal proprioceptive and tactile sensations [104].

Unfortunately, there are a host of safety issues associated with implanting penetrating microelectrode arrays into neural tissue. Electrode insertion results in mechanical damage to the tissue followed by glial scarring [105] which isolates the electrode from the neurons [106], and in the periphery, shifts the fiber composition towards smaller fibers [107]. Additionally, peripheral nerves are highly stretchable structures that undergo large changes in length as the limbs move through range of motion [108, 109], causing movement of the electrodes relative to their neural targets. All of these effects cause changes in the response to stimulation over time [62].

The dorsal root ganglia (DRG) and dorsal rootlets (DR) are attractive targets for delivering sensory feedback via electrical stimulation. The DRG contains a heterogenous population of cutaneous, muscle and nociceptive afferents all of which can be further divided into receptor classes that convey specific information about the state of the limb [80]. Three to four ganglia account for the innervation of an entire limb [98] while DRG at a single spinal level may provide access to the entire sensory representation of the foot [110]. Importantly, the separation of the sensory and motor pathway at the spinal roots allows for stimulation of afferents in the DRG without concomitant stimulation of motor efferents which could directly activate muscles and contaminate a myoelectric control interface. Additionally, the spine provides mechanical stability, limiting the movement of the DRG and spinal cord, which may improve the stability of stimulation. DRG and DR stimulation can also be used with high-level amputations (above-knee, above-elbow) where access to peripheral nerves is limited. In fact, ongoing work in our lab has demonstrated that electrical stimulation of the dorsal rootlets and spinal cord can evoke somatosensory percepts in the missing limbs of upper-limb amputees [111]. In that study, the stimulation electrodes were relatively large (3x1 mm), and

stimulation evoked sensations that covered entire digits or regions of the palm. Stimulation through smaller electrodes might evoke substantially more focal sensations. Prior work in our lab has demonstrated that microstimulation via penetrating microelectrodes in the DRG can achieve a highly selective neural interface, recruiting many distinct distal branches of the sciatic and femoral nerves [112]. This would likely translate into focal percepts in the foot and leg in humans. However, in chronic experiments, we found a substantial degree of instability in the response to DRG microstimulation over time [113]. Additionally, these electrode insertion techniques require extensive exposure of the DRG (e.g. via foraminotomy), which may pose significant challenges for clinical translation.

One method of overcoming these disadvantages is to use non-penetrating epineural electrodes. Existing minimally invasive surgical techniques for implanting electrodes on or near the spinal cord and DRG to manage pain [57, 56, 114] can potentially be adapted for implanting epineural arrays on the DRG for sensory feedback. Clinically approved epineural stimulation leads [115, 116, 117] may be amenable to use for sensory feedback easing the clinical translation process and provide a significant advantage over penetrating technologies. Additionally, our lab has recently demonstrated that it is possible to achieve single-unit recording of DRG neurons with electrodes placed on the epineural surface [84] which could be extended to study the mechanism of DRG stimulation or develop a closed-loop neuroprosthesis that uses evoked responses to adjust stimulation parameters, similar to other currently available spinal cord stimulation systems [118].

Because it is challenging or impossible to have animals report on the characteristics of evoked sensations, nerve cuff recordings from multiple nerve branches have been used by our lab and others to measure the selectivity of peripheral nerve [119] and DRG stimulation [112]. In this study, we compare the recruitment properties of epineural and penetrating electrodes when stimulating afferents in the L5, L6 and L7 DRG. Electroneurographic recordings of evoked responses in many distal branches of the femoral (saphenous, vastus medialis, vastus lateralis, sartorius) and sciatic (tibial, distal tibial, medial and lateral gastrocnemius, common peroneal, distal common peroneal, sural, cutaneous) nerve were used to assess the selectivity of DRG stimulation. Compound action potentials (CAPs) recorded from each

instrumented nerve were used to determine the threshold and dynamic range for selective recruitment, the distribution of projected fields per DRG, and the conduction velocity of the recruited afferents.

2.2 Methods

All experiments were performed under the approval of the University of Pittsburgh Institutional Animal Care and Use Committee (IACUC) and the US Army Animal Care and Use Review Office. Acute experiments were performed in six anesthetized male cats.

2.2.1 Instrumentation

Anesthesia was induced with a ketamine/acepromezine cocktail and maintained via inhaled isoflurane (1-2%) throughout the experiment. Vital signs (i.e heart rate, core temperature, SpO_2, and $ETCO_2$) were monitored continuously. Distal branches of the femoral and sciatic nerves (Figure 2.1A) were instrumented with two-contact nerve cuffs, which were either custom made or purchased (Microprobes, Gaithersburg, MD). Both types of electrodes were made from split silicone tubing with circumferential fine-wire stainless steel electrodes with an interelectrode spacing of 3 or 4 mm. The nerve cuff inner diameters ranged from 1 mm to 3 mm depending on the size of the targeted nerve. The sciatic and femoral nerves were instrumented with five-contact nerve cuffs (Ardiem Medical, Indiana, PA), which had an interelectrode spacing of 4 mm. Proximal, center, and distal contacts were shorted together and were used as a reference in a virtual tripole configuration when recording from the second and fourth contacts within the cuff [120].

Custom book electrodes were designed to match the characteristic branching pattern at the tibial nerve where it branches into the distal tibial, medial gastrocnemius and lateral gastrocnemius nerves (Figure 2.1B). A 3-D printed negative mold of this branching geometry

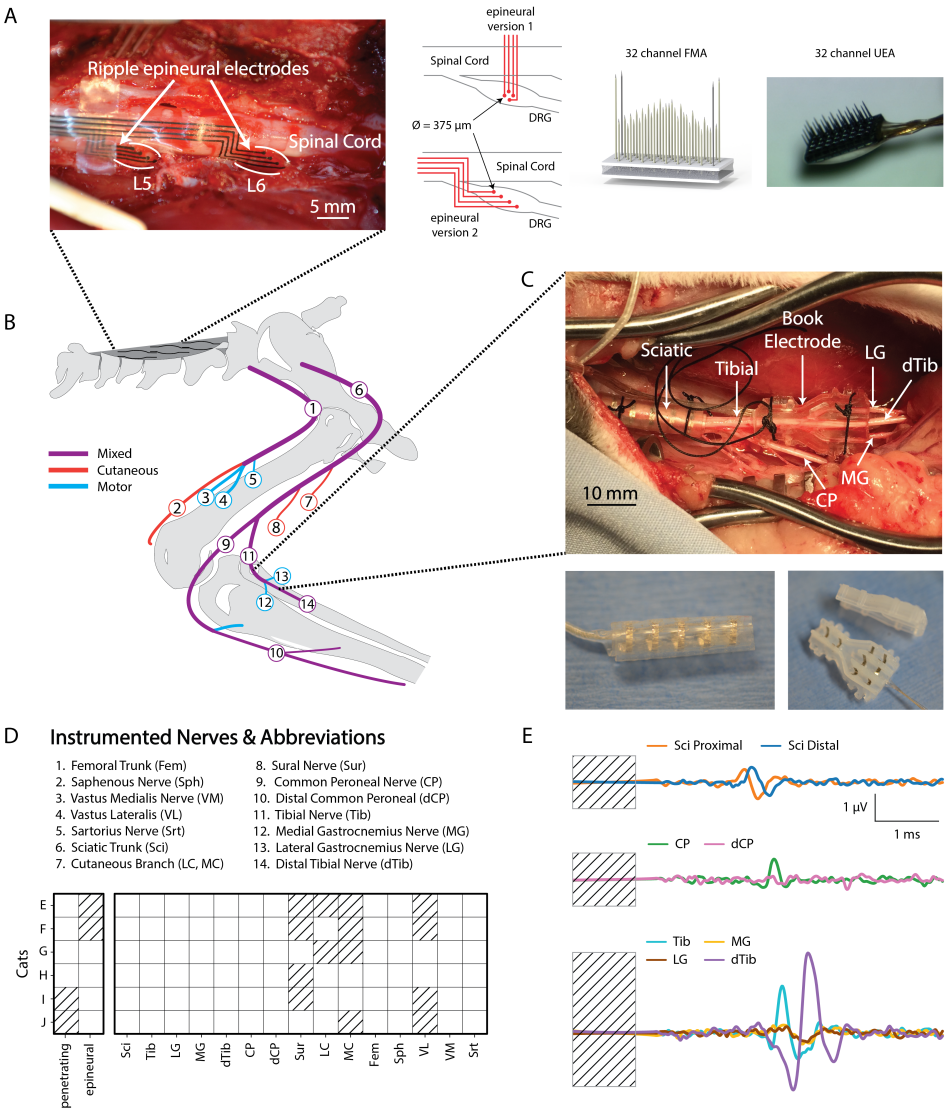

Figure 2.1: A) Placement of Ripple stimulation electrodes on the epineurium of the L5 and L6 DRG (left) along with a representation of the 2 epineural electrode designs and images of 32-channel UEA and FMAs (right). B) Schematic of nerve cuff location in the left hindlimb. C) Nerve cuffs and book electrodes implanted on the sciatic trunk and distal branches. D) Summary of nerves instrumented and DRG stimulation electrodes used across 6 acute experiments. Hatching represents instances where a nerve was not instrumented or a DRG stimulation electrode was not used. E) Example stimulation triggered average ENG recorded from the sciatic nerve and its common peroneal (middle) and tibial (bottom) branches.

was used to fabricate the spine and cover of the book electrode. Each channel in the book electrode contained 2 stainless steel electrodes to mimic a two-contact nerve cuff implanted on each branch.

Where possible, nerves projecting to members of each major muscle group innervated by the sciatic and femoral trunks were instrumented. The sciatic branches innervating the hamstrings were often very proximal, complicating surgical access, although a cuff was implanted around the nerve innervating biceps femoris in cat G. It was not possible to instrument the branch of the common peroneal nerve innervating ankle dorsiflexors without reflecting the biceps femoris tendon; however, the common peroneal nerve was always instrumented proximal and distal to this important branch point. Nerve identities were determined using known anatomical landmarks and verified by stimulation using a voltage-controlled stimulator (Grass, Warwick, RI) and finding coarse motor thresholds (supplementary table A.1). Sensory nerves, such as the sural and the sciatic cutaneous branch, were tested to the maximum stimulation intensity (20 V, 200 μs pulse width) to verify that there were no evoked movements. Across the 6 cats, instrumented nerves included the Sciatic (Sci) and Femoral (Fem) trunks, lateral gastrocnemius (LG), medial gastrocnemius (MG), distal tibial (dTib), common peroneal (CP), distal common peroneal (dCP), sural (Sur), cutaneous branches of the sciatic nerve (Cut), saphenous (Sph), vastus lateralis (VL), vastus medialis (VM) and Sartorius (Srt) nerves (Figure 2.1D).

After nerve cuff implantation, the left L5, L6 and L7 DRG were exposed via laminectomy. Epineural electrodes (4-channel Ripple LLC, Salt Lake City, UT) were placed on the epineurium of the L5, L6 and L7 DRG of cats G, H, I and J (Figure 2.1C). For cats G and H, there was no fixation of electrodes to the epineural surface and a threshold search was repeated for multiple placements of a single array on multiple ganglia. For cats I and J the epineural electrodes were fabricated with tabs that were used for fixation to the spinal cord dura. Following epineural testing, penetrating arrays were implanted in the L5-L7 DRG and threshold search was repeated. Testing epineural arrays first limited the effects of surgical manipulation and the tissue damage that might occur during high-speed insertion of the penetrating arrays.

Penetrating floating microelectrode arrays (32-channel FMA; Microprobes, Gaithersburg, MD) were inserted in the L6 and L7 DRG of cats E and F. The platinum-iridium electrodes of each FMA (Figure 2.1) had a variety of lengths (0.7-2.1 mm) designed to span the depth of the DRG with a pitch of 400 μm and exposed tip sizes of 50 or 150 μm. Utah electrode arrays (32-channel UEA; Blackrock Microsystems, Salt Lake City, UT) were inserted in the L5, L6 and L7 DRG of cats G and H. Each UEA contained 32 electrodes in a 4x8 grid and electrodes were 1 mm long with a pitch of 400 μm. During implantation, a custom vacuum holder attached to a micromanipulator was used to position the array over the DRG. The array was positioned so that its long axis was aligned with the proximal/distal axis of the spinal root. A pneumatic inserter with 1.5 mm of travel (Blackrock Microsystems, Salt Lake City, UT) was used to rapidly insert the array through the epineurium in the DRG. For all electrodes, a stainless-steel screw in the iliac crest was used as the return for stimulation and all stimulation was applied in a monopolar configuration. The cat was placed in a spinal frame for the duration of the experiment. Motor thresholds were measured again after transfer to the frame to verify that the cuffs still made adequate contact and that the instrumented nerves were still intact.

2.2.2 Epineural Electrode Design

The epineural electrode array fabrication process was based on patterned robotic deposition of alternating layers of insulating medical-grade silicone/polyurethane co-polymer and a conductive polymer. The conductive polymer traces and electrode sites were formed by mixing platinum microparticles with the silicone/polyurethane substrate material. This provided mechanical matching of all the materials throughout the device for high flexibility and flexural durability. The flexibility of these electrodes allowed for conformation to the surface of the DRG. The initial design of these arrays, used in cats G and H, comprised of traces along the length of the array that terminated in 4 contacts arranged in a square layout (Figure 2.1A). This electrode design was highly susceptible to mechanical perturbations when placed on the epineural surface. For cats I and J the array design was modified such that the leads from the array ran parallel to the spinal cord, providing additional friction with the

epidural surface of the spinal cord to improve mechanical robustness. For these arrays, the traces terminated in 4 contacts arranged along the length of the DRG. Additionally, tabs were added to the array substrate to allow fixation to the spinal cord dura. The diameter of the exposed electrode contacts for both electrode arrays was 375 μm and spacing between the centers of neighboring contacts was 750 μm (mean $\pm$ std post-implant impedance was 16.03 $\pm$ 5.29 kΩ).

2.2.3 Experiment Design

The objective of this study was to evaluate the recruitment properties of epineural electrodes in terms of threshold, selectivity, dynamic range, and distribution of recruited nerves. Threshold charge was defined as the minimum charge injection at the DRG required to elicit activity in any instrumented nerve. If a single distal nerve branch was activated at threshold, stimulation was deemed to be selective for that nerve. For each instance of selective recruitment, the dynamic range was determined as the range of stimulation charge over which selectivity could be maintained before a second nerve was recruited. In the event of non-selective recruitment, functionally synergistic innervation pathways (e.g. nerves innervating multiple heads of the gastrocnemius) were identified.

Electroneurogram (ENG) signals were recorded from all nerve cuffs using a Grapevine Neural Interface Processor (Ripple, Salt Lake City, Utah), using a differential headstage (Surf-D) with an input range of 5 mV, resolution of 0.2 μV, 0.3 Hz cutoff high-pass filter and 7.5 kHz cutoff low-pass filter. Signal digitization was performed directly on the headstage at 30 kHz. Stimulation was performed using two IZ2 16-channel stimulus isolators (TDT, Alachua, FL) and custom LabVIEW software in cats E, F, G and H or nano2+stim headstages (Ripple, LLC) for cats I and J. ENG signals typically have a low signal-to-noise ratio. To reduce this noise and reveal the underlying compound action potential (CAP), high pass filtering and stimulus triggered averaging was performed for all ENG recordings. Stimulation artifacts were blanked in software using a 1 ms window, which was at least 0.5 ms longer than each stimulation pulse and did not exceed the minimum conduction latencies of the most proximal nerves. Following blanking, ENG data were high-pass filtered at 300 Hz.

Table 2.1: Epineural stimulation binary search parameters. "Total Electrodes" represents the number of electrodes that were tested, "Active Electrodes" represents the number of electrodes that were capable of recruiting any nerve at any charge. "Selective Electrodes" represents the number of electrodes that recruited a single nerve at threshold. The binary search was conducted independently at 2 threshold resolutions for cat G at the L5 DRG.

Subject	**Threshold resolution** (nC)			**Maximum charge** (nC/phase)	**Total Electrodes**	**Active Electrodes**	**Selective Electrodes**
	L5	**L6**	**L7**				
G	0.08, 0.82	-	0.21	16.38, 15.35	20	10	6
H	0.41	0.41	0.41	16.38	24	23	16
I	1.02	1.02	1.02	61.43	12	11	8
J	0.4	0.4	0.4	28.0	12	8	5
Total					**68**	**52**	**35**

Custom software was written in C++ and MATLAB (Mathworks, Natick, MA) to capture and display stimulus triggered ENG recordings from all cuff electrodes, to detect responses, and to coordinate a binary search for threshold as a function of the injected charge.

The methodology for determining recruitment threshold online is detailed elsewhere [112]. Briefly, a high amplitude survey trial was conducted to identify electrodes that evoked CAPs in the sciatic and femoral nerve branches. During this survey, stimulation was delivered through each electrode at a rate of 55-58 pulses/second with either 82 or 205 μs/phase cathodic-leading symmetric pulses. The maximum charge injection for epineural stimulation was varied between 15-60 nC/phase (Table 1). For penetrating electrodes, the maximum charge injection was varied between 3-8 nC/phase (Table 2). This maximum amplitude was chosen to avoid electrode degradation and to avoid activating spinal reflexes that would cause muscle contraction and movement artifact in the ENG signal. Stimulation electrodes that did not evoke a response in any nerve branch were excluded from the binary search. For all other electrodes, a binary search over stimulation charge was carried out to determine the recruitment threshold for each instrumented nerve. For epineural electrodes, the resolution for binary search was varied between 0.06 and 0.95 nC/phase (Table 1) and for penetrating

Table 2.2: Penetrating stimulation binary search parameters. The binary search was conducted independently at 2 threshold resolutions for cat G at the L7 DRG.

Subject	**Threshold resolution** (nC)			**Maximum charge** (nC/phase)	**Total Electrodes**	**Active Electrodes**	**Selective Electrodes**
	L5	**L6**	**L7**				
E	-	0.20	0.20	3.07	192	61	49
F	-	0.20	0.20	8.19	256	38	28
G	0.08	0.12	0.12, 0.41	2.45	128	123	96
H	0.25	0.25	0.25	3.27	96	86	67
Total					**672**	**308**	**240**

electrodes the resolution was varied between 0.17 and 0.71 nC/phase (Table 2). The binary search resolution used for epineural testing was lower relative to penetrating electrode testing (i.e. stimulation charge was sampled more coarsely) to compensate for the higher survey trial amplitude. For cat G, the binary search with penetrating electrodes at L5 DRG and epineural electrodes at L7 was conducted at 2 separate resolutions within the same experiment to reduce the time spent performing a binary search per electrode. A non-parametric Kruskal-Wallis test confirmed that resolution had no effect on the detected threshold ($p > 0.01$) for cat G. During the online threshold search, stimulation was repeated 400-600 times at each amplitude, ENG responses were detected by comparing the RMS of the stimulus triggered averaged ENG response between pre-stimulus baseline and stimulation epochs. The windowed RMS was calculated using a 250 μs sliding window with 25 μs overlap between consecutive windows. RMS values exceeding 0.5 μV and one standard deviation of baseline RMS for four consecutive windows were annotated as stimulation evoked responses. These parameters were selected empirically to improve accuracy during online detection.

All recorded ENG signals were reanalyzed offline for rigorous statistical testing using a non-parametric subsampling approach described previously [112]. Briefly, a 99% confidence interval about the baseline mean was established and the detection threshold for post-stimulation ENG responses was set to one standard deviation above the upper bound of this interval. For each stimulation amplitude, a random subsample of 90% of the repeti-

tions were selected 100 times to generate a distribution of ENG responses for each electrode. The windowed RMS was calculated for each of these subsampled responses using the same 250 μs sliding window with 25 μs overlap. For a time window in the ENG response to be considered significant, 95% of the subsampled averages had to be supra-threshold during that time window (supplementary figure A.1A). Additionally, all ENG responses from epineural stimulation were validated by a human expert. The sensitivity and accuracy of the automated detection algorithm was calculated using the manual annotations as ground truth. ENG responses per trial for both epineural and penetrating electrodes along with validated annotations can be downloaded from the Blackfynn Discover Repository. Additionally, all ENG responses and selectivity results per trial can be viewed here.

2.2.4 Conduction Velocity

For instances where a CAP was detected at the sciatic or femoral nerve trunks, the local cross correlation (LCC) was calculated between signals recorded from the second and fourth contacts of the 5-pole nerve-cuff to determine the conduction velocity of recruited afferents. The process for calculating LCC is described in detail elsewhere [120]. Briefly, the cross-correlation between the stimulus-triggered averaged signal recorded on the second contact and fourth contact was calculated (supplementary figure A.1B). A 0.5 ms sliding window of the signal recorded from the fourth contact was moved through a 1-10 ms time window of the stim-triggered average ENG signal recorded on the second contact at 50 μs steps. If the peak of the LCC exceeded one standard deviation above the cross-correlation of the noise for 3 consecutive windows, the trial was identified as containing a compound action potential. The distance between the second and fourth contact (8 mm) was divided by the cross-correlation lag for the window with the highest LCC to calculate the conduction velocity of the recruited afferent.

2.3 Results

Across the four cats (G, H, I, J) where epineural stimulation was delivered, a total of 64 electrodes were tested in 11 ganglia. Fifty-two electrodes produced a response in at least one nerve at threshold and 67% of these electrodes were able to selectively recruit a single nerve at threshold. In contrast, for the four cats (E, F, G, H) where penetrating arrays were tested, a total of 672 electrodes were tested in 10 ganglia, of which 308 produced a response at maximum amplitude and 79% of these electrodes selectively recruited a single distal nerve branch at threshold. While the percentage of responsive electrodes evoking selective responses were higher for penetrating arrays, stimulation at maximum amplitude evoked responses in fewer penetrating electrodes (45%) compared to epineural electrodes (76%). The percentage of responsive electrodes varied across subjects for both electrode types. For penetrating electrodes, the yield of responsive electrodes at maximum amplitude for cats E, F, G, and H was 31.7%, 14.8%, 96.0%, and 89.6% respectively. For epineural electrodes the yield for cats G, H, I, and J was 50%, 95.8%, 91.7%, and 66.7%. The maximum amplitude delivered during epineural stimulation was higher than that for penetrating stimulation and may explain overall greater recruitment.

2.3.1 Coactivation at Threshold

Threshold responses for stimulation at each DRG were used to generate coactivation matrices for each electrode type (Figure 2.2). The rows in each coactivation matrix correspond to the nerve recruited at threshold and the columns represent the coactivated nerves. The non-normalized counts for recruitment and coactivation were calculated to highlight the differences in recruitment and coactivation per DRG. Additionally, non-normalized counts allow comparison across multiple nerves recruited at threshold whereas normalizing (supplementary figure A.2A and B) allows a comparison of the instances of coactivation within a given nerve.

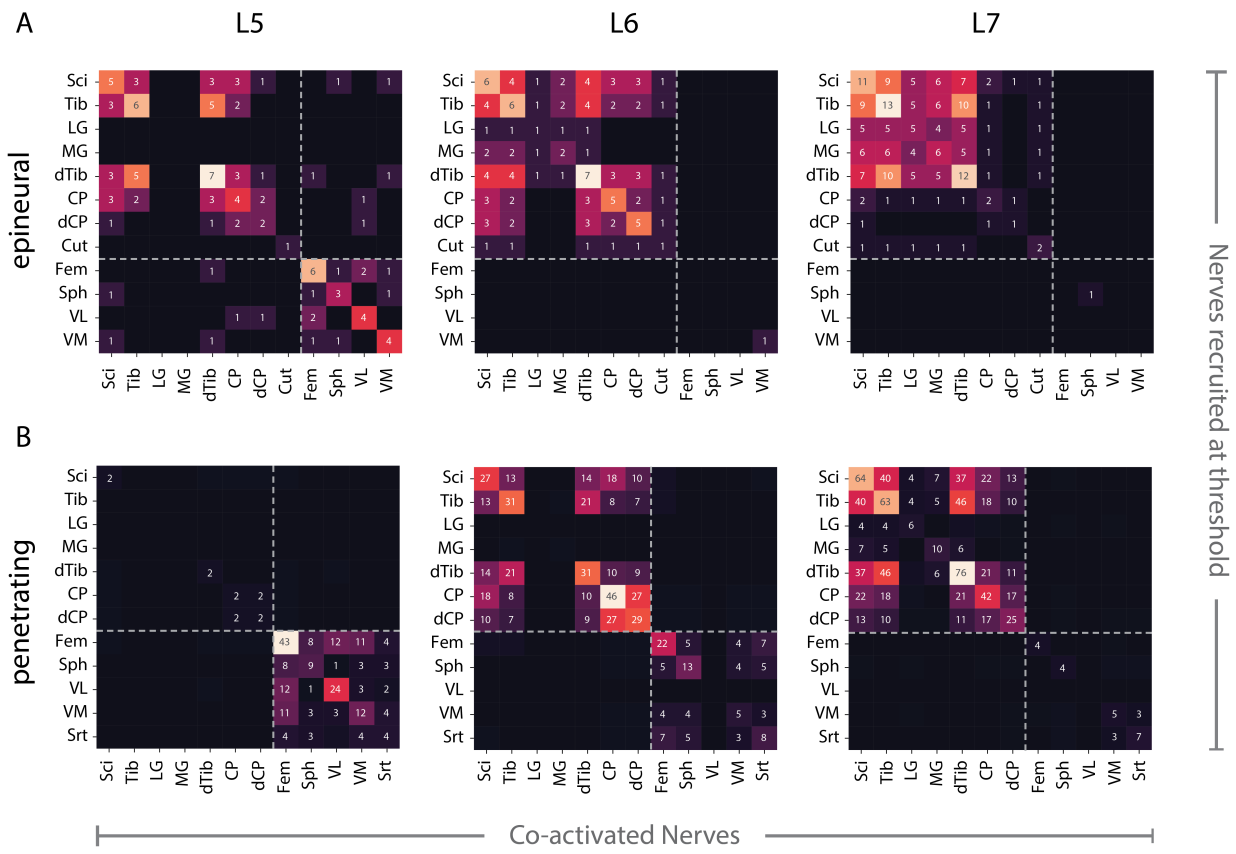

Figure 2.2: Count of nerves coactivated at threshold per DRG for stimulation via A) epineural and B) penetrating electrodes. Dashed line indicates division between femoral and sciatic nerve branches. Rows represent the nerves recruited and columns represent the nerves coactivated at threshold

With epineural electrodes, stimulation at the L5 DRG recruited femoral and sciatic nerve branches at threshold. Stimulation at the L6 and L7 DRG exclusively recruited the sciatic nerve and its branches at threshold except for one instance of vastus medialis recruitment at L6 and one instance of saphenous recruitment at L7. Epineural stimulation at L6 recruited the common peroneal and the tibial branch of the sciatic nerve, however LG and MG were rarely recruited. Whereas stimulation at L7 preferentially recruited the tibial branch of the sciatic nerve over the common peroneal branch and had a higher recruitment rate for MG and

LG. With penetrating electrodes, stimulation at L5 primarily recruited the femoral trunk and its branches (Sph, VL, VM and Srt) with minimal sciatic nerve recruitment. Penetrating electrode stimulation of the L6 DRG recruited sciatic and femoral branches approximately equally at threshold with no activation of the LG, MG and VL. While penetrating L7 stimulation predominantly recruited sciatic nerve branches with rare activation of LG and MG, unlike epineural stimulation at L7. Both electrode types demonstrated preferential activation of sciatic nerve branches for stimulation at L6 and L7 DRG. However, stimulation with penetrating electrodes at the L6 DRG showed more coactivation of sciatic and femoral branches than epineural stimulation. This trend was reversed for stimulation at the L5 DRG where epineural stimulation produced more coactivation of femoral and sciatic nerve branches at threshold than stimulation with penetrating electrodes. The combined coactivation matrices for each electrode type (supplementary figure A.2A and B) were calculated by adding the coactivation matrix at each DRG and normalizing the counts in each row by dividing by the total number of times that a given nerve was recruited. This was used to determine the overall tendency of multiple nerves to be coactivated at threshold. The overall pattern of coactivation at threshold for penetrating and epineural electrodes showed a strong linear relationship (supplementary figure A.2C) i.e. the likelihood of two nerves being coactivated at threshold was similar for both electrode types. The Pearson correlation coefficient between the coactivations for epineural and penetrating stimulation was 0.80 ($R^2 = 0.64$). We expected that distal nerves would be coactivated with their proximal parents (e.g. tibial or common peroneal with sciatic nerve). However, this was not always true and is likely a result of the difficulty in detecting threshold-level ENG signals in large-diameter nerves, where the signal may be smaller if the electrode is further from the source [112]. Furthermore, the sciatic and femoral nerves were infrequently coactivated at threshold (<20% of the time).

2.3.2 Selectivity and Dynamic Range

The instances of selective recruitment for each nerve were tallied for each DRG (Figure 2.3A). Stimulation that recruited a single distal nerve at threshold was deemed selective. Nerves in the same innervation path (e.g. tibial and distal tibial) could be coactivated while

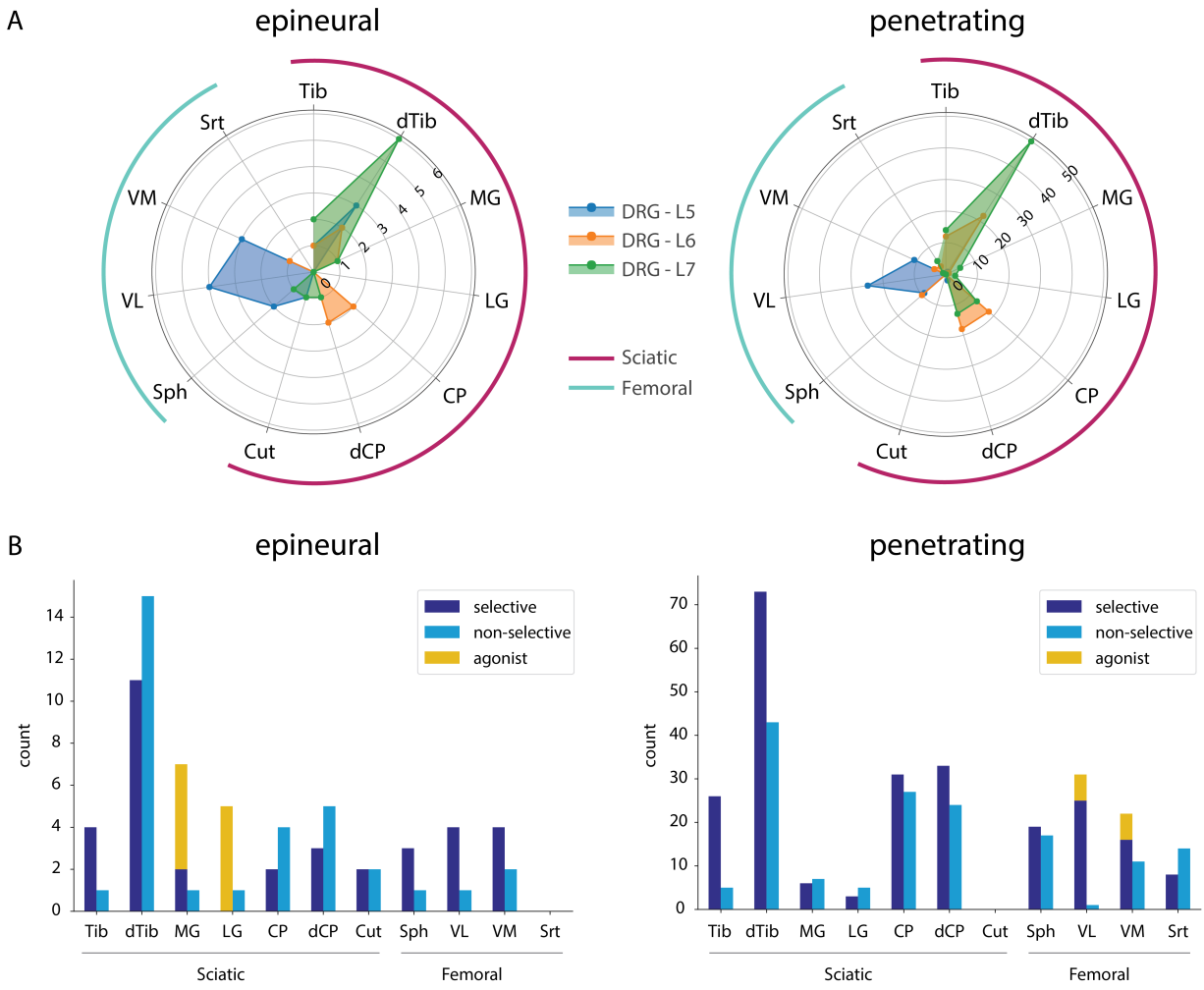

Figure 2.3: A) Counts of selectively recruited nerves for stimulation via epineural and penetrating electrodes at each DRG. B) Counts for selective recruitment, non-selective recruitment and coactivation of agonists at threshold. Counts for selective recruitment were obtained by adding the counts at each DRG for each nerve in 3A. Nerves in the same innervation path (e.g., tibial and distal tibial) were allowed to be coactivated while still being considered selective; however, only activation of the distal most nerve was counted to highlight differential recruitment of proximal branches

still being considered selective. However, only activation of the distal most nerve was counted to highlight differential recruitment of proximal branches [112]. Epineural stimulation at the

L5 DRG recruited more sciatic branches (28%) than penetrating stimulation (6%). For both electrode types, the distal tibial nerve was most often recruited selectively. This was followed by the tibial, vastus lateralis, and vastus medialis branches for epineural stimulation and distal common peroneal and common peroneal branches for penetrating stimulation. For both electrode types, stimulation at the L5 DRG produced selective responses in the femoral nerve and its branches. For the L6 and L7 DRG, the likelihood of recruiting the sciatic nerve or its branches was higher than for L5. Additionally, for functional groups of agonist muscles, (i.e. quadriceps: VL, VM and plantarflexors: LG, MG), selective recruitment of each nerve and each functional agonist group was counted separately (2.3B). For epineural stimulation, the quadriceps were never coactivated at threshold while the plantarflexors were often (55%) coactivated at threshold. Overall, epineural stimulation yielded at least one instance of selective recruitment at threshold for all the instrumented nerves except LG. For penetrating electrodes, plantarflexors (MG and LG) were never coactivated at threshold while the quadriceps were coactivated infrequently (8.3%).

Using an expert observer as the gold standard, the overall sensitivity, specificity, and accuracy for ENG response detection was 96.4%, 80.9% and 85.7% respectively (supplementary table A.2). In several instances, the ENG response detection algorithm erroneously detected the stimulation artifact as an ENG response, which was greater in the femoral nerve trunk due to the short distance between the DRG and the femoral nerve cuff. This high false positive rate (Fem: 30%, Sci: 3%) contributed to the lower detection accuracy in the femoral nerve and its branches, particularly for cat G and H.

We also quantified the distribution of threshold charge and dynamic range of stimulation for each instance of selective activation. A D'Agostino-Pearson test was used to determine that the distributions for threshold and dynamic range for each electrode type (Figure 2.4) were non-normal ($p < 0.01$), so a non-parametric Kruskal-Wallis test was used to test for differences in thresholds and dynamic range across epineural and penetrating stimulation. The median recruitment threshold and dynamic range for epineural electrodes were 9.67 nC and 1.01 nC respectively. For penetrating electrodes, median recruitment threshold and dynamic range were 0.90 nC and 0.36 nC respectively. Both threshold and dynamic range were significantly higher ($p < 0.001$ for both) for epineural than penetrating electrodes.

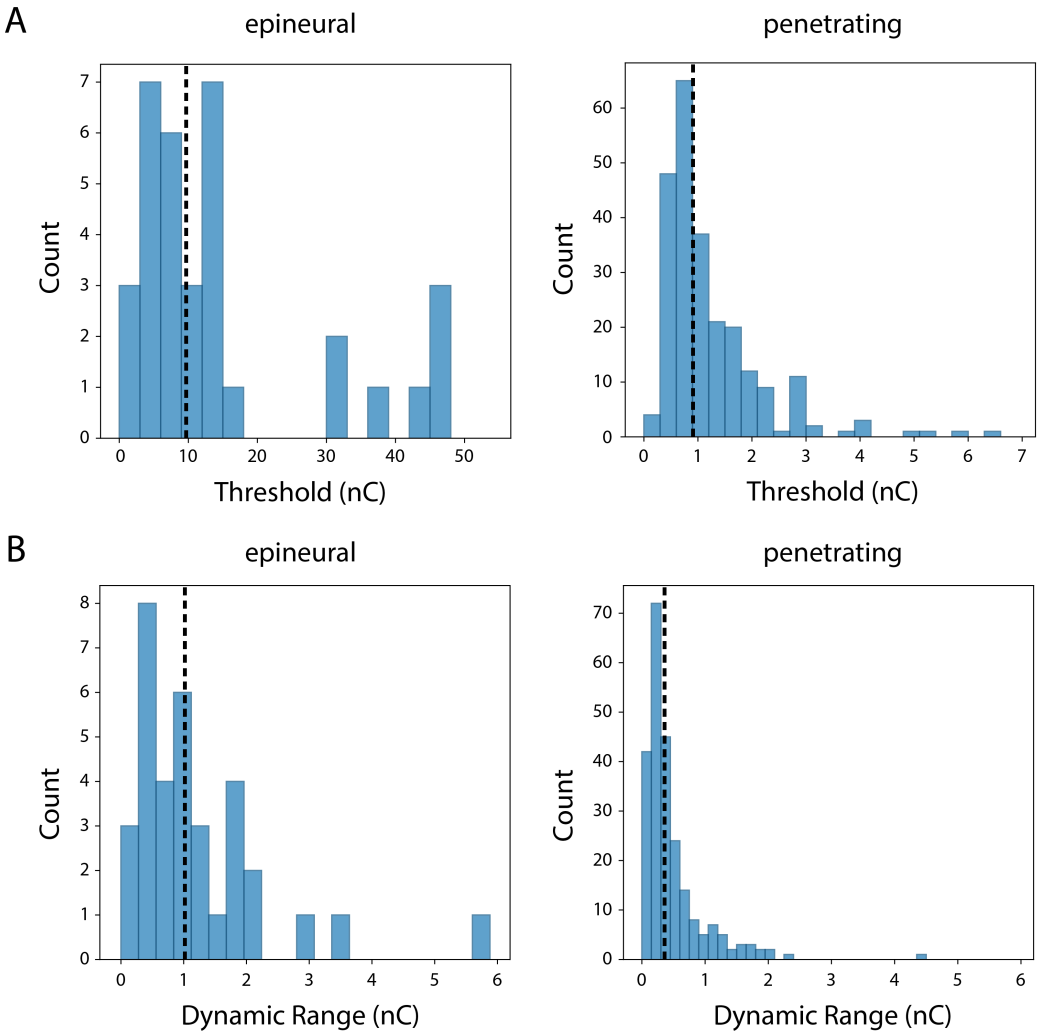

Figure 2.4: A) Distribution of selective recruitment thresholds for stimulation via epineural (median = 9.67 nC/phase) and penetrating (median = 0.905 nC/phase) electrodes. B) Distribution of dynamic range for selective recruitment for epineural (median = 1.01 nC/phase) and penetrating (median = 0.36 nC/phase) stimulation. Dashed lines show median for each plot.

The choice of resolution for binary search could impact the dynamic range (i.e. a lower resolution could give the appearance of a higher dynamic range). Since the resolution was varied between epineural and penetrating electrode experiments, we used a non-parametric

Kruskal-Wallis test to test for differences in dynamic range across binary search resolutions for each electrode type (supplementary Figure A.3). For the same binary search resolution (0.41), there were significant differences ($p < 0.01$) in the distribution of dynamic range for penetrating and epineural stimulation. Additionally, the dynamic range for penetrating stimulation at a lower resolution of 0.082 nC was not significantly different from the dynamic range detected with a resolution of 0.41 and 1.024 nC with epineural electrodes. These results indicate that the observed differences in dynamic range were not due to the resolution of binary search.

Additionally, we used a nonparametric Kruskal-Wallis test (as data were non-normal) to test for differences in dynamic range and threshold between FMA and UEA penetrating electrodes. There were significant differences in the thresholds ($p < 0.01$) between the two types of penetrating electrodes however no difference was observed in the distribution of dynamic range. We also tested if there were differences in threshold and dynamic range across electrode length and exposed tip sizes for the FMAs and no significant differences were observed. We also tested for differences between the two designs of epineural electrodes used and found a significant difference in the thresholds ($p < 0.01$). However, there was no difference in the dynamic range between both designs. Because of variations in the experimental setup between cats G-H and I-J, there were multiple covarying factors that could have led to these differences such as the layout of contacts (linear vs square) and fixation to the spinal dura.

2.3.3 Conduction Velocity

Finally, the conduction velocity of recruited afferents in the femoral and sciatic nerve were compared at threshold and supra-threshold stimulation amplitudes (Figure 2.5). For epineural stimulation, at threshold only 60-80 m/s (group 1/Aβ) fibers were recruited in the femoral nerve while slowly conducting fibers (< 50 m/s, group 2) were recruited at higher amplitudes. For the sciatic nerve, epineural stimulation recruited 40-120 m/s fibers at threshold while slowly conducting fibers were never recruited at threshold. The relationship

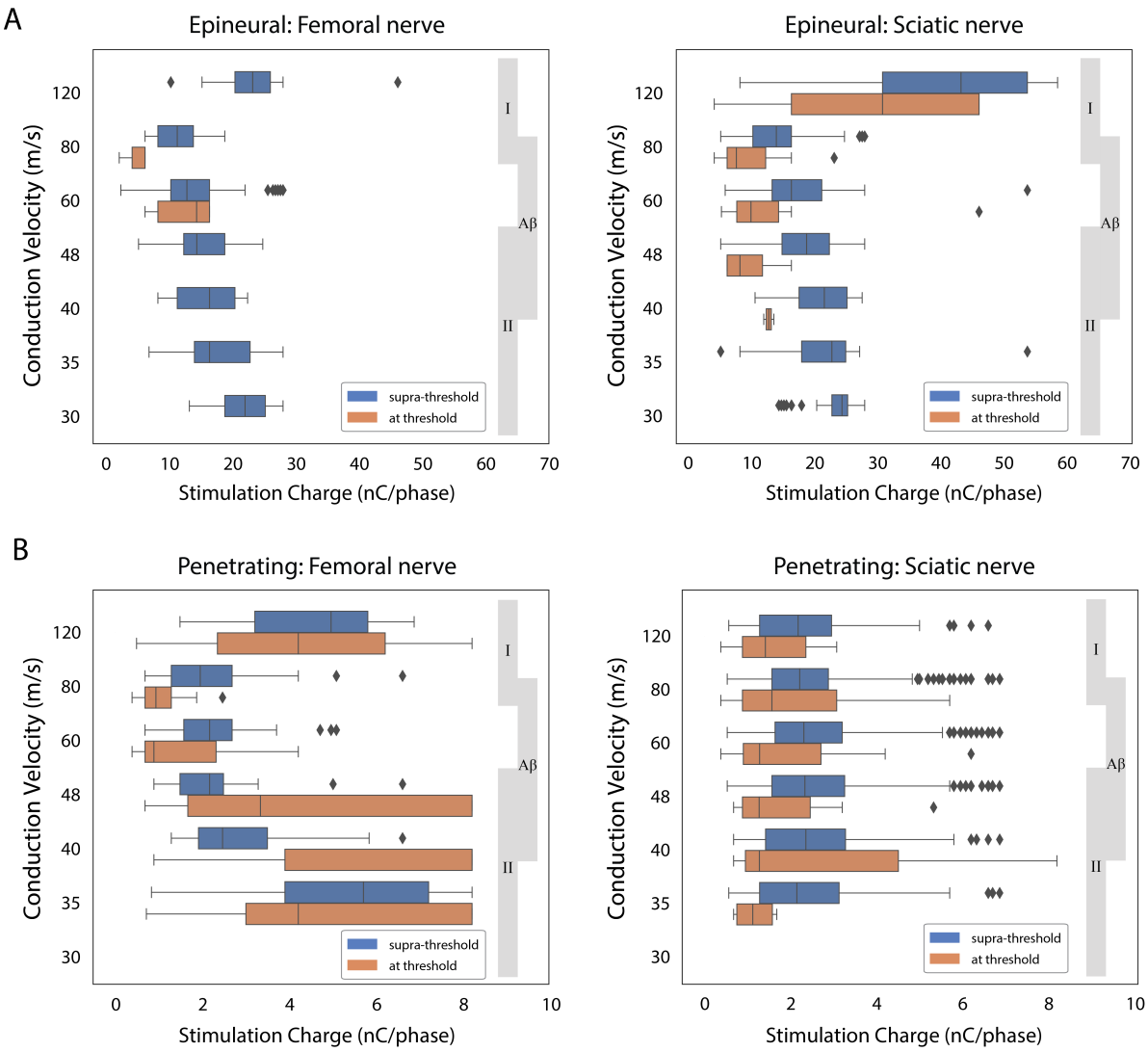

Figure 2.5: Comparison of stimulation charge injected and the CV of the nerve cuff response recorded across all stimulation amplitudes (blue) and at recruitment threshold (orange) for stimulation via A) epineural and B) penetrating electrodes at the lumbar DRG. CV values were discretized due to sampling frequency limitations of the recording setup. The vertical grey bars indicate the range of CVs corresponding to group I, Aβ and II afferents.

between stimulation amplitude and conduction velocity of recruited fibers displayed a weak negative correlation at threshold for the femoral nerve (R^2 = 0.39, slope = -2.26 $ms^{-1}nC^{-1}$,

$p < 0.01$) and a weak positive correlation for the sciatic nerve ($R^2 = 0.35$, slope = 1.19 $ms^{-1}nC^{-1}$, $p<0.001$) nerve. For penetrating stimulation, the range of fibers (35-120 m/s) recruited at threshold and supra-threshold stimulation amplitudes was the same for sciatic and femoral nerves. Stimulation via penetrating electrodes did not recruit any afferents with a conduction velocity below 35 m/s. For the femoral nerve, the conduction velocity of recruited afferents at threshold showed a weak negative correlation with the stimulation charge ($R^2 = 0.17$, slope = -2.44 $ms^{-1}nC^{-1}$, $p<0.001$) whereas for afferents in the sciatic nerve no linear correlation between stimulation amplitude and conduction velocity was observed.

2.4 Discussion

The goal of this study was to determine whether epineural stimulation of the DRG selectively recruits distal branches of the sciatic and femoral nerves and to compare the distribution of recruited nerves and recruitment properties with stimulation via penetrating electrodes. While epineural electrodes provide a clearer path to clinical translation than penetrating devices, the epineurium is a resistive barrier [121] that increases the separation between electrodes sites and target neural tissues. Additionally, the size of the active sites on the epineural electrodes used in these experiments meant that charge density delivered per pulse of stimulation was lower than with penetrating electrodes. Given the diffuse nature of epineural stimulation, we expected less selective recruitment and frequent coactivation of the sciatic and femoral branches. Surprisingly, a majority (67%) of epineural electrodes selectively recruited a single distal branch of the sciatic or femoral nerve at threshold.

The pattern of recruitment was consistent with known dermatome maps [98] and selectivity was consistent across both electrode types. Stimulation of the L5 DRG selectively recruited femoral nerve branches innervating the quadriceps while stimulation at the L6 and L7 DRG recruited sciatic nerve branches innervating ankle plantarflexors and distal branches of the common peroneal and tibial nerves, both of which innervate the skin on the foot. Several studies have demonstrated that sensory feedback from peripheral afferents is necessary to modulate locomotor muscle activity and the timing of phase transitions in

the gait cycle [122, 123, 124, 125, 126]. Specifically, feedback from Golgi tendon organs and secondary spindle afferents provides approximately $1/3^{rd}$ of ankle plantarflexor muscle tone [127]. In the context of clinical translation, these results imply that delivering stimulation at the caudal lumbar DRG may be sufficient to evoke relevant percepts that are localized to the missing limb in a somatosensory neuroprosthesis for people with trans-tibial amputation.

Other than the lateral gastrocnemius nerve, epineural stimulation selectively recruited every instrumented nerve branch at least once. Interestingly, for both epineural and penetrating electrodes the distal tibial nerve was frequently recruited selectively. It is unlikely that distal tibial afferents have an intrinsically low activation threshold. However, it is possible that afferents innervating the distal tibial nerve represent a greater fraction of afferents than other nerves in the L6 and L7 DRG, increasing the likelihood of recruitment. While our primary method to determine selectivity was to identify nerves that were recruited to the exclusion of all others, another way to consider selectivity is at a functional level. For example, there were 5 instances in which the lateral and medial gastrocnemius nerves were coactivated at threshold. Although this coactivation does not represent selectivity in terms of a single nerve branch, both nerves innervate the agonist muscles that are responsible for ankle plantarflexion and knee flexion. In terms of delivering relevant sensory feedback, it may not be necessary to selectively recruit these functionally synergistic nerves. The same holds for the vastus lateralis and medialis nerves that innervate the quadriceps, although coactivation at threshold was not observed during epineural stimulation.

As anticipated, epineural stimulation had a higher threshold for selective recruitment when compared to penetrating electrodes. However, the dynamic range of selectivity was also significantly higher than that for penetrating electrodes. This means that selectivity for a given nerve could be maintained over a larger range of charge injection during stimulation. In the context of clinical translation, a higher dynamic range for selective recruitment may provide a somatosensory interface that is resilient to electrode encapsulation since increasing stimulation charge may still recruit the same population of afferents. A larger dynamic range also provides a larger parameter space within which stimulation can be varied in order to modulate the subjective quality of an evoked percept. The inherent assumption that epineural stimulation is diffuse may be true in the context of current spread through neural

tissue. However, it is plausible that the mechanism of afferent recruitment itself is different between epineural and penetrating stimulation and serves to counter this diffusivity. The DRG houses the cell bodies for all sensory afferents that project from the limbs, and in cross-section, these cell bodies are concentrated near the circumference of the DRG while axons are concentrated near the center [83]. Additionally, the cell soma and initial segment are excitable and adapted for spike initiation [128]. Taken together, these observations suggest a possible mechanism of recruitment wherein epineural stimulation activates regions of the neuron closer to the epineurium such as the axon hillock or stem, while penetrating electrodes directly recruit axons present near the center of the DRG. Future work should explore these potential mechanisms and their implications for the design of electrodes at the DRG. The subjective quality of evoked percepts may also be modulated by activating fibers of specific sensory modalities. Afferents can be loosely segregated into separate populations based on their axonal diameters and corresponding conduction velocities, though those populations have some overlap [129, 130, 131]. By measuring the conduction velocity of CAPs traveling through the nerve-cuff electrode, it is possible to infer the most likely sensory modalities of the activated neurons. Our prior work in acute and chronic preparations using penetrating electrodes has demonstrated the ability to recruit medium to large diameter fibers in the DRG [113, 120].

Additionally, modeling studies examining the recruitment of fibers via stimulation of the DRG have demonstrated that intraneural microstimulation may recruit medium diameter fibers with greater probability than large diameter fibers [132] while non-penetrating DRG stimulation drives activity of large myelinated Aβ fibers but does not directly activate small nonmyelinated C-fibers [79]. In the present study, recruitment of fibers in the L5, L6 and L7 DRG showed a similar trend. Across all stimulation amplitudes, epineural electrodes recruited fibers with conduction velocities between 30-120 m/s. Stimulation with penetrating electrodes recruited a similar range of fibers (35-120 m/s). These conduction velocities correspond to medium and large diameter fibers such as muscle spindle afferents, Golgi tendon organs and a variety of cutaneous sensory axons. At threshold, epineural stimulation recruited fibers in the femoral nerve with conduction velocities between 60-80 m/s, roughly corresponding to medium diameter fibers.

Interestingly, fast conducting (120 m/s) fibers were not activated selectively at threshold. For the femoral nerve, stimulation via epineural and penetrating electrodes displayed a similar negative correlation between the conduction velocity of recruited afferents and the stimulation charge. For the sciatic nerve, epineural stimulation at threshold predominantly recruited fibers with conduction velocities between 40-80 m/s with some instances of 120 m/s fibers being recruited. As with the modeling study, this result may occur because of the higher percentage of cutaneous afferents than fast conducting proprioceptive afferents in the DRG [133]. In contrast, stimulation via penetrating electrodes recruited a diverse population of afferents projecting to the sciatic nerve at all stimulation amplitudes. Still, we have demonstrated that epineural electrodes can recruit a range of sensory afferents and future work may focus on selective recruitment and activation thresholds for each modality of sensory afferents with epineural DRG stimulation.

2.4.1 Challenges and Future Work

In this study we have demonstrated that selective recruitment of distal nerve branches that innervate the hindlimb via epineural stimulation is comparable to the selectivity achieved via penetrating electrodes. Despite the diffuse nature of epineural stimulation, individual nerves and functionally synergistic innervation pathways were recruited at threshold and the dynamic range for selectivity was higher than anticipated. However, there are a few shortcomings that could be addressed in future work. A large inter-subject variability was observed in the percentage of epineural electrodes that produced a response at maximum charge injection. It is possible that this variability is an example of anatomical differences and inconsistent dermatomes between animals. However, successful array placement and fixation typically determined the efficacy of stimulation. There was no fixation of electrodes to the epineural surface for cat G and H while epineural electrodes used with cats I and J were fabricated with tabs on the arrays that were used for fixation to the spinal cord dura. For a potential somatosensory interface with the DRG, ensuring electrode positioning and contact with neural tissue throughout the lifetime of the device is critical. Additionally, in terms of measuring conduction velocity, we were limited by the sampling frequency of the surf-D

headstage (i.e. 30 kHz). This meant that the resolution for measuring conduction velocity decreased for higher conduction velocities and we could only detect conduction velocities at 30, 34, 40, 48, 60, 80 and 120 m/s. While no afferents were recruited below 40 m/s it is possible that the reported conduction velocities are only a close approximation (to the nearest sample) and selective recruitment by sensory modality may be possible. The difficulty of selectively recruiting neurons varies throughout the nervous system based on underlying neural organization. Neural interfaces based in the primary somatosensory [134, 135], and the visual cortex [136, 137], rely upon the somatotopy and retinotopy of these regions, respectively. The cochlear implant relies on the well-defined tonotopic map of the cochlea [138] which facilitates recruitment of auditory fibers with similar frequency responses in spatial restricted locations. While there is dermatomal segregation of afferents from large regions of the limb across DRG, selective recruitment is important due to the lack of a consistent somatotopic organization of sensory fibers within each DRG [99, 100]. As with peripheral nerves, neighboring neurons may innervate different regions within a dermatome or may convey different modalities of sensory information. This means that particular afferent types and subregions of the limb cannot be targeted a priori with DRG stimulation, making broad and diverse electrode coverage especially important. In the context of developing a clinical somatosensory interface, further work is necessary to evaluate the effect of modulating stimulation parameters on recruitment properties. In this study all stimulation was applied in a monopolar configuration with respect to a distant ground. Maximizing the utility of epineural electrodes may ultimately require pursuing bipolar stimulation and more complex current steering techniques to achieve more focal recruitment. The epineural electrodes used in this study had only four contacts. We tried multiple placements of these electrodes to compensate for this limitation. Additionally, the large electrode contacts meant multiple electrodes may have recruited redundant populations of afferents. The size and spacing of electrodes used in this study was constrained by the fabrication process. Ripple is currently able to manufacture devices with features of 150 μm that are comparable in size to the cell body of afferents found in the DRG (20-100 μm) [139]. Ongoing work in our lab is focused on identifying the optimal electrode size, channel count, spacing, and fixation required for maximal coverage, selectivity and electrode independence. The primary limiting factors for

achieving a high-channel epineural interface will possibly be related to anatomy (e.g. surface area and curvature of the DRG) and stimulation safety (e.g. charge density limits) rather than electrode properties.

Finally, a fundamental assumption underlying these experiments is that selective recruitment of distal nerve branches corresponds to focal percepts localized to the limb. However, it is possible that the salience of an evoked percept is more relevant than focality for a somatosensory neural interface. Stimulation parameters that recruit a nerve may not necessarily evoke a percept and coactivation and non-selectivity may be permissible if evoked percepts are differentiable. However, addressing the subjective modality of percepts evoked via DRG stimulation may only be possible by replicating epineural DRG stimulation in humans. In summary, epineural electrodes represent a compromise between selectivity, safety, and stability and have been used in several successful neuromodulation devices. The selectivity of epineural stimulation at the DRG represents a viable path forward for clinical translation for a DRG-based somatosensory neuroprosthesis.

3.0 Modeling sensory fiber recruitment via epineural and penetrating stimulation at the DRG

3.1 Introduction

Computational models of neural tissue are a valuable scientific tool that have been used to analyze and design neurostimulation devices used to treat several neurological diseases and disorders. Modeling in this context serves two main purposes. First, it provides insight into the mechanism by which the target neural population is activated [140]. Second, it serves as a virtual testing platform to explore a large parameter space (lead design, stimulation configurations, waveform parameters etc) that would be challenging if not impossible to explore in a clinical or preclinical setting [140, 141].

Additionally, with regards to personalized medicine, patient-specific models that account for the unique anatomy, electrode position and measured physiological response to stimulation have shown superior clinical efficacy and can be used to optimize clinical application of technologies, such as deep brain stimulation [142] and spinal cord stimulation [143]. Epidural stimulation of the spinal cord for treatment of chronic pain was one of the first applications of computational modeling where a finite element model of the electrical field generated within the spinal cord was used to estimate the threshold and recruitment of myelinated axons in response to bipolar stimulation [144, 145]. Subsequent studies have focused on identifying the population of nerve fibers recruited as a function of the stimulation parameters [146] and electrode geometry [105] along with refinements to the biophysical model of the neurons [147] and anatomical models of the spinal cord [148] to explain the mechanism of action of SCS.

More recently, DRG stimulation was approved by the FDA for treatment of complex regional pain syndrome of the groin and lower limbs [149, 116] and has been used off-label for a wide array of pain etiologies, such as phantom limb pain, diabetic neuropathy, etc [150, 151, 152, 153]. This has also led to several modeling studies focused on understanding the mechanism of action of DRG stimulation [79, 154]. Prior DRG modeling work has focused

on building a model of afferent fibers to predict the probability of recruiting a distribution of fibers as a function of stimulus intensity [132]. This model demonstrated that as stimulation amplitude increased the number of fibers recruited increased exponentially. Furthermore, it also predicted that medium-diameter fibers may be recruited with greater probability than large-diameter fibers. While these results formed the basis for our in vivo experimentation with penetrating stimulation electrodes, the model does not account for the presence of cell bodies, the pseudounipolar morphology of DRG afferents, the glomerular structure of the T-stem axon [81] and assumes that the site of activation always occurs at the nodes of Ranvier in axons.

Results from our epineural stimulation experiments may contradict this assumption about the site of activation within afferents in the DRG. When the DRG is viewed in cross-section, the cell bodies of afferents are clustered around the circumference, while axons are more densely located near the center of the structure [83]. This unique anatomical structure may explain the surprising selectivity results we observed. Epineural electrodes are much closer to cell bodies than to axons, and given that voltage drops exponentially with distance from an electrode and that epineural stimulation can achieve a high degree of selectivity, it is possible that the site of activation may not always be the axons.

Several studies modeling the behavior of neurons at the DRG have confirmed empirical observations regarding the excitability of the soma. The cell soma is adapted for spike initiation and the excitability of the soma and initial segment is essential for spike invasion of the soma [128]. Our data present the possibility that epineural stimulation at the DRG may activate other regions of neurons (e.g. axon hillock, stem), that are closer to the epineurium while penetrating electrodes directly recruit axons present in higher densities near the center of the DRG.

In this study, we developed a computational model of the DRG that replicates the unique geometric arrangement of afferents to identify response to electrical stimulation at the DRG. By building a model that accurately replicates the anatomy and dynamics of electrical stimulation at the DRG, we can begin to understand how these surprising results occur, and to take advantage of the unique anatomical structure of the DRG to develop electrodes that can optimally target PAs for a somatosensory neuroprosthesis. Contemporary studies

have used a similar model-based approach to design epineural electrodes that maximize the selectivity of peripheral nerve stimulation [155, 156, 157] for motor and somatosensory neuroprostheses. Their simulations investigated multiple electrode configurations to determine the optimal number and location of contacts for maximum selectivity. The advantage of such an approach is that it allows for rapid iteration on the design of electrodes to determine the effects of electrode size, shape, arrangement, and number on the selectivity of stimulation. While this approach has been used extensively in designing electrodes for stimulation of peripheral nerve, this study marks the first attempt at model-based design for epineural electrodes at the DRG.

3.2 Methods

To develop an understanding of the underlying mechanisms of stimulation through penetrating and epineural electrodes at the DRG, we 1) developed a computational finite element model (FEM) that replicates the anatomical and electrical properties of the DRG and surrounding tissues, 2) calculated the extracellular voltages generated by stimulation of the tissue through epineural and penetrating electrodes, and 3) simulated the dynamics of transmembrane ionic current flow with multi-compartmental models of pseudounipolar neurons placed in this extracellular voltage field.

3.2.1 Models of Sensory Neurons in the DRG

We used the open-source software package NEURON (v7.7) [158] and the pyneuron [159] library in Python (v3.6) [160] to construct a multi-compartment model of Aβ afferents. The morphology of these afferents was adapted from previous studies [128, 161]. The Aβ afferents have a large soma (50-80μm) that leads into a long unmyelinated initial segment followed by four myelinated internodes (neck), ending at the t-junction. At the t-junction the neuron

bifurcates into a peripheral and dorsal root axon branch. The dorsal root axon branches were smaller in diameter than the peripheral branches [162] and were parametrized to the diameter of the peripheral branch [139] (figure 3.1A).

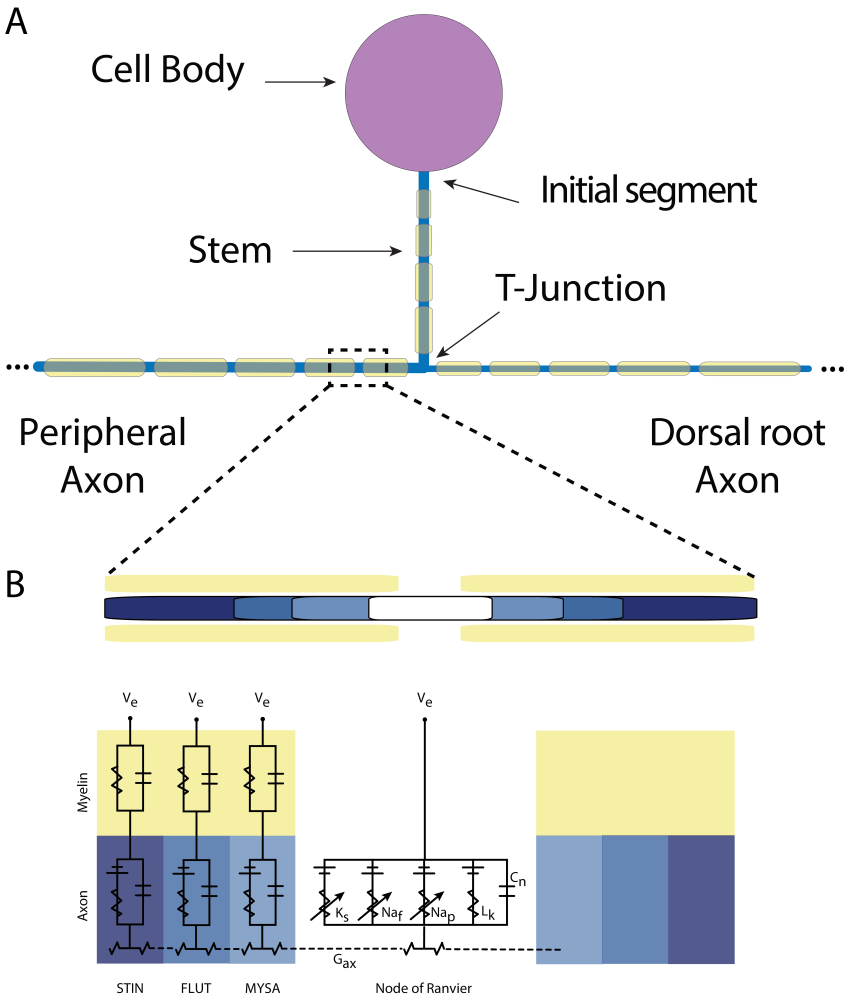

Figure 3.1: A) Multi-compartment model of primary sensory (Aβ) afferent B) Equivalent circuit representation of mammalian axon described in the MRG model

A model of the mammalian axon (the MRG model) [147] was used to construct the neck and axon branches of the neuron model. The MRG model is a double cable model of a mammalian motor axon that contains nodes of Ranvier separated by ten internodal segments with an explicit representation for the myelin attachment segment (MYSA), paranodal main segment (FLUT) and internode segment (STIN). Nodes in the MRG model

include fast and persistent sodium (Na_f, Na_p respectively), slow potassium (K_s) and linear leakage (L_k) conductances in parallel with the nodal capacitance as shown in figure 3.1B. Internodal conductance was represented by a single conductance value (G_i) in parallel with the membrane conductance. To accurately predict the behavior of Aβ sensory afferents, the membrane conductances at the nodal and internodal compartment of the MRG model were modified [163, 164]. Specifically, fast potassium (K_f) channels were added to the nodal and internodal compartments and slow potassium (K_s), leak (L_k) and hyperpolarization activated cyclic-nucleotide gated (HCN) channels were added to the internodal compartments. Additionally, the nodal L_k was increased to 8 mS/cm^2 to reduce membrane hyperpolarization at simulation onset. The A parameter of the K_s β rate constant was increased to 0.06 to better fit experimental values of afterhyperpolarization (AHP) amplitude and duration as has been described in previous studies [79].

The Na_f and Na_p channel densities at the nodes of Ranvier in the MRG model are 2000 channels/μm^2. Freeze fracture studies of the DRG soma and axon hillock describe the soma and initial segment as having the same active channels as the nodes, differing only in the sodium channel densities [82]. Accordingly, for our Aβ afferent model the Na_f and Na_p channel densities at the soma were modified to 300 channels/μm^2. The initial segment was divided into a proximal (0 to 6 μm from the soma) and distal section. The Na_f and Na_p channel densities were 1000 channels/μm^2 at the proximal section and 600 channels/μm^2 at the distal section of the intial segment.

Additionally, the myelin thickness and internode length of our Aβ afferent model were parametrized to replicate the increased myelination in the neck near the t-junction and the variable internode length in the first several nodes of the peripheral and dorsal root branches.

3.2.2 Histological Data from Feline Lumbar DRG

Histological data collected from the L6 and L7 DRG in six cats was used to determine the arrangement of sensory afferent cells within the DRG. We observed that cell bodies were distributed densely within an annulus of 400 μm beneath the epineurium. With increased depth from the epineural surface, cell bodies become sparse and most of the endoneurium is

occupied by axon branches projecting towards the periphery and dorsal root (figure 3.2A). Nissl staining showed that PA soma are large, roughly round cells with diameters ranging from about 50-80 μm [165]. These observations were in agreement with a recent study where the cross sectional area of the DRG was partitioned based on the density of cell bodies. The highest density of cell bodies was reported in the outer 24% radially and the dorsal $\pm$ 61° [83] (figure 3.2B). Additionally, we used published data for fiber size distributions in the L7 DRG of a cat to obtain a log-normal probability distribution for fiber size within a 4-16 μm range of diameters. We used these observations to determine the placement of the multi-compartment Aβ afferent model within the FEM and the fiber size of the neck and axon branches.

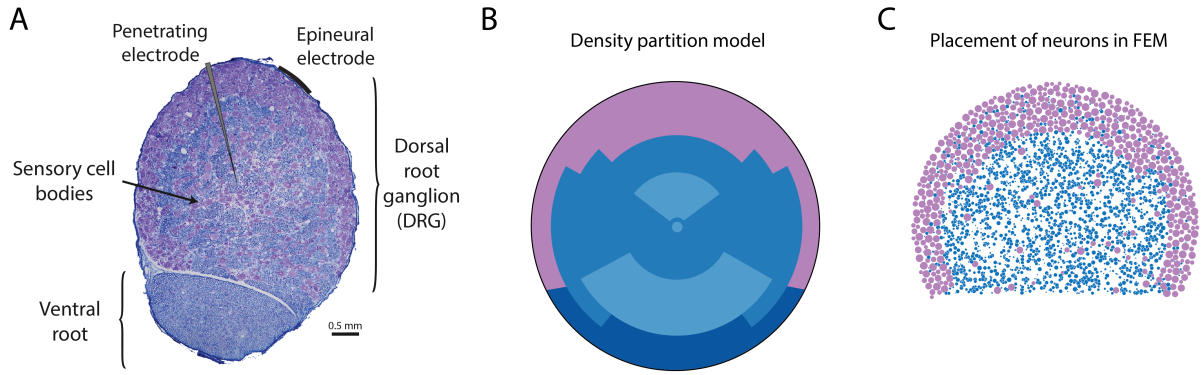

Figure 3.2: A) Cross section of feline lumbar DRG with schematic representation of epineural and penetrating electrodes relative to cell soma and axons. B) Density partition model describing regions of high neuronal soma density (purple). Blue shading represents sectors where the soma density was significantly different from other regions. Adapted from [83]. C) Example of multi-compartment Aβ afferent models placed in the FEM

3.2.3 Anatomy Based Model of the DRG and Surrounding Tissue

We constructed a 3-dimensional finite-element model of the feline L7 dorsal root ganglion based on anatomical measurements taken from previous acute experiments. Across multiple cats, the L7 DRG measured after a laminectomy was 5-8 mm long and 3-3.5 mm in diameter

at its widest point. The enlargement of the dorsal root ganglion was modeled as an ellipsoid (prolate spheroid) with a semi-major axis of 3.7 mm and a semi-minor axis of 1.5 mm. The peripheral and dorsal root branches were modeled as 15 cm long cylinders with a radius of 0.75 mm. The peripheral and central branches connected to the DRG at 3.25 mm from the center of the ellipsoid. The epineurium and connective tissue was modeled as a 20μm thick layer that ensheaths the DRG and extends uniformly along the length of the peripheral and dorsal branches. The DRG and epineurium were placed within 2 concentric cylinders of 3.25 mm and 17.2 mm radius to represent the intraforaminal tissue and bone (figure 3.3).

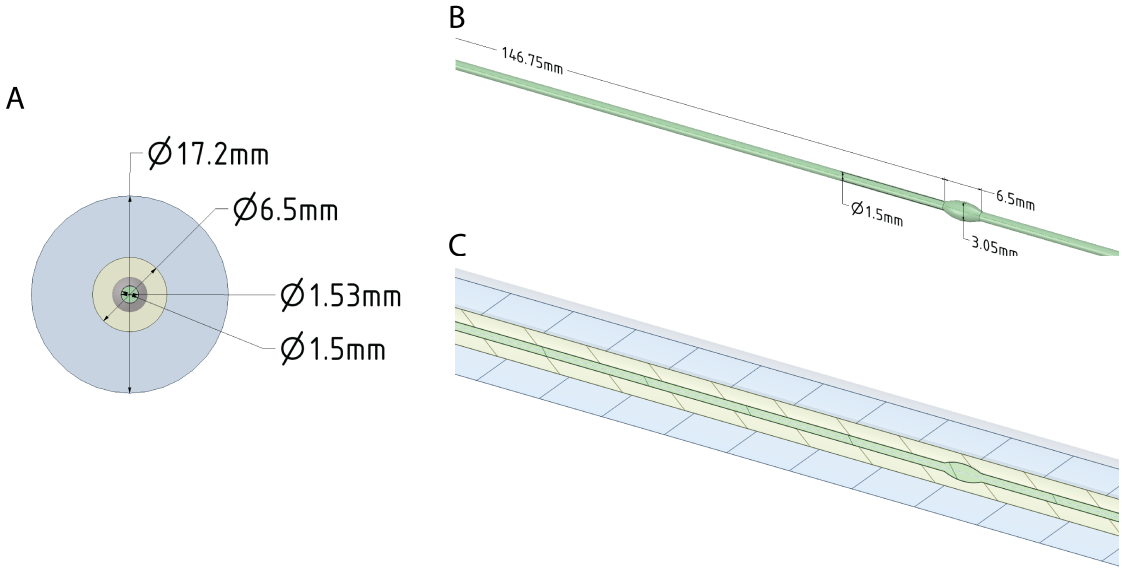

Figure 3.3: Schematic of DRG finite element model A) Cross section B) 3-dimensional rendering of the DRG C) Longitudinal section of the DRG and surrounding tissue modeled as concentric cylinders

A single platinum epineural electrode with a contact diameter of 375 μm and a height of 100 μm was constructed. Except for the surface of the electrode in contact with the epineurium all surfaces were encased in a perfect silicone insulator (figure 3.4A). A model of a single 1mm long Utah array electrode was constructed with a 0.05 mm exposed tip and parylene-c insulation on all remaining surfaces (3.4B). Additionally, a cylindrical stimulation return electrode made of stainless steel was inserted into the bone to replicate the stimulation

ground inserted in the iliac crest during the acute experiments. All model components were constructed using the SpaceClaim 3D modeling software. Anatomical and electrical properties of the finite element model were obtained from previous studies [154].

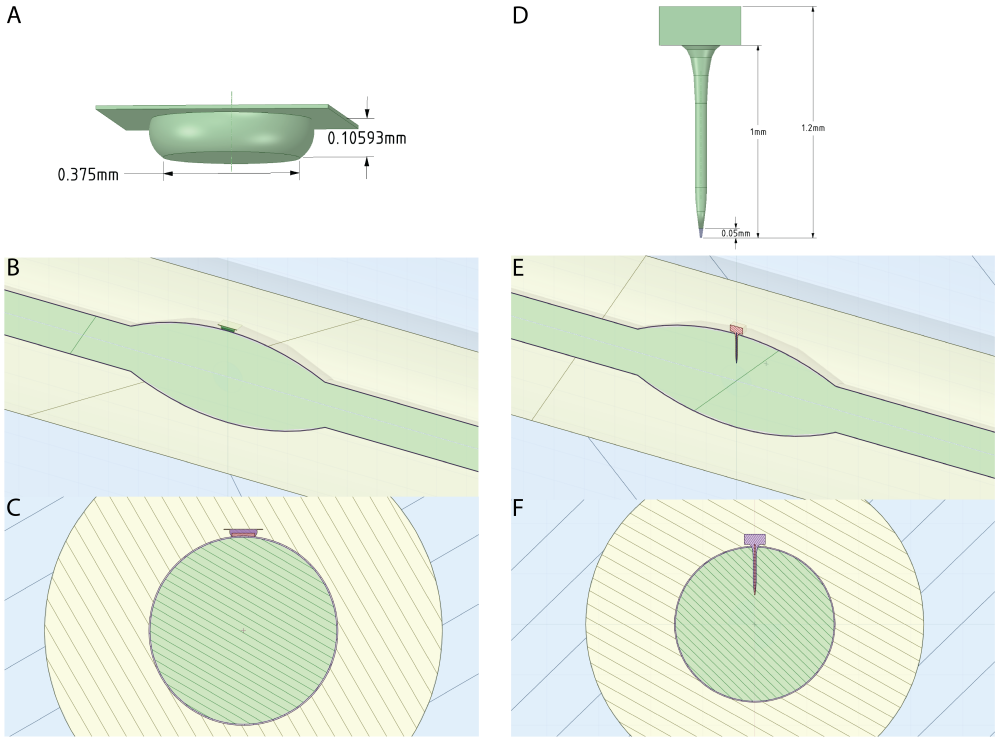

Figure 3.4: Schematic of A) epineural and B) penetrating electrode design

3.2.4 Extracellular Voltage Generated by DRG Stimulation

The 3-dimensional model of the DRG, surrounding tissue and stimulation electrode was imported into Maxwell 3D (v2020, ANSYS, Canonsburg, Pennsylvania). All biological tissues were modeled with isotropic conductivity except the DRG and spinal root which was modeled as a two-dimensionally anisotropic material. The longitudinal conductivity (along the x-axis) was higher than the transverse conductivity (y-z plane).

The epineural electrode was placed on the epineurium such that the longitudinal axis coincided with the y-axis at the middle of the DRG. The exposed contact of the epineural electrode was designed to conform to the curved surface of the DRG. The penetrating

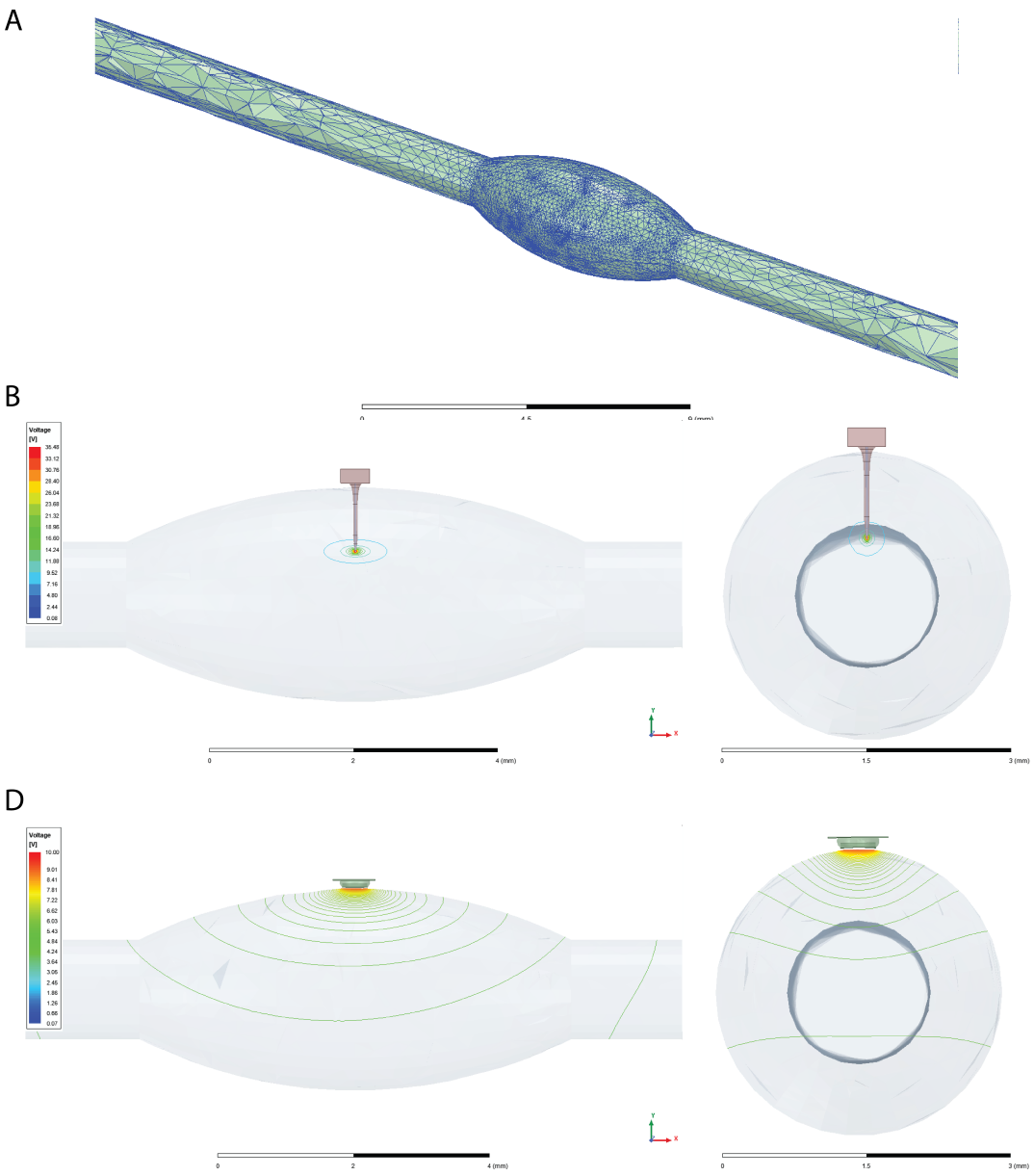

Figure 3.5: A) Result of meshing operation in Maxwell. Extracellular voltages generated by B) penetrating and C) epineural stimulation calculated from the FEM

electrode was inserted to a depth of 0.9 mm inside the DRG such that its longitudinal axis coincided with the y-axis at the middle of the DRG. For both electrodes, besides the 'active' platinum surfaces where charge injection occurred all surfaces were encased in a perfect insu-

lator to prevent any off-target current spread. The stimulation return electrode was inserted into the bone component of the model 10 cm from the stimulation electrode to approximate the distance between the L7 DRG and the iliac crest.

The DC conduction solver in ANSYS Maxwell was used to run frequency-independent simulations for each electrode. Stimulation was applied by setting a 1 mA current excitation through the exposed contact surface for each electrode. The edge faces of the bone and the stimulation return electrode were set to ground boundary conditions (0 V). The voltage field was calculated by solving the Laplace equation using the conjugate gradient method. The mesh resolution was set to 0.0001 and auto-adaptive mesh refinement converged to a final mesh with less than 1% error in the voltage distribution.

For penetrating electrode simulations, the calculated voltages were piece-wise exported to Python (v3.6) [160] by splitting the DRG structure into 2 regions. The voltage field within a 10 μm radius of the entire electrode (including insulation) was exported with a 2 μm resolution. For the remaining volume, the voltage field was exported with a 50 μm resolution. This piece-wise export was done to ensure that the voltage field was accurately captured within close proximity of the electrode. Past the 10 μm around the electrode the voltage change was uniform hence a lower resolution was used. This method also reduced export time from $\sim$6 hours (at an intermediate resolution) to $\sim$1.5 hours.

For epineural electrode simulations, the calculated voltage field was exported with a 50 μm resolution. Since the voltage distribution varied smoothly and the DRG volume was intact (unlike with penetrating electrodes), a piece-wise export was not necessary.

3.2.5 Simulating the Neuronal Response to DRG Stimulation

For each simulation, the position of the soma of the Aβ afferent was assigned. The neck and t-junction were constrained to the plane of the soma (y-z plane) and the angle of the neck with the horizontal (z-axis) was determined. The peripheral and dorsal root branches of the neuron contained 50 nodes each. The trajectories of both branches curved ventrally prior to entering the nerve roots.

The extracellular voltage for each compartment of the model was interpolated using a 2-D cubic spline (*CloughTocher2DInterpolator* using scipy in Python). These values were applied to the model using the *extracellular* mechanism in NEURON. For every simulation the time-course of the membrane potential for each compartment was calculated by solving the cable equation using a backward Euler implicit integration method with a timestep of 0.01 or 0.005 ms. These simulations were run for cathodic-leading biphasic asymmetric pulses with a pulse width of either 80 or 200 μs to mimic stimulation parameters used during acute experiments.

3.2.6 Determine Afferent Recruitment via DRG Stimulation

We validated the Aβ afferent model by simulating a single axon placed in the DRG when epineural stimulation was applied. The soma of this single afferent model was placed 100 μm from the boundary of the DRG, ventral to the stimulation electrode. Characteristics of the somatic action potential reported in experimental studies were used to validate our model [79].

To determine the threshold of activation of Aβ afferents we placed the soma of the neuron along a uniform grid in the y-z plane with a 100 μm spacing. The stem axon projected toward the center of the DRG. Thresholds were calculated to an accuracy of 0.1 μA using a binary search algorithm. This was repeated at each placement of the soma for neurons with peripheral axon diameters of 8 and 16 μm. Separate simulations were run for epineural and penetrating electrodes.

To determine the site of action potential initiation along the neuron the DRG FEM was populated with Aβ afferents to resemble the organization of soma and axons reported in studies of DRG histology discussed previously. A 2-dimensional cross section of the DRG at the middle of the ganglion (y-z plane at x=0, radius of cross section = 1.5 mm) was populated with a total of 2500 neurons. The fiber diameter of these neurons was drawn from the log-normal function described previously [133] and the afferents were organized according to parameters described in the partition model of the DRG [83] (i.e. soma were clustered towards the dorsal annulus and axons were clustered towards the center). Of the

Table 3.1: Validation metrics for multicompartment model of Aβ afferent

Parameter	**Model value**	**Experimental range**
Soma AP amplitude	111.5 mV	109.72 ± 11.21 mV [166, 128]
AP duration	0.95 ms	1.29 ± 0.59 ms [167]
Rise time	0.41 ms	0.61 ± 0.13 ms [168]
Fall time	0.54 ms	0.89 ± 0.41 ms [168]
AHP amplitude	4.6 mV	7.9 ± 4.2 mA [167]
Resting potential	-79 mV	-80 mV [164]

2500 neurons in a given cross section, 500 neurons had a soma in the same plane as the DRG cross section while the remaining 2000 neurons had cell somas distributed randomly along the length of the DRG. For epineural stimulation a threshold search was carried out for all neurons where the t-junction or cell soma was placed above the x-z plane at y=750 μm. For penetrating stimulation a threshold search was carried out for all neurons where the t-junction or cell soma was placed within a 600 μm radius of the tip of the pentrating electrode. For each electrode, multiple simulations were run where the position of the 2500 neurons were varied.

3.3 Results

3.3.1 NEURON Model Validation and Recruitment Thresholds

We created a multi-compartment model of an Aβ afferent to investigate the mechanism of recruitment via DRG stimulation. This model combined the psuedounipolar morphology [128] of the DRG afferents, the membrane dynamics of sensory specific MRG axons [147] and the differential distribution of ion channels at the soma and initial segment [82, 79] reported in previous studies. We compared the somatic action potential characteristics, with experimental values reported in the literature to validate our model (Table 3.1).

3.3.2 Recruitment Thresholds for Epineural and Penetrating Electrodes

We quantified the threshold for recruiting Aβ afferents and the location of spike initiation for neurons with peripheral branch fiber diameters of 8 and 16 μm. For epineural stimulation, (figure 3.6) the thresholds for recruitment followed the gradient of extracellular voltage as expected, i.e. thresholds increased with distance from the electrode. Within a 100 μm annulus, on the dorsal side of the DRG, roughly corresponding to the region of densely populated cell soma, the threshold for recruitment was 22.29 $\pm$ 0.94 μA across all fiber diameters. The minimum threshold for recruitment (20.9 μA) was observed for cell somas placed directly beneath the electrode inside the DRG. The distribution of thresholds was similar for cell soma placed near the electrode, for each fiber diameter. As the distance increased, neurons with fiber diameters of 16 μm displayed a lower threshold whereas 8 μm fibers were not recruited.

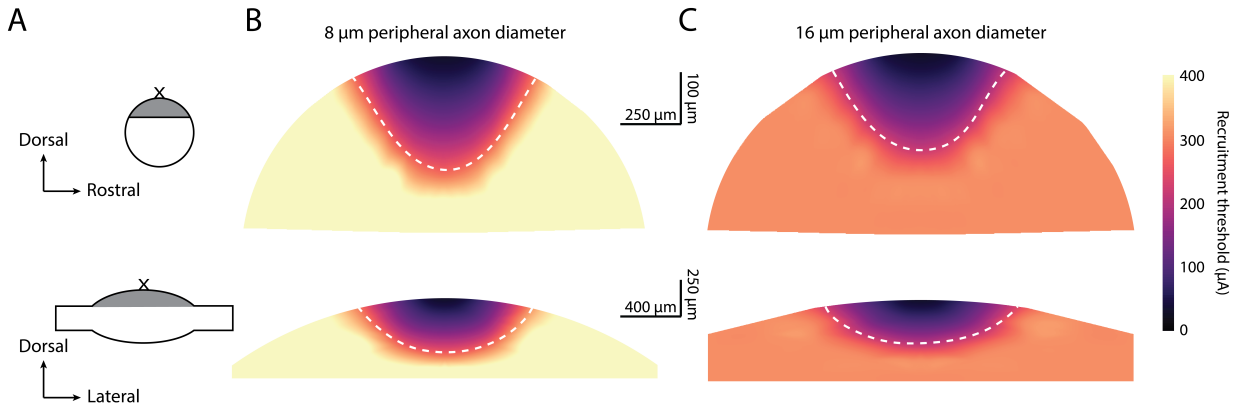

Figure 3.6: Distribution of recruitment thresholds for epineural stimulation. Neurons were placed on a uniform grid at 100 μm spacing. The approximate location of the stimulating electrode is denoted by an X

When the location of spike initiation was overlaid on the distribution of thresholds (figure 3.6 dotted lines), we observed that the region of low thresholds close to the electrode, coincided with instances where spike initiation occurred in the neck and initial segment of the neuron. However, spike initiation at the initial segment was constrained to a narrow region of tissue that extended 500-600 μm deep and 800-1000 μm along the length of the DRG.

This pattern of recruitment mirrors the anisotropy of the DRG. For neurons placed beyond this region, spike initiation occurred at the t-junction, peripheral or central axon branch. For instances where spike initiation occured at the initial segment, univariate analyses for the effect of fiber diameter on the threshold did not show a significant difference. Univariate analyses for the effect of spike initiation on the threshold showed a significant difference in the threshold ($p<0.01$) and follow-up non-parametric tests (Tukey-HSD) showed that there was a significant difference between thresholds for spike initiation at the initial segment and t-junction, and initial segment and the axon branches.

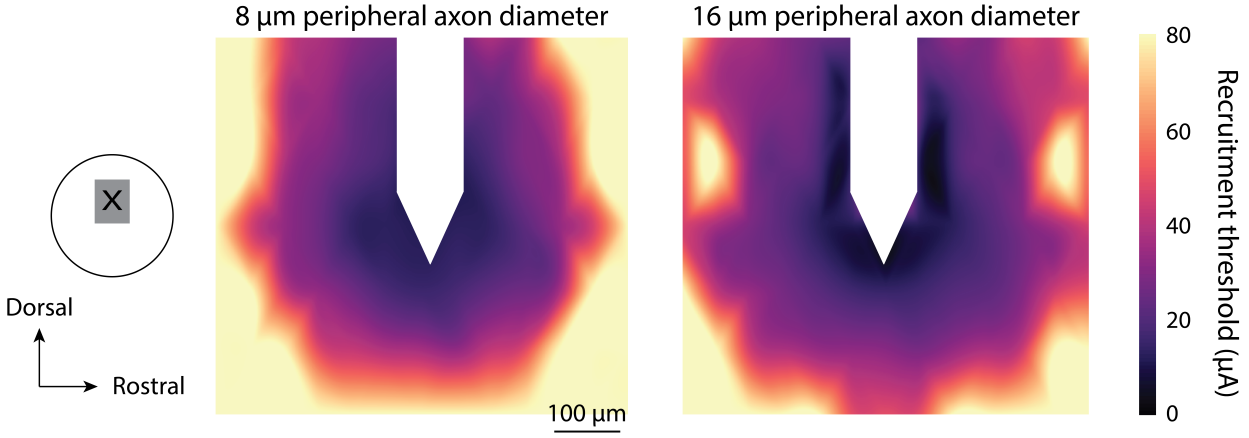

Figure 3.7: Distribution of recruitment thresholds for penetrating stimulation

For stimulation via penetrating electrodes, recruitment thresholds within a 200 μm radius of the electrode were similar for all fiber diameters. Univariate analyses for the effect of fiber diameter on the threshold did not show a significant difference. This observation is similar to the pattern of recruitment reported in prior DRG modeling work [132]. When the location of spike initiation was overlaid on the distribution of thresholds, we observed that spike initiation predominantly occurred at the axon branches. For the range of stimulation amplitudes tested during our acute experiments, spike initiation rarely occured at the initial segment. A univariate analysis showed no significant difference between thresholds for instances where spike initiation occured at the t-junction and the axon branches. These results implied that recruitment via penetrating electrodes was governed by distance of the fiber from the electrode only.

3.3.3 Mechanism of Selective Recruitment of Afferents via DRG Stimulation

We populated the DRG model with Aβ afferents to resemble a realistic distribution of neurons (in terms of fiber diameter and soma density) in order to identify the possible mechanism of recruitment observed during our acute experiments. For the range of stimulation amplitudes tested during our experiments, epineural stimulation resulted in spike initiation at the initial segment for a majority (61%) of the recruited neurons. Conversely, penetrating electrodes primarily recruited peripheral or central axon branches in nearly 65% of the instances of afferent recruitment while spike initiation occured at the t-junction 30% of the time (figure 3.8A).

The distribution of thresholds as a function of distance from the electrode, (figure 3.8B) was used to identify the order of recruitment of afferents. For epineural stimulation at stimulation amplitudes below 50 μA, spike initiation occurred primarily at the initial segment of the neuron. As stimulation amplitude was increased neurons placed farther from the electrode were recruited at the t-junction and axon branches. Recruitment of afferents selectively at the initial segment was possible up to a distance of approximately 350 μm from the electrode. Conversely, for penetrating electrodes there was no obvious order in which afferents were recruited. Spike initiation occurred at the peripheral branch, central branch or t-junction with nearly equal probability within 200 μm of the electrode.

We also constructed recruitment curves for each electrode type to quantify the number of neurons recruited for a unit increase in the stimulation amplitude (figure 3.8C) for a typical population of DRG afferents. The slope of the recruitment curve at 50% activation was 0.03 and 0.005 for penetrating and epineural stimulation respectively. The steeper slope for penetrating electrode stimulation resembles the narrower dynamic range for stimulation via penetrating electrodes observed in acute experiments. Across 10 simulations, penetrating electrodes recruited a single neuron at the minimum stimulus amplitude in six instances and recruited as many as five neurons at threshold for one simulation. At the minimum threshold, epineural stimulation recruited a single neuron in four instances and recruited a

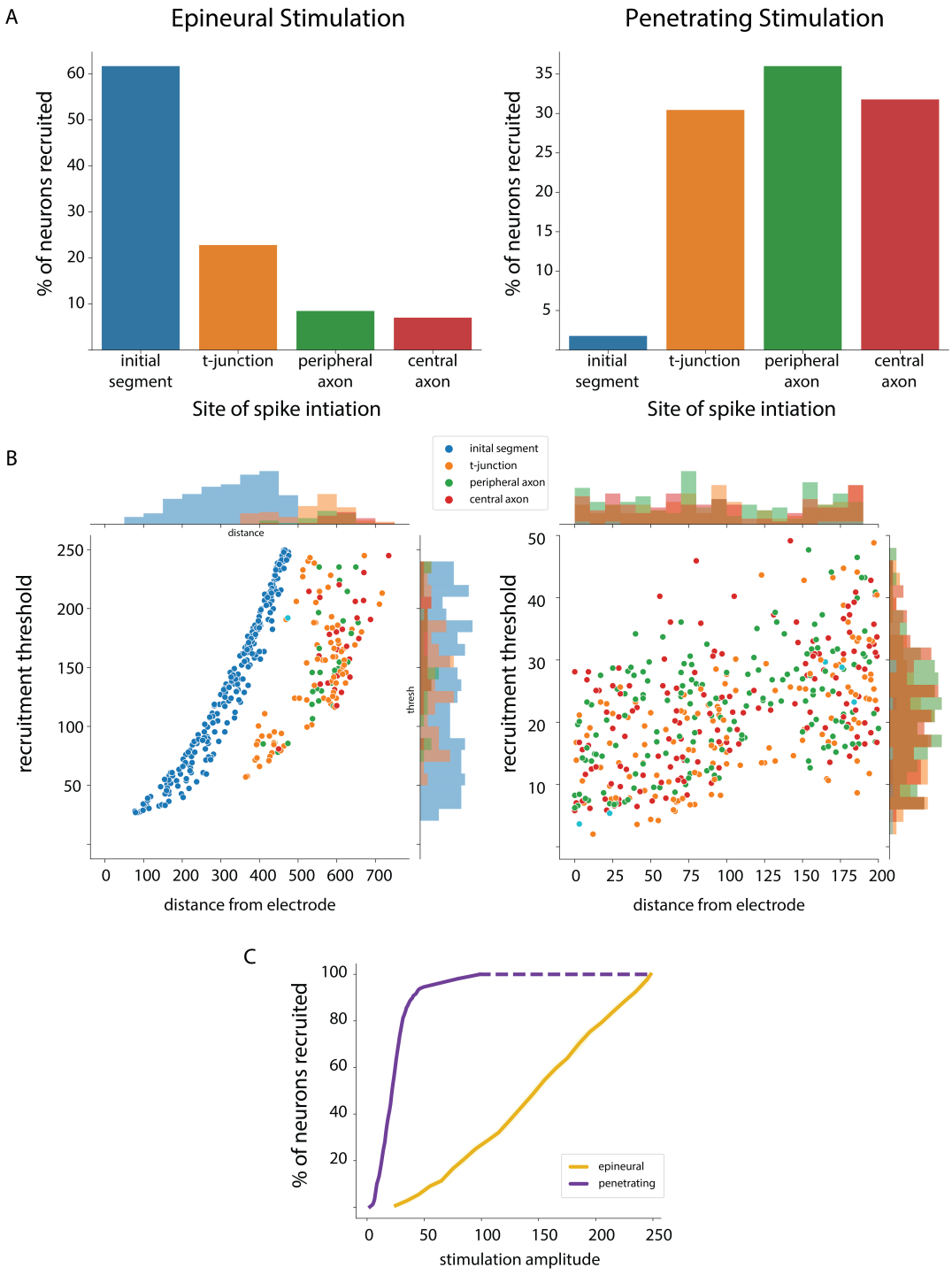

Figure 3.8: Summary of results showing A) locus of spike initiation for epineural and penetrating stimulation B) distribution of thresholds as a function of distance from stimulating electrode and locus of spike initiation C) recruitment curves for epineural (yellow) and penetrating (purple) electrodes

maximum of three neurons in two separate instances. These results suggest that epineural stimulation can recruit individual neurons near the periphery of the DRG by initiating spikes at the initial segment.

3.4 Discussion

The unique electrical and morphological properties of the sensory afferents, combined with data showing selective recruitment via epineural stimulation at the DRG suggest an alternative mechanism of recruitment than what has been reported for peripheral nerve stimulation. The goal of this study was to develop a computational model of sensory (Aβ) afferents and replicate their unique geometric arrangement within a structural model of the DRG to shed light on the mechanisms of action and locus of activation of epineural and penetrating stimulation.

3.4.1 Electrical Properties of the Initial Segment

We constructed a model of an Aβ afferent that produced somatic action potential characteristics that agreed with reported experimental data. A key modification in our model was the inclusion of an initial segment where the Na_f and Na_p conductances varied along the length of the compartment.

Recruitment via penetrating electrode stimulation was primarily driven by proximity of the neuron to the electrode and was unaffected by the presence of an excitable initial segment and soma. Epineural stimulation generated action potentials at the initial segment more frequently than any other location along the neuron. However, the initial segment does not have an inherently lower threshold than the t-junction or the nodes of Ranvier. In terms of excitability, the initial segment has nearly half the sodium channel density of the nodes of Ranvier making it far less excitable. In fact, for distances greater than 400 μm from the electrode, the threshold for generating an action potential at the initial segment was almost

equal to the threshold for generating an action potential at a t-junction (figure 3.8B). This indicates that initial segment excitability alone is not responsible for selective recruitment via epineural DRG stimulation.

3.4.2 Mechanism of recruitment via DRG Stimulation

Sensory afferents have a characteristic arrangement within the DRG such that the soma are densely packed near the circumference and the axons of these neurons are clustered towards the center. This organization is consistent throughout the length of the DRG and has been observed for lumbar and sacral DRG. The number of densely packed cell bodies exceeds the number of axons interspersed at the periphery, by 2-3 orders of magnitude. These observations imply that at the periphery of the DRG, there are fewer t-junctions than cell soma and initial segments. Additionally, due to the size of the soma, the number of excitable entities (initial segments) packed into a unit volume at the periphery is much lower than the number of excitable axons packed into a unit volume at the center. Our results show that at low amplitudes of epineural stimulation neurons are activated at their initial segment and the probability of recruiting a t-junction or axon increases with amplitude and distance of the soma from the stimulation electrode. We also replicated the greater dynamic range of recruitment observed with epineural electrodes by modeling a realistic packing of cell soma at the periphery. Ongoing work is focused on identifying the effect of soma size and packing density on the dynamic range of recruitment. Our results indicate that the greater distribution of excitable initial segments at the periphery may enable selective recruitment via epineural stimulation.

3.4.3 Limitations and Future Directions

While we were able to achieve our objective of building a model of the DRG and positing a possible mechanism for selective recruitment of afferents via DRG stimulation, there are a number of improvements to our model that may inform future studies. We made several simplifications with regards to the morphology of the neuron model where the soma, initial segment and neck were in the same plane, the stem axon projected towards the center of the

DRG and the trajectories of the axon and central branches were idealized. In reality, the axon hillock, initial segment and neck wrap around the cell soma forming a tight glomerulus. It is unclear how this glomerulus affects the electrical excitability of the neuron, but it would certainly affect how densely we can pack the soma in our model.

The properties of the epineurium used in our model were drawn from previous literature pertaining to electrical properties of the dura. In fact, at the spinal roots, the dense irregularly arranged collagen fibers and fibroblasts of the dura blend with the epineurium of peripheral nerves [169]. These matrix differences between the dura and epineurium likely alter the volume of tissue activated during epineural stimulation. As such future work should focus on studying the electrical and structural properties of the epineurium and the impact on recruitment.

An initial objective of this study was to develop a platform to allow testing of stimulation paradigms and optimize the design of novel epineural electrodes to maximize coverage and selectivity. Alas, that proved a bridge too far for the scope of this thesis however, the model described in this chapter is a starting point for ongoing efforts in the lab to determine the ideal number, location, and size of stimulation electrode contacts, and designing stimulation parameters that maximize the dynamic range and selectivity of stimulation. Additionally, the model developed herein included Aβ primary sensory neurons only. In reality, the DRG contain a heterogenous population of sensory afferents that include high and low threshold mechanoreceptors (Aα fibers), small diameter sensory fibers (Aδ fibers) and nociceptive fibers (C-fibers) [154]. Incorporating these neurons into our model may further highlight the differences in the mechanism of recruitment across fiber types and help develop stimulation paradigms that are relevant for providing somatosensory feedback in a potential somatosensory neuroprosthesis.

4.0 Sensory restoration by epidural stimulation of the lateral spinal cord in upper-limb amputees

The contents of this chapter are published as: *Chandrasekaran S*, Nanivadekar AC*, McKernan GP, Helm ER, Boninger ML, Collinger JL, Gaunt RG, Fisher LE (2020). Sensory restoration by epidural stimulation of the lateral spinal cord in upper-limb amputees. eLife. 2020 July 21; 9:e54349.* * These authors contributed equally to this work.

4.1 Introduction

Individuals with amputations consistently state that the lack of somatosensory feedback from their prosthetic device is a significant problem that limits its utility [11] and is often a primary cause of prosthesis abandonment [12, 170]. In the case of upper-limb amputations, the absence of somatosensory feedback particularly affects the ability to generate the finely controlled movements that are required for object manipulation [11, 171, 172, 170]. Although sophisticated myoelectric prostheses with multiple degrees of freedom [173] are becoming increasingly available, their potential is limited because they provide little or no somatosensory feedback [10, 12, 174, 175]. In fact, body-powered devices are often preferred because of the feedback they provide through their harness and cable system [176, 177, 178, 179]. Partially addressing this limitation, advanced robotic prosthetic arms have been designed with embedded sensors that could be harnessed to provide somatosensory signals to a neural interface [180, 181, 182]. Thus, developing a robust and intuitive means to deliver somatosensory information to the nervous system is an important endeavor to ensure the adoption and use of the latest advancements in prosthetics.

Several research groups have explored the potential of peripheral nerve stimulation to provide sensory feedback to people with amputation and examined the effects of feedback on prosthetic control. Sensory restoration has been achieved using a variety of neural interfaces including epineural cuff electrodes like the spiral cuff [46, 45] and flat interface nerve electrode

[30] or microelectrodes that penetrate the epineurium, such as the longitudinal intrafascicular electrode [33], transverse intrafascicular multichannel electrode [34], or Utah slant array [36]. Targeted sensory reinnervation is another approach that can allow vibrotactile or electrotactile feedback on the residual limb to be perceived as emanating from the missing limb [16, 51]. This is achieved by first surgically redirecting nerves that formerly innervated the missing limb to patches of skin on the residual limb or elsewhere, and then providing electrical or mechanical stimulation to the newly innervated site [53, 52]. These approaches can evoke focal sensations that are perceived to emanate from the upper-limb, even decades after injury, and can improve the control of prosthetic limbs. However, all of these approaches involve specialized electrodes and/or surgeries that are not part of common surgical practice. Further, these approaches often target nerves in the distal limb, which could limit their use in people with proximal amputations such as shoulder disarticulations.

Spinal cord stimulation (SCS) systems are an FDA-approved, commercially available technology that could potentially be used to restore somatosensation. SCS leads are currently implanted in approximately 50,000 patients every year in the USA to treat chronic back and limb pain [54]. The standard clinical approach begins with a week-long trial phase with temporarily implanted leads, and if patients experience pain relief, permanent implantation occurs during an hour-long follow-up procedure. For the trial phase, SCS leads are inserted percutaneously into the epidural space on the dorsal side of the spinal cord via a minimally invasive, outpatient procedure [55]. Clinically effective stimulation parameters typically evoke paresthesias (i.e. sensation of electrical buzzing) that are perceived to be co-located with the region of pain. SCS leads are usually placed over the dorsal columns along the midline of the spinal cord which limits the evoked paresthesias to the proximal areas of the trunk and limbs. However, recent studies have demonstrated that stimulation of lateral structures in the spinal cord and spinal roots can evoke paresthesias that selectively emanate from the distal regions of the body [58, 59, 57, 56], likely by stimulating the same sensory afferent neurons that are targeted by peripheral nerve stimulation for prosthetic applications [183]. As such, these devices provide an attractive option for widespread deployment of a neuroprosthesis than can evoke somatosensory percepts from distal aspects of the amputated limb, including the hand and fingers.

In this study, we implanted percutaneous SCS leads into the lateral epidural space of four people with upper-limb amputations and characterized the sensations evoked when the cervical spinal cord and spinal roots were stimulated. The goals of the study were to demonstrate the feasibility of lateral SCS to restore somatosensation and to guide technical development for future studies that will include full implantation of SCS leads and stimulators. In all subjects, lateral SCS evoked sensations that were perceived to emanate from the missing limb, including focal regions in the hand, regardless of the level of amputation (trans-radial to shoulder disarticulation). These sensations were stable throughout the 29-day testing period and showed only minor changes in area and location. Additionally, in some cases, it was possible to evoke naturalistic, rather than paresthetic sensations, though the incidence of naturalistic sensations varied by subject. Considering these results along with the extensive clinical use of SCS, this approach to somatosensory restoration could be one that is beneficial to a diverse population of amputees, including those with proximal amputations. Further, these percutaneously implanted SCS devices are a useful tool for the development of somatosensory neuroprosthetic systems, especially for research projects that focus on advanced prosthetic control but have not developed their own technologies and techniques for restoring sensory feedback.

4.2 Methods

4.2.1 Study Design

The aim of this study was to investigate whether electrical stimulation of lateral structures in the cervical spinal cord could evoke sensations that are consistently perceived to emanate from the missing hand and arm. We also aimed to characterize those sensations and establish the relationship between stimulation parameters and the perceptual quality of evoked sensory percepts. Four subjects with upper-limb amputations (three females, one male; Table 4.1) were recruited for this study. Three amputations were between the elbow and shoulder and one was below the elbow. The time since amputation ranged from 2 to 16

years. All procedures and experiments were approved by the University of Pittsburgh and Army Research Labs Institutional Review Boards and subjects provided informed consent before participation.

Table 4.1: Demographic, amputation, and study-related information for each subject.

Subject	**Age**	**Gender**	**Amputation characteristics**				**Implant**
			Years since	**Side**	**Level**	**Cause**	**duration**
1	67	Female	>5	Right	Shoulder disarticulation	Necrotizing fasciitis	29 days
2	33	Male	>16	Left	Transhumeral	Trauma	15 days
3	38	Female	>2	Right	Transhumeral	Trauma	29 days
4	44	Female	>3	Right	Transradial	Compartment syndrome	29 days

4.2.2 Electrode Implantation

SCS leads were implanted through a minimally invasive, outpatient procedure performed under local anesthesia. With the subject in a prone position, three 8- or 16-contact SCS leads (Infinion, Boston Scientific) were percutaneously inserted into the epidural space on the dorsal side of the C5–C8 spinal cord through a 14-gauge Tuohy needle. Contacts were 3 mm long, with 1 mm inter-contact spacing. Leads were steered via a stylet under fluoroscopic guidance, and electrode placement was iteratively adjusted based on the subjects' report of the location of sensations evoked by intraoperative stimulation. The entire procedure usually took approximately 3–4 hours. The leads were maintained for up to 29 days and subsequently explanted by gently pulling on the external portion of the lead. Subjects attended testing sessions 3–4 days per week during the implantation period. The testing sessions lasted up to a maximum of 8 hours. Lead location and migration were monitored via weekly coronal and sagittal X-rays throughout the duration of implant.

4.2.3 Neural Stimulation

During testing sessions, stimulation was delivered using three 32-channel stimulators (Nano 2+Stim; Ripple, Inc.). The maximum current output for these stimulators was 1.5 mA per channel. In order to achieve the higher current amplitudes required for SCS, a custom-built circuit board was used to short together the output of groups of four channels, thereby increasing the maximum possible output to 6 mA per channel resulting in a total of 8 effective channels per stimulator. Custom adapters were used to connect each stimulator to 8 contacts on each of the implanted leads. Custom software in MATLAB was used to trigger and control stimulation.

Stimulation pulse trains were charge-balanced, cathodic-first square pulses, with either asymmetric or symmetric cathodic and anodic phases. For asymmetric pulses, the anodic phase was twice the duration and half the amplitude of the cathodic phase. Stimulation was performed either in a monopolar configuration, with the ground electrode placed at a distant location such as on the skin at the shoulder or hip, or in a multipolar configuration with one or more local SCS contacts acting as the return path. Stimulation frequencies and pulse widths ranged from 1–300 Hz and 50–1000 μs, respectively. The interphase interval was 60 μs. All stimulus amplitudes reported in this manuscript refer to the first phase amplitude.

4.2.4 Recording Perceptual Responses

The first few sessions of testing were primarily devoted to recording the location and perceptual quality of sensory percepts evoked with various stimulation configurations. An auditory cue was provided to denote the onset of stimulation. At the offset of each stimulation train, the subject used a touchscreen interface developed in Python (Figure 4.1) to document the location and perceptual quality of the evoked sensation. This interface can be downloaded from Github. The location of the sensory percept was recorded by the subject using a free-hand drawing indicating the outline of the evoked percept on an image of the appropriate body segment (i.e., hand, arm or torso). The percept quality was recorded using several descriptors: mechanical (touch, pressure, or sharp), tingle (electrical, tickle, itch, or pins and needles), movement (vibration, movement across skin, or movement

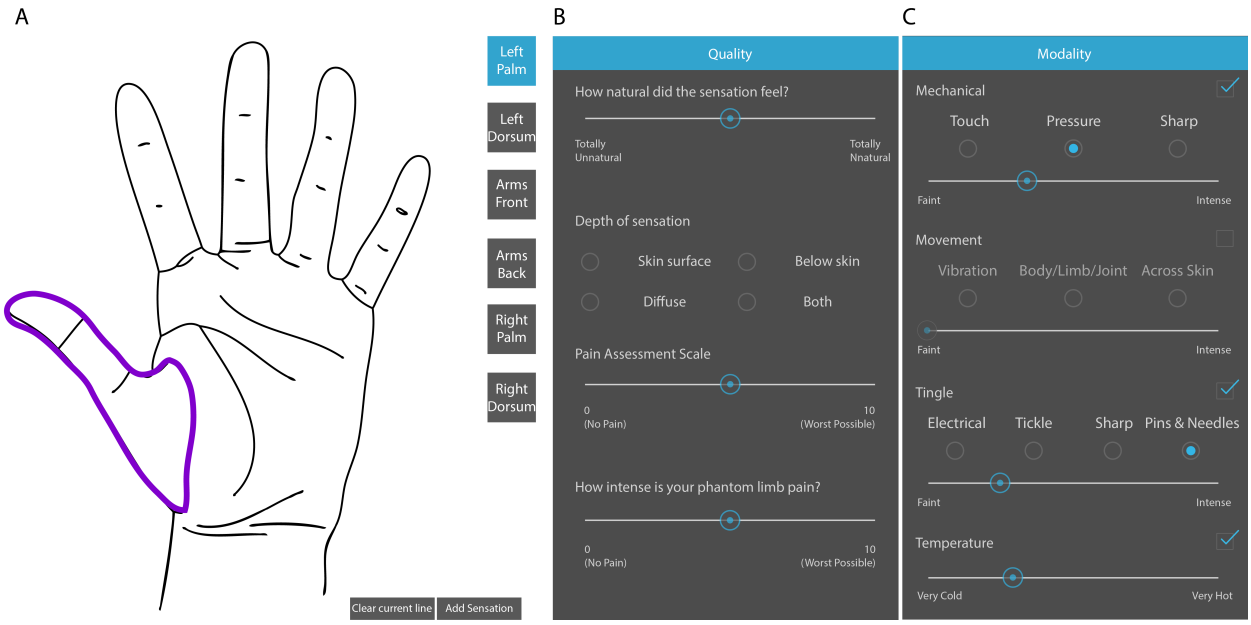

Figure 4.1: Touchscreen interface for describing evoked sensory percepts. (A) Panel for free hand drawing to show the location and extent of the sensory percept. (B) and (C) Questionnaire to describe the modality and intensity of the sensory percept and associated phantom limb pain, if any.

of body/limb/joint), temperature, pain due to stimulation, and phantom limb pain. Each descriptor had an associated scale ranging from 0–10 to record the corresponding perceived intensity. Additionally, the subject was instructed to rate the naturalness (0–10) and the depth of the perceived location of the percept (on or below the skin, or both). This set of descriptors have been used previously to characterize evoked sensory percepts [184, 185]. The order of stimulation electrodes and amplitudes was randomized to prevent subjects from predicting the location and perceptual qualities of sensations from previous trials. All percepts that were localized ipsilateral to the amputation were included for analysis in this work. In Figure 4.2, only those percepts which show less than 70% area overlap (as in [32]) with any other percept are shown for clarity.

4.2.5 Analyzing Sensory Percepts

For each trial, subjects were allowed to report more than one descriptor simultaneously. Each unique combination of 'mechanical', 'movement', and 'tingle' descriptors was considered a separate modality for the evoked percept. All percepts that contained a descriptor for tingle ('electric current', 'tickle', 'sharp', 'pins and needles') were considered paresthetic and were grouped together. A sunburst plot was constructed for each subject to analyze the fraction of paresthetic and non-paresthetic percepts that contained mechanical or movement components. Therefore, all unique modalities were divided in to three groups: paresthetic percepts that had 'tingle' but no 'mechanical' or 'movement' component (Figure 4.4, teal sectors), mixed percepts that had a 'mechanical' and/or 'movement' component and 'tingle' (Figure 4.4, grey sectors), and non-paresthetic percepts that only had 'mechanical' and/or 'movement' components (Figure 4.4 red sectors). For each sunburst plot, the inner, middle, and outer annuli represent 'tingle', 'mechanical', and 'movement' modality descriptors, respectively. Each sector represents a unique descriptor and the size of each sector represents the fraction of all percepts that contained the corresponding descriptor. This allows us to identify the distribution of unique modalities, such that, for a given sector in the tingle annulus (for example, $n = 761$ for Subject 2, 'tingle'), we can identify the fraction of percepts that had a specific mechanical descriptor (e.g. 'sharp' $n = 245$) and the fraction of these percepts that had a specific movement descriptor (e.g. 'vibration' = 104).

The spinal cord segment targeted by stimulation through each electrode was inferred from the X-ray images. We used the pedicles of each vertebra to mark the boundaries that separated each spinal root (Figure 4.3B). These boundaries provided an anatomical marker to establish where each electrode was located, in the rostrocaudal axis. Similarly, boundaries were drawn on the body segment outline images to divide them into 7 anatomical segments (Figure 4.3A) including thumb, D2–D3, D4–D5, wrist, forearm, elbow, and upper arm. The sensory percepts were categorized as being associated with one of the seven anatomical segments based on which segment contained the maximal area of the perceived sensation. For this analysis, only those electrodes that evoked a sensory percept ipsilateral ($n = 315$) to the amputation were included. Electrodes that only evoked bilateral ($n = 64$) and contralateral

($n = 68$) sensations at threshold would not be useful for neuroprosthetic applications for people with unilateral amputation and were excluded. Dermatome maps were generated per subject, by determining the proportion of electrodes situated at each spinal level that evoked a sensation in a specific anatomical region.

4.2.6 Quantifying Lead and Percept Migration

The intraoperative fluoroscopy image, superimposed over the X-rays from the first and last week of testing, gave an indication of gross movements of the leads. Using bony landmarks, the X-ray from the first week was aligned to the intraoperative fluoroscopy image, and each subsequent X-ray was aligned to the X-ray from the previous week using an affine transformation method in MATLAB. The SCS contact that appeared to be most parallel to the plane of imaging was used to determine the scale length for the image (SCS contacts are 3 mm in length). For each lead, the distance between the rostral tips of the electrodes as seen in the aligned image pairs (Figure 4.7) was measured to determine the rostro-caudal migration. Positive values signified caudal migration and negative values signified rostral migration.

For all electrodes that evoked a percept in the missing hand, the threshold charge was calculated for each week. A one-way ANOVA was performed for each subject to test for differences in thresholds across weeks. For subjects where a significant difference was reported, a post-hoc multiple pairwise comparison analysis using the Tukey HSD was performed to identify the pairs of consecutive weeks with a significant difference in thresholds. To quantify migration of perceived sensations, we measured the change in the position of the centroid and the change in area of each percept that was localized to the hand. For sensations that included a percept outside the hand, we only used the hand percept in these calculations, as this is the most relevant location for a somatosensory neuroprosthesis. We chose the minimum stimulus amplitude that was tested at least once per week for the highest number of weeks during the implant. We quantified the migration of the mean percept centroid for each week, with respect to the mean percept centroid for the previous week. This analysis was repeated for all electrodes. Similarly, to quantify the change in percept area, the mean

area of the percept for each week was compared to the mean area for the previous week. The distances were converted to millimeters using the average hand length of 189 mm (as measured from the tip of the middle finger to the wrist) and average palmar area of 75 cm2 of a human male [186, 187, 188, 189, 190, 191]. All electrodes that were tested in at least two of the weeks were included in the analysis.

We also constructed separate auto-regressive time series models to examine the changes in distributions for both area and centroid migration over time, adjusting for autocorrelations in the data. The AUTOREG procedure in SAS estimates and forecasts linear regression models for time series data when the errors are autocorrelated or heteroscedastic. If the error term is autocorrelated (which occurs with time series data), the efficiency of ordinary least-squares (OLS) parameter estimates is adversely affected and standard error estimates are biased, thus the autoregressive error model corrects for serial correlation. For models with time-dependent regressors, the, AUTOREG procedure performs the Durbin t-test and the Durbin h-test for first-order autocorrelation and reports marginal significance levels.

4.2.7 Detection Thresholds

A two-alternative forced choice task was used to determine detection thresholds. The subject was instructed to focus on a fixation cross on a screen. Two one-second-long windows, separated by a variable delay period, were presented and indicated by a change in the color of the fixation cross. Stimulation was randomly assigned to one of the two windows. After the second of the two windows, the fixation cross disappeared, and the participant was asked to report which window contained the stimulus. The stimulus amplitude for each trial was varied using a threshold tracking method [192, 193] with a 'one-up, three-down' design. In this design, an incorrect answer resulted in an increase in stimulus amplitude for the next trial while three consecutive correct trials were required before the stimulus amplitude was decreased. Stimulus amplitude was always changed by a factor of 2 dB. Five changes in direction of the stimulus amplitude, either increasing to decreasing or vice versa, signaled the end of the task. Using this task design, the detection threshold was determined online as the average of the last 10 trials before the fifth change in direction. A detection

threshold calculated this way corresponds approximately to correctly identifying the window containing the stimulus 75% of the time [194]. To get a finer estimate of the detection threshold we also used a non-adaptive design in a subset of trials for Subject 4, where we presented a predetermined set of stimulus amplitudes. This block of stimulus amplitudes was repeated up to 8 times and the presentation sequence was randomized within each block. A cumulative-normal psychometric curve was fit to both types of detection experiments post-hoc using the Palamedes toolbox [195] with the guessing rate γ and lapse rate λ held fixed at 0.5 and 0 respectively. The detection threshold was calculated as the stimulus amplitude at the 75% accuracy level. Tasks in which accuracy levels for all stimulus amplitudes were < 0.6 or > 0.9 were omitted from this analysis. We carried out a goodness-of-fit analysis with 1000 simulations using the Palamedes toolbox and discarded any fit with probability of transformed likelihood ratio ($pTLR$) less than 0.05. $pTLR$ signifies the proportion of simulated likelihood ratios that were smaller than the likelihood ratio obtained from the data and it spans 0–1 with a higher value signifying a better fit and values below 0.05 signifying an unacceptable fit. Thresholds calculated for the same electrodes on different days were averaged together to obtain a mean detection threshold for each electrode, with all other stimulus parameters (e.g. frequency, pulse width) held constant.

4.2.8 Just-Noticeable Differences

A similar two-alternative forced choice task was used to determine just-noticeable differences (JND) for stimulation amplitude. The design of the task was identical to the detection task except stimulation was provided in both the windows and the subject was instructed to choose the window where the stimulus was perceived as being at a higher intensity. One of the stimulation amplitudes in every trial was held constant while the other was chosen randomly from a list of stimulus amplitudes constituting a block. The constant amplitude was either fixed at 2.5 mA for the lower standard amplitude or at 4.0 mA for the higher standard amplitude. The windows in which standard and the test amplitude were administered was randomized as well. This block of stimulus amplitudes was repeated up to 8 times and the presentation sequence was randomized within each block. A cumulative-normal

psychometric curve was fit to the data post-hoc using the Palamedes toolbox [195] with the guessing rate γ and lapse rate λ held fixed at 0.5 and 0 respectively. The JND was calculated as the stimulus amplitude at the 75% accuracy level. Tasks in which accuracy levels for all stimulus amplitudes were < 0.6 or > 0.9 were omitted from this analysis. We carried out a goodness-of-fit analysis with 1000 simulations using the Palamedes toolbox and discarded any fit with $pTLR< 0.05$. To determine average JNDs at the two different standard amplitudes, we included data from only those electrodes for which testing at both standard amplitudes were carried out in the same session. JNDs calculated for the same standard amplitude on different electrodes were averaged together to obtain a mean JND for each standard amplitude. As JNDs were expected to be highly subject-specific, data from different subjects were not pooled together.

4.2.9 Perceived Intensities of the Evoked Sensory Percepts

A free magnitude estimation task was used to determine the relationship between stimulus amplitude and perceived intensity of the evoked sensations [196, 197, 198, 199]. In this task, subjects were instructed to rate the perceived intensity on an open-ended numerical scale as stimulation amplitude was varied randomly. A block of stimulus amplitudes consisted of 6–10 values linearly spaced between the detection threshold of the electrode being tested and the highest value that did not evoke a painful percept up to 6 mA. This block of chosen amplitudes was presented six times and the presentation sequence was randomized within each block. The subject was instructed to scale the response appropriately such that a doubling in perceived intensity was reported as a doubling in the numerical response. Zero was used to denote that no sensation was perceived in response to the stimulus. During the first block, the subject experienced the full range of stimulation amplitudes while establishing their subjective scale, so data from this block were not included in the analysis. Data across electrodes or across different testing sessions were compared after normalizing each electrode to its mean response.

We performed a post-hoc analysis to determine the maximum number of intensities a subject would likely be able to discriminate. For each electrode, stimulation amplitude was normalized to the maximum amplitude tested and the range of stimulation amplitude was partitioned into three or five linearly spaced discrete values. Similarly, the perceived intensities reported by the subjects were normalized to the maximum reported intensity and partitioned into three or five discrete linearly spaced ranges. Across all subjects, the distribution of the binned reported intensity for each discretized stimulation level was used to estimate how reliably subjects would be able to to distinguish feedback at three or five different amplitudes (Figures 4F, B.3).

To determine whether stimulation amplitude had differential effects on the area and intensity of evoked percepts, we computed the least-squares regression line for the relationship between stimulation amplitude and percept intensity and from magnitude estimation trials and stimulation amplitude and percept area from percept mapping trials. The two-side p-values (p_{int} and p_{area}, respectively) for each line were obtained for the null hypothesis that the slope of the regression line was zero and the slopes of the two lines were compared for each electrode. Instances where the slopes of each line were significantly different indicate electrodes where stimulation amplitude can modulate percept intensity independent of the area of the percept.

4.3 Results

4.3.1 SCS Evokes Sensory Percepts Localized to the Missing Limb

Three SCS leads were implanted in the cervical epidural space in each of four individuals with upper-limb amputation (Table 4.1). The percutaneous implant was maintained for the full 29-day duration of the study for all subjects except Subject 2, who requested removal of the leads after two weeks due to personal factors and discomfort from caudal migration of one

of the leads. We stimulated with both monopolar and multipolar electrode configurations. Stimulus amplitudes, frequencies, and pulse widths ranged 0–6 mA, 1–300 Hz, and 50–1000 μs, respectively.

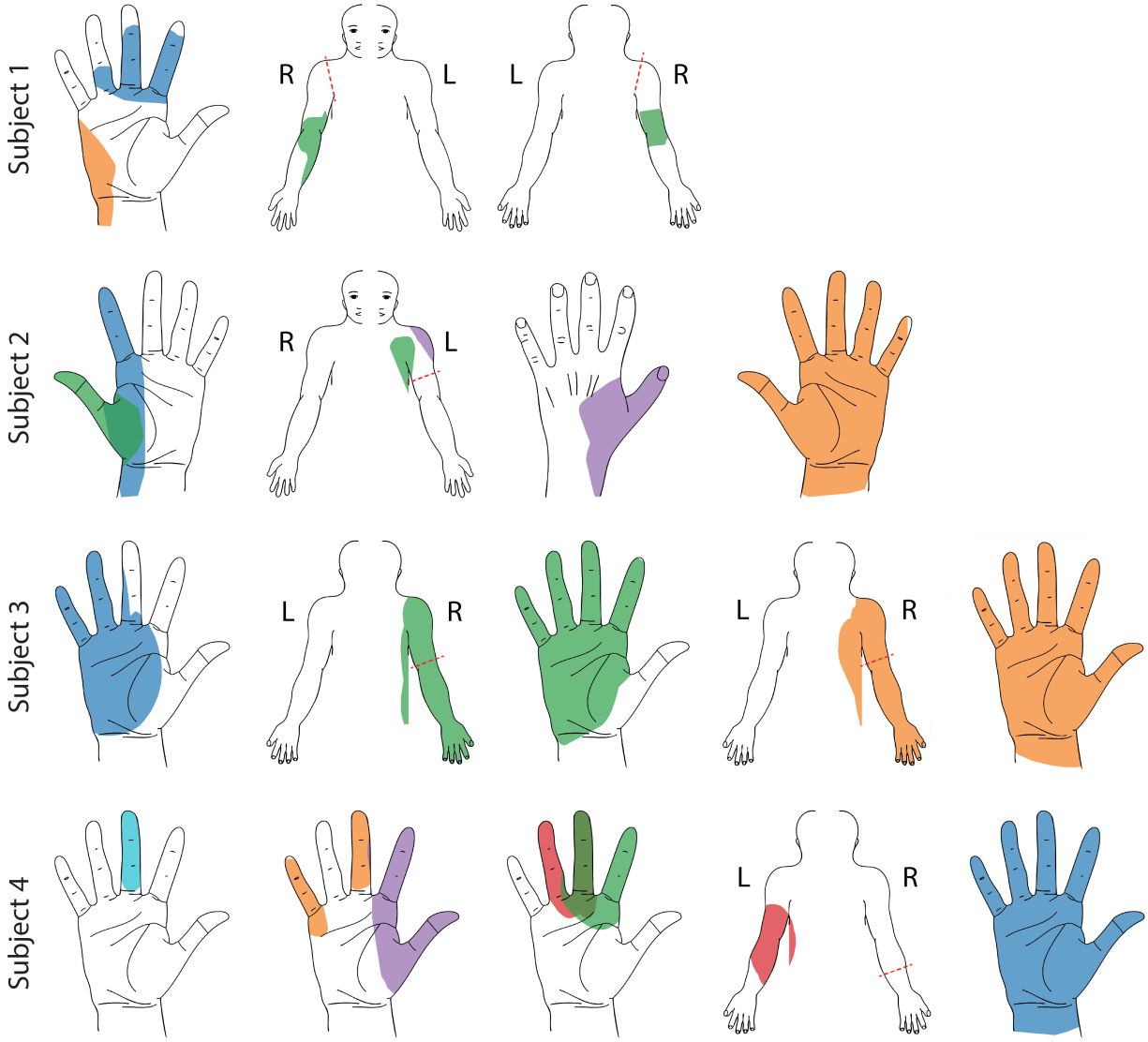

Figure 4.2: Representative sensory percept locations. Colored areas represent selected projected fields that were reported for more than two testing sessions and remained stable for at least two weeks. Each color represents a unique stimulation electrode per subject. If a pair of percepts had more than 70% overlap, only the more focal percept is shown here [32].

In all four subjects, epidural SCS evoked sensory percepts in distinct regions of the missing limb including the fingers, palm, and forearm. While some sensory percepts were diffuse and covered the entire missing limb, other percepts were localized to a very specific area, such as the ulnar region of the palm or wrist, or individual fingers. Figure 4.2 shows select representative percepts for all subjects. In Subjects 1 and 2, only multipolar stimulation evoked sensory percepts that were localized to focal regions of the missing hand and fingers (B.1). In Subjects 2 and 3, most percepts were accompanied by a sensation on the residual limb. This was the case even when there was a percept that was focally restricted to a distal region of the missing limb, such as a finger (e.g. purple thumb/shoulder sensation in Subject 2, Figure 4.2). These additional proximal sensations emanated predominantly from the end of the residual limb. The incidence rate of such simultaneous sensations varied from 0% and 8% for Subjects 1 and 4 to 92% and 98% for Subjects 2 and 3. There were also a subset of mono- and multi-polar electrodes that evoked sensations bilaterally or only in the contralateral intact limb (14.3% and 15.4% of all electrodes that generated a sensation across all subjects n=447). While these sensations might be useful in a neuroprosthesis for people with bilateral amputation, they were not a focus of this study and were not included in any of the analyses presented here.

We sought to determine if stimulation of specific regions of the spinal cord consistently evoked sensations that were perceived to emanate from specific regions of the arm and hard across subjects. We hypothesized that the location of the perceived sensation would be driven by the location of the cathodic electrode with respect to the spinal cord according to expected dermatomes. Figure 4.3 shows the proportion of sensory percepts in a specific anatomical region (dashed lines, Figure 4.3A) evoked by electrodes situated at each spinal level (Figure 4.3B, C). There were notable similarities between the perceived locations and dermatomes [200, 201], however there was considerable inter-subject variability and sensations were not evoked in all regions of the hand in all subjects (Figure 4.3C). For example, sensations reported in the thumb were predominantly evoked by electrodes located near the C6 root in Subjects 2 and 4 (0%, 67%, 26%, and 50% for Subjects 1-4 respectively). Similarly, a high proportion of the percepts localized to the 2nd and 3rd digits were evoked by electrodes near the C7 root in Subjects 2 and 3 (0%, 50%, 66%, and 23%, for Subjects

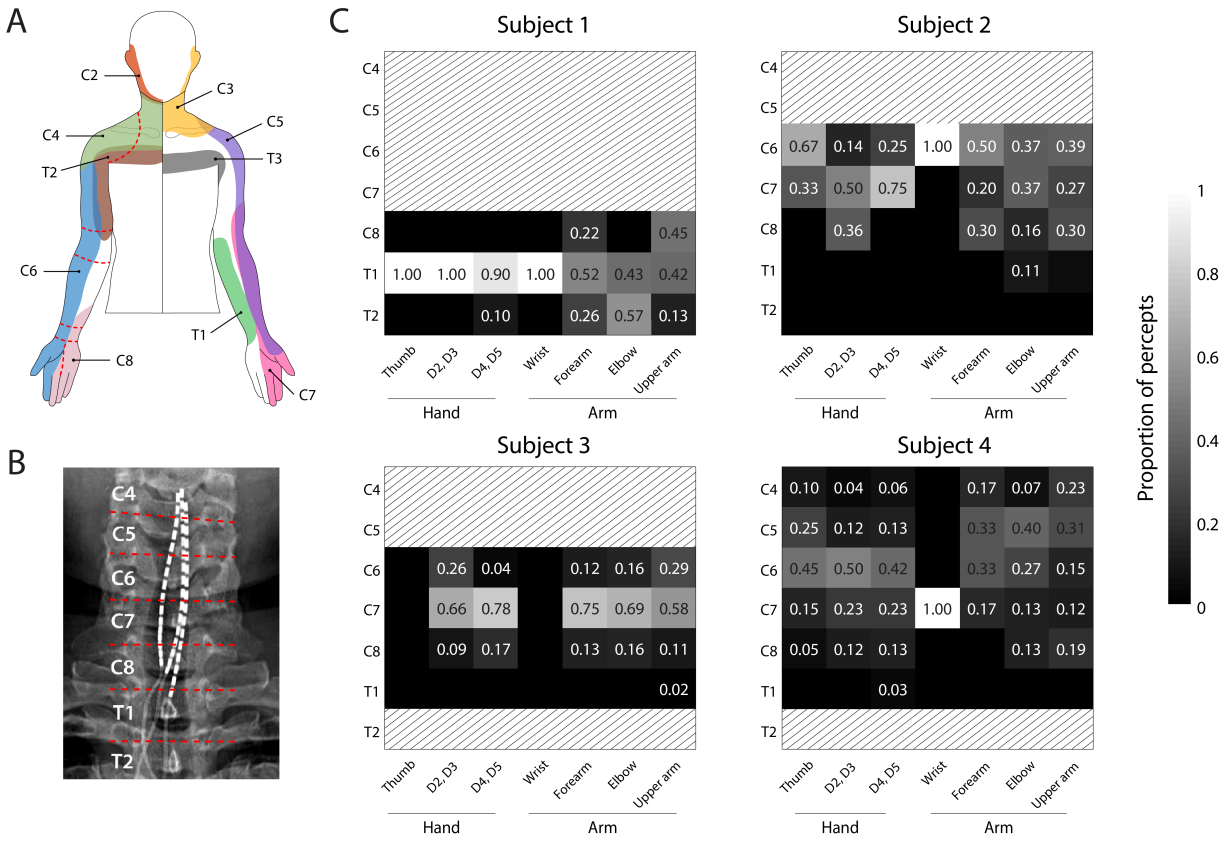

Figure 4.3: Schematic of dermatomes, adapted from Lee et al., 2008. Overlapping dermatome areas are shown in lighter shades. Dotted lines indicate our division of different regions of the fingers, hand, and arm. B) An example of the segmentation of the spinal cord (from Subject 4) used to determine the location of each stimulation electrode. C) Heat maps show the relative proportion of electrodes located at different spinal levels to the total number of percepts emanating from a specific region of the arm. The spinal level of each electrode was defined by the position of the cathode with respect to the spinal levels as seen in the X-rays. Spinal levels that have no electrodes nearby are marked with gray hatching.

1-4, respectively). However, sensations in 4th and 5th digits (within the C8 dermatome) were evoked predominantly by electrodes near the C7 root in Subjects 2 and 3 (0%, 75%, 78%, and 23% in Subjects 1-4, respectively). Interestingly, for Subject 4, electrodes near the C6 root produced most of the percepts in the hand (2nd and 3rd digits: 52%, 4th

and 5th digits: 45%). Moreover, almost all the electrodes in Subject 1, including those that evoked focal percepts in the fingers and palm, were located near the T1 root. Overall, these results demonstrate that, while there was some consistency between the locations of stimulation and dermatomes, there was considerable inter-subject variability in many of the evoked sensations.

Table 4.2: Descriptors provided for characterizing the evoked percepts. The various descriptors that subjects were asked to choose from while describing the modality and intensity of the evoked sensory percept. Visual analog scales (VAS) were presented as a slider bar and no specific numbers were shown.

Naturalness	**Depth**	**Mechanical**	**Tingle**	**Movement**	**Temperature**
	Skin surface	Touch	Electrical	Vibration	
	Below Skin	Pressure	Tickle	Body/limb/joint	
	Diffuse	Sharp	Itch	Across skin	
	Both		Pins & Needles		
VAS (Totally Unnatural to Totally Natural)	VAS (intensity)	VAS (intensity)	VAS (intensity)		VAS (Very Cold to Very Hot

We asked the subjects to describe the evoked sensations using a set of words provided in a predefined list (Table 4.2). This allowed us to standardize the descriptions of the percepts across subjects and put them in context of previous research [184, 185]. Subjects could report more than one modality simultaneously. All sensations that had an 'electrical tingle', 'pins and needles', 'sharp' or 'tickle' component were considered paresthetic. If these sensations also included descriptors for mechanical, movement, or temperature modalities, they were considered mixed modality sensations. Sensations that did not include any paresthetic descriptors were considered naturalistic. The unique combinations of percept descriptors used by each subject along with the fraction of naturalistic, paresthetic, and mixed modality sensations are shown in Figure 4.4. For Subjects 1, 2, and 4, most sensory percepts were either paresthetic or of mixed modality (90.2%, 75.2%, and 96.5%, respectively). Subject 1 reported 74.2% of these percepts as purely paresthetic, whereas only a small fraction of these percepts were reported as purely paresthetic by Subjects 2 and 4 (4.1% and 0.3%). For Sub-

Figure 4.4: Sunburst plot showing the combination of paresthetic (teal), naturalistic (red), and mixed (grey) percept descriptors used by each subject. Each annulus represents a modality descriptor that the subjects could select. The innermost annulus represents sensations where a 'tingle' descriptor was used. The middle annulus represents the fraction of each tingle descriptor that co-occurred with a 'mechanical' descriptor. The outermost annulus represents the fraction of tingle and mechanical descriptors that co-occurred with a 'movement' descriptor. For Subjects 1, 2, and 4, most sensory percepts were either paresthetic or of mixed modality (90.2%, 75.2%, and 96.5%, respectively). Subject 3 predominantly reported naturalistic sensations (79.9%) with most of those percepts described as pure vibration.

ject 2 the evoked percept was most frequently described as tingle-pressure and for Subject 4 the evoked percept was most frequently described as tingle-pressure-vibration. Subject 3 predominantly reported naturalistic sensations (79.9%) with most of those percepts described as pure vibration. In fact, for this subject, 80% of all evoked percepts contained a 'vibration' component, and most mixed modality percepts (97.8%) were described as tingle-vibration with only one instance of a purely paresthetic percept.

More naturalistic modalities, like "touch" and "pressure", were elicited to varying degrees among the subjects (0.5%, 60.5%, 25.2% and 75.8% of unique stimulation parameter combinations for Subjects 1-4, respectively). Interestingly, sensation described as purely touch or pressure were reported in 8.25% and 19.5% of all evoked percepts in Subjects 2 and 3, respectively. Otherwise, these naturalistic sensations were commonly accopmanied by a paresthesia, as particularly seen in Subject 4. Percepts containing a dynamic ('movement') component that may be described as proprioceptive were evoked at least once in all subjects. Subjects were able to describe distinct proprioceptive sensations in the phantom limb such as opening and closing of the hand, movement of the thumb, and flexing of the elbow. However, unlike the tactile percepts that were predominantly stable across days, these proprioceptive sensations could be repeatedly evoked only for a few minutes even with consistent stimulus parameters. Only in the case of Subject 4 (the subject with trans-radial amputation), were we able to evoke sensations of thumb and wrist movement reliably over longer time courses, spanning multiple days and weeks. Interestingly, these proprioceptive percepts were elicited by a set of three closely situated electrodes over a narrow range of stimulus parameters (stimulus amplitude = 3 mA, stimulus frequency = 1–5 Hz).

Varying the stimulation frequency influenced the modality of the evoked sensation in Subject 3, but not in the other subjects. For Subject 3, the sensory percepts that were described as "touch" or "pressure" occurred in up to 90% of trials at low stimulation frequencies (below 20 Hz) while stimulation frequencies above 50 Hz evoked percepts that were always characterized as mixed modality. Subject 1 never reported these naturalistic sensations, which could be because we never stimulated at frequencies below 20 Hz, while Subjects 2 and 4 reported naturalistic, mixed, and paresthetic sensations independent of the stimulus frequency.

4.3.2 Psychophysical Assessment of Evoked Percepts

We quantified the detection threshold for sensations in the missing limb in all four subjects using a two-alternative forced-choice paradigm. Because Subjects 2 and 3 frequently experienced co-evoked sensations in the phantom and on the residual limb, for psychophysical assessments, we asked them to focus only on the distal phantom percept whenever stimulation co-evoked a sensation in the residual limb. In this task, the subject reported which of two intervals contained the stimulus train. With a randomized presentation of various stimulation amplitudes, we measured the detection threshold as the minimum amplitude at which the subject could correctly report the interval containing the stimulation train with 75% accuracy (Figure 4.5A). Mean detection thresholds (Figure 4.5B) for Subjects 1-4 were 3.75 mA ($n = 2$ electrodes), 1.25 ± 0.36 mA ($n = 5$ electrodes), 1.58 ± 0.39 mA ($n = 14$ electrodes) and 1.94 ± 0.27 mA ($n = 14$ electrodes), respectively.

We measured just-noticeable differences (JND) in stimulation amplitude with a two-alternative forced choice task in Subjects 3 and 4. We evaluated the goodness-of-fit using the probability of transformed likelihood ratio ($pTLR$), which spans 0–1 with a higher value signifying a better fit and values below 0.05 signifying an unacceptable fit. In Subject 3, for one electrode, the subject could perceive a change of 86 μA (slope, $\beta = 0.045$, $pTLR = 0.58$) at 75% accuracy when the standard amplitude was 2.5 mA, and a higher standard amplitude of 4 mA increased the JND to 280 μA (slope, $\beta = 0.073$, $pTLR = 0.83$; Figure 4.5C). In Subject 4, the JNDs showed a similar dependence on standard amplitude with mean $\text{JND}_{2.5}$ = 60 ± 21 μA (median slope, $\beta = 0.040$, median $pTLR = 0.79$) and mean $\text{JND}_{4.0}$ = 338 ± 98 μA (median slope, $\beta = 0.005$, median $pTLR = 0.40$, $n = 5$ electrodes; Figure 4.5D and B.2). To put these numbers in context, for Subject 4, with mean threshold at approximately 2 mA and maximum stimulation amplitude at 6 mA, the JNDs represent 1.3% (at standard amplitude of 2.5 mA) and 9% (at standard amplitude of 4 mA) of the available stimulation range.

To measure the relationship between stimulation amplitude and sensation intensity, subjects performed a free magnitude estimation task, in which they were instructed to rate perceived intensity on an open-ended numerical scale as stimulation amplitude was varied

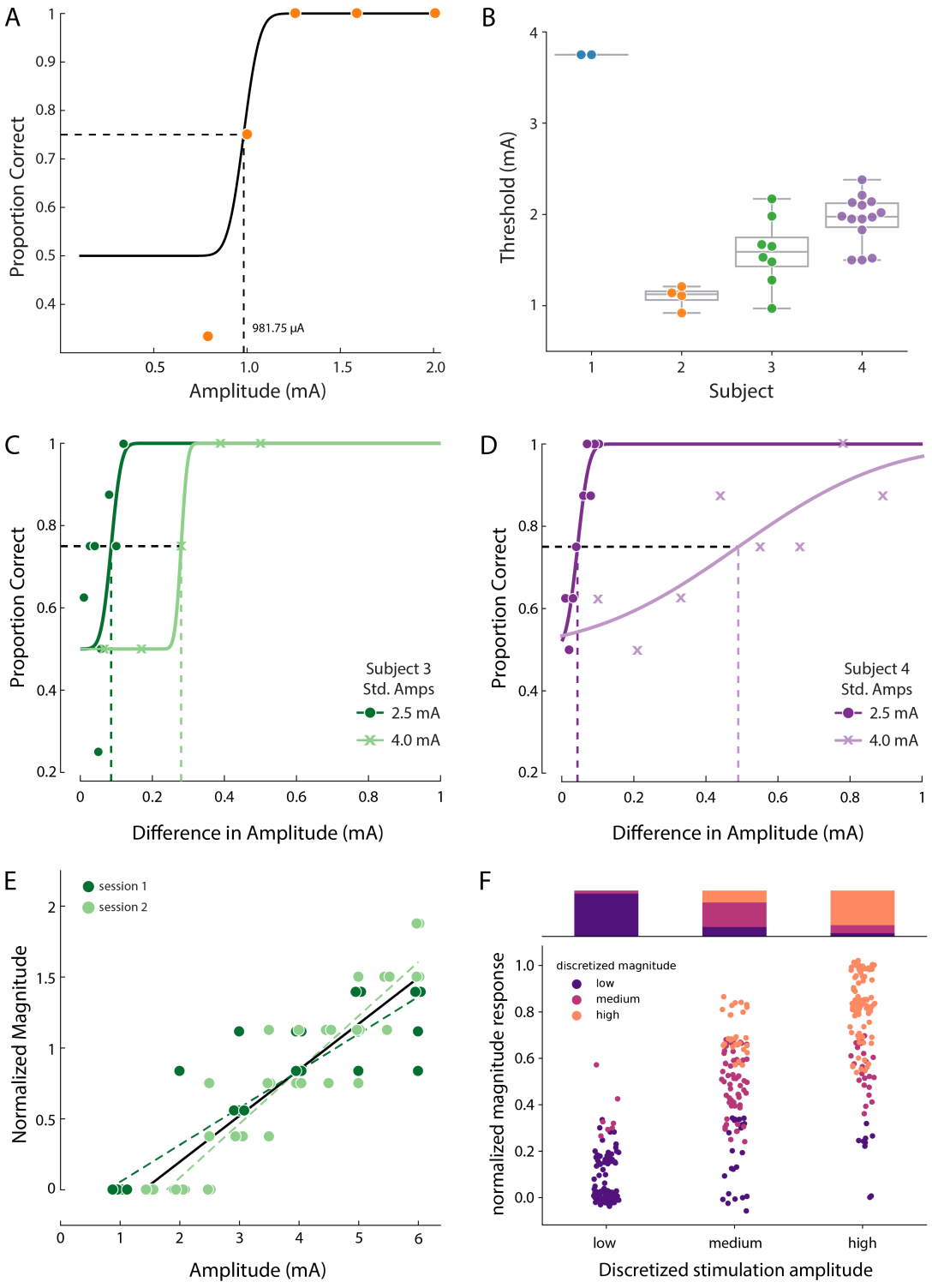

Figure 4.5: A) Example data from a detection task for a single electrode from Subject 2. Data were collected using a threshold tracking method and a psychometric function was fit to the data. The detection threshold was determined to be 982 μA.

Figure 4.5: B) Scatter plot showing the distribution of all the detection thresholds for Subjects 1 (blue), 2 (orange), 3 (green) and 4 (purple). C) Example data for the just-noticeable differences at two different standard amplitudes for one electrode in Subject 3 and D) Subject 4. Error bars represent SD. E) Example data from Subject 3 of a free magnitude estimation task carried out on two different days (light and dark green circles) for a single electrode. Data from multiple days was compared after normalizing each electrode to its mean response. Perceived intensity varied linearly with stimulus amplitude for each individual testing session (dashed and solid green lines) as well as when taken together (black solid line). The slope of these lines was measured in units of mA-1 F) Distribution of the stimulation amplitude and the reported intensity of the evoked percept for all subjects. Stimulation amplitude and reported intensity were independently discretized into three linearly spaced (low, medium, and high) bins and subject ratings of sensation intensity accurately predicted these bins. The stacked bar graph represents the percentage of times a binned magnitude response occurred for the corresponding discretized amplitude.

randomly. They were instructed to scale their response such that a doubling in perceived intensity was reported as a doubling in the numerical response. To control for variability across different electrodes and across different testing sessions, we normalized each electrode to the mean of its response. We observed that as stimulation amplitude was increased, the perceived intensity of the sensory percept increased linearly for all subjects; an effect that was consistent across repetitions of the task on multiple days (Figure 4.5E). A linear fit was determined to be better than or at least as good as a sigmoid or logarithmic fit based on adjusted R^2 values, and all electrodes had a significant linear relationship between stimulus amplitude and perceived intensity, ($p_{int} < 0.01$, F-test, where p_{int} is the two-sided p-value for the null hypothesis that the slope of the regression line was zero). This linear relationship between amplitude and intensity was maintained even though different electrodes were tested with different pulse widths and frequencies. Table 4.3 shows a complete list of stimulation parameters used for these experiments.

Table 4.3: Summary of psychophysics testing for each subject. For detection and discrimination trials the threshold (TH) and JND per stimulation channel are listed along with the corresponding frequency and pulse width that were used.

Subject	Electrode	Receptive Field	Minimum modal amplitude (mA)	Detection			Discrimination				Magnitude estimation	
				TH (mA)	F (Hz)	PW (μs)	JND_{low} (μA)	JND_{high} (μA)	F (Hz)	PW (μs)	slope	R^2
1	1	D1-D2	5.48	2.05	100	200		618	100	1000	0.37	0.62
	2	Palm (ulnar)	5.0	1.86	100	800					1.07	0.42
	3	Palm (ulnar)	4.0	2.13	100	200					1.7	0.68
2	1	Hand	4.0	1.14	20	200					3.18	0.78
	2	Thumb	3.0	1.21	20	200	245		20	200	2.36	0.71
	3	Hand	4.0								2.21	0.76
	4	Palm, D1	3.0	1.11	20	200					2.74	0.7
	5	Thumb	3.0	0.92	20	200					1.2	0.33
3	1	Hand	6.0	1.98	50	200					0.94	0.74
	2	Hand	5.0	2.85	50	200					1.33	0.73
	3	Hand	5.0	1.77	50	200	151		50	200	1.27	0.76
	4	Palm, D1-D4	3.0	0.97	50	200						
	5	Palm, D3-D4	4.0	1.28	50	200					1.22	0.87
	6	Palm, D1-D4	5.0	1.53	50	200					1.18	0.74
	7	Palm, D1-D4	4.0								1.58	0.79
	8	Palm, D3-D4	5.0	1.65	50	200					1.39	0.81
	9	Palm, D2-D4	3.0								1.43	0.69
4	1	Hand	3.0	1.52	50	200						
	2	D2, D4	4.0	2.13	50	200						
	3	D2	2.0									
	4	D1, D2	3.0	2.05	50	200	62	222	50	200	1.37	0.88
	5	Thumb, D1, D2	3.0	2.13	50	200		527	50	200	1.39	0.83
	6	Thumb, D1, D2	3.0								1.33	0.87
	7	Thumb, D1	3.0	1.97	50	200						
	8	Thumb, D1	3.0	1.98	50	200	27	647	50	200	1.49	0.92
	9	Palm, Thumb, D1-D3	3.0	2.05	50	200	59	516	50	200	1.32	0.91
	10	D2, D3	3.0	1.99	50	200	44	488	50	200	1.29	0.86
	11	Thumb, D1, D2	3.0	2.01	50	200	54	300	100	200	1.32	0.91
	12	Hand	3.0									
	13	Hand	3.0									
	14	Hand	2.0	1.95	50	200						
	15	Hand	3.0	2.1	50	200						
	16	Thumb, D1	3.0	1.86	50	200	96	360	50	200	1.36	0.89

These results taken together show that subjects should be able to perceive graded sensory feedback for linearly spaced gradations greater than the JND for each electrode. The number of gradations in stimulation determines the number of discrete targets (such as identifying three different levels of force) that can be represented in a functional task. To identify the optimal gradation for functionally relevant sensory feedback via SCS, we partitioned

stimulation amplitudes and subject responses during the free magnitude estimation task into three or five discrete linearly spaced ranges. The partitioned data were used to estimate how reliably subjects can distinguish sensations for each of these amplitude ranges. Figure 4.5F shows the distribution of the normalized subject responses for a 3-target task where the overal accuracy was 72%. All subjeccts reported sensations in the low and high range of stimulation with a high accuracy (79% and 95% accuracy, respectively) with medium targets having an accuracy of 54%. When the data were partitioned into 5 discrete ranges, the overall accuracy was 46% (Figure B.3). In the context of clinical translation, these results indicate that it may be possible for the user to discriminate three specific intensity levels based on stimulation amplitude alone.

Since we found a consistent linear relationship between percept intensity and stimulation amplitude, we quantified the changes in percept area that occurred as the stimulation amplitude was increased. In a prosthetic device, being able to modulate the percept intensity independent of the area is critical to deliver graded feedback that remains focal. Figure 4.6A shows an example of a percept where the area and centroid remain stable as the stimulation amplitude is increased. To examine the effect of stimulation amplitude on the area and intensity of the evoked percept, we computed the least-squares regression line for area versus stimulation amplitude and obtained the two-sided p-value (p_{area}) for the null hypothesis that the slope of the regression line was zero. We also compared the slope of this regression line with the slope of the linear fit between stimulation amplitude and reported intensity (obtained from magnitude estimation trials) for each electrode to identify whether percept area and intensity were modulated independently (Figure 4.6B). Across all electrodes ($n = 24$), the slope of the linear fit for area was less than the slope for intensity. For three electrodes, both area and intensity were modulated by stimulation amplitude ($p_{area} < 0.01$, median $\beta = 0.25$ and $p_{int} < 0.01$ median $\beta = 1.36$). For the remaining 21 electrodes, only intensity, but not area, was modulated by stimulation amplitude ($p_{area} > 0.05$, median $\beta = 0.01$ and $p_{int} < 0.01$, median $\beta = 1.33$). This indicates that for most electrodes, it is possible to modulate percept intensity independent of percept area.

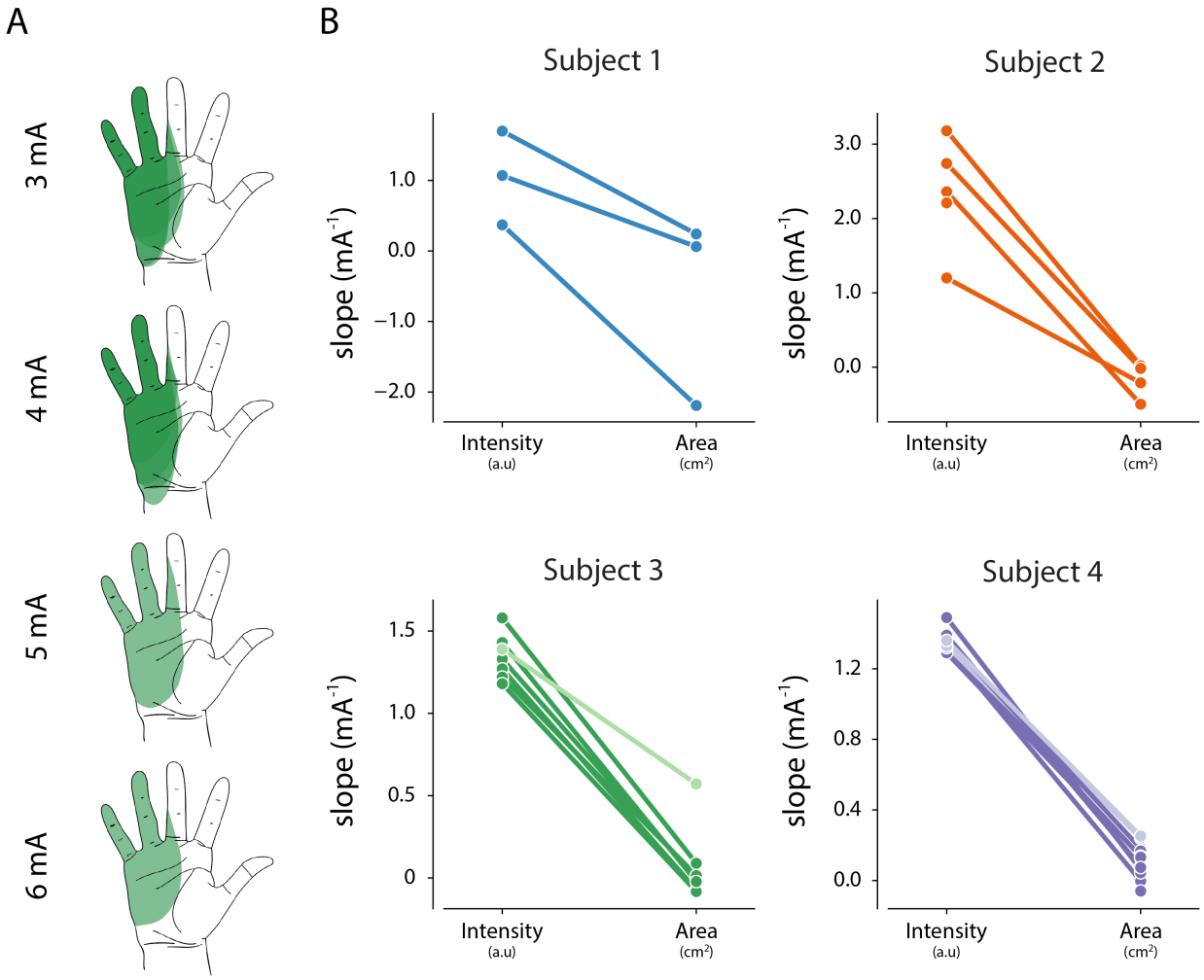

Figure 4.6: A) Example of the stability of percept area with increasing amplitude for one electrode in Subject 3. B) Summary of the relationship between stimulation amplitude and percept characteristics for each electrode that evoked a percept in the phantom hand. The slope of the linear fit between stimulation amplitude and reported intensity was obtained from magnitude estimation trials. The slope of the linear fit between stimulation amplitude and percept area was obtained from percept mapping trials. Lighter shades represent electrodes where parea < 0.01. The null hypothesis is that the slope of the linear fit is zero.

4.3.3 Stability of SCS Electrodes and Evoked Sensory Percepts

Lead migration is a common clinical complication for SCS, with an incidence rate as high as 15–20% [202, 55, 203, 204]. Lead migration would change the location and modality of evoked sensations, which could limit the long-term viability of SCS and would also complicate the scientific utility of percutaneous SCS as a testbed for novel neuroprosthetic techniques. We performed weekly X-rays that allowed us to monitor the position of the leads and quantify migration over the duration of the implant. Superimposing the intraoperative fluoroscopy image and the final X-ray (Figure 4.7A) revealed that lead migration was largely restricted to the rostro-caudal axis. In all subjects, the largest caudal migration was observed when comparing the intraoperative fluoroscopy image with the X-ray at the end of first week (Figure 4.7B). One of the leads in Subject 2 almost completely migrated out of the epidural space in this post-operative period (Figure 4.7B), rendering it unusable for stimulation experiments. In contrast to the migration that occurred during the first week, X-rays from the first and last week of testing showed minimal lead migration (Figure 4.7B). In the weeks following the initial migration, the median migration in the rostro-caudal direction across the three leads in any subject never exceeded 5 mm. For all subjects, the initial placement of the leads rostral to the target cervical levels prevented loss of coverage of those spinal levels following the caudal migration of the leads.

We assessed the stability of each evoked percept throughout the duration of the study (e.g. Figure 4.8A) in terms of the threshold charge (Figure 4.8B) for evoking a percept in the missing hand. A one-way ANOVA performed for each subject confirmed that there was no significant difference in the threshold charge for each week for Subjects 1, 2 and 3 ($p > 0.01$, F = 2.3, 1.1, 1.7 respectively). For Subject 4, there was a significant change in threshold after weeks one and three ($p < 0.01$, F = 9.0). A post-hoc multiple pairwise comparison analysis using the Tukey HSD test confirmed that there was a significant increase in the thresholds between weeks one and two ($p < 0.01$) and a significant decrease between weeks three and four ($p < 0.01$).

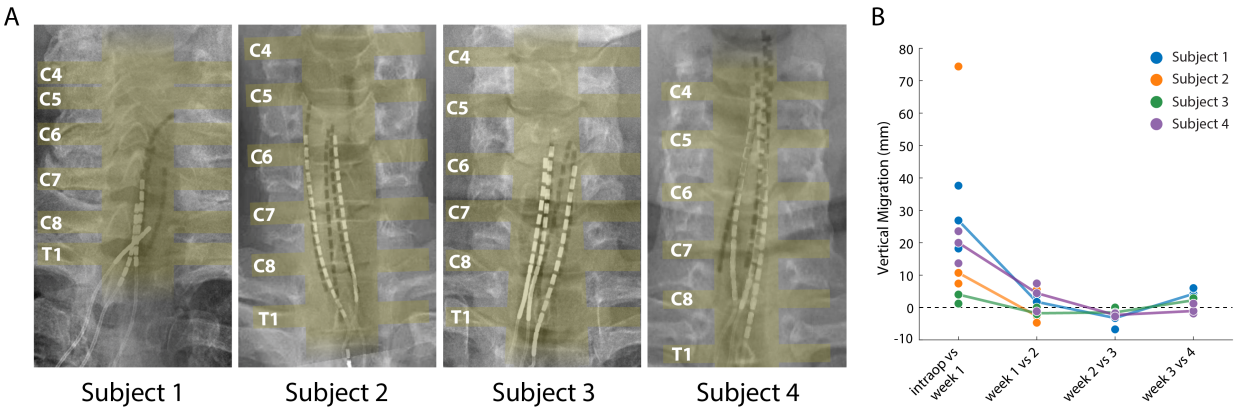

Figure 4.7: A) Composite image showing the changes in the position of the SCS leads in the epidural space. The intraoperative fluoroscopy image (contacts appear black) showing the position of the leads immediately after implantation is superimposed over the X-rays (contacts appear white) from week 4 for each subject. The labels on the left mark the dorsal root exiting at that level. The approximate location of the spinal cord and the roots is also shown in yellow overlay. For scale, each contact is 3 mm long. B) Weekly migration of the rostral tip of each of the leads for the four subjects (blue, orange, green, and purple circles for Subjects 1–4, respectively). For week 1, the comparison was between the weekly X-ray and the intraoperative fluoroscopic image. For subsequent weeks, the comparison was done between the weekly X-ray and the one from the preceding week. Median migrations are shown (solid lines). The X-ray for Subject 2 was taken from week 2, before leads were explanted.

We also characterized stability in terms of the size (area) and location (centroid) of percepts evoked in the missing hand. The centroid and area were calculated for all percepts evoked at the minimum stimulus amplitude that was tested at least once each week during the implant. If no stimulus amplitude was tested during every week of testing, the lowest stimulus amplitude that was tested for the next highest number of weeks (for at least two weeks) was chosen. We quantified the migration of the mean centroid location across all stimulus repetitions for each week with respect to the mean centroid location of the previous

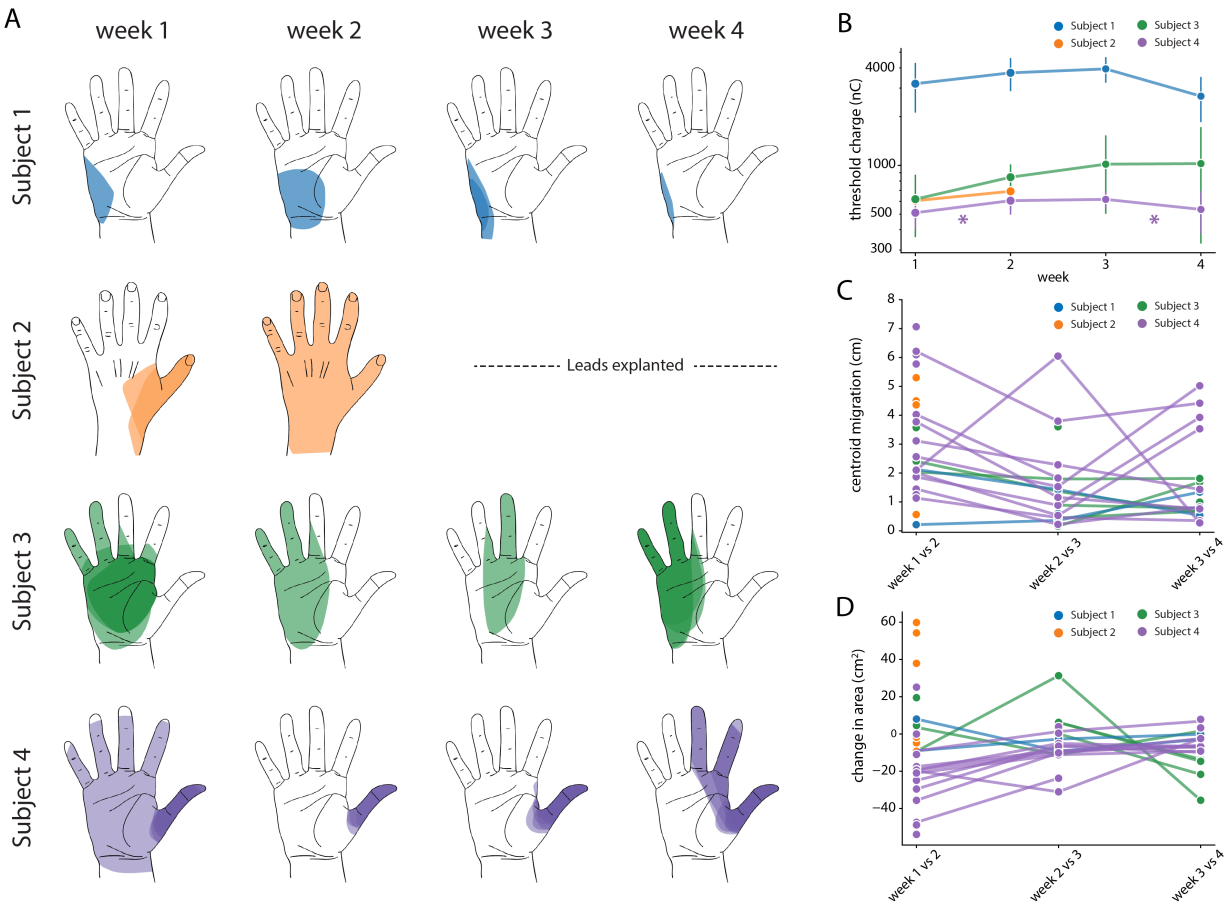

Figure 4.8: A) Example sensory percepts from the hand for a single electrode in Subjects 1–4. For Subject 2, the percepts are shown for weeks 1 and 2 only, as the leads were explanted after that. The percepts shown were evoked by the minimum stimulus amplitude that was tested at least once per week for the maximal number of weeks. Each column shows the location of all percepts evoked for that week of testing. Multiple examples of the percepts evoked during the week are superimposed on each other as indicated by different shades. B) Time course of the average stimulation threshold (in nC) for evoking a percept in the phantom hand for each subject. Weeks with a significant change in threshold are annotated with an asterisk. C) Stability of the location of the evoked percept in the phantom hand. For each electrode, the centroid location of the evoked percept was compared between successive weeks. D) Stability of the area of the evoked percept in the phantom hand. For each electrode, the area of the evoked percept was compared between successive weeks.

week for each electrode (Figure 4.8C). Across all subjects, the evoked percepts exhibited a median migration of 25.2 mm between weeks 1 and 2, 11.6 mm between weeks 2 and 3, and 9.9 mm between weeks 3 and 4. This week-to-week decrease in centroid migration follows the trend of decreased week-to-week vertical electrode migration (Figure 4.8B). Similarly, the change in area for each week was calculated with respect to the mean area of the previous week for each electrode (Figure 4.8D). Across all subjects, the median change in area of percepts evoked in the missing hand was 8.1 cm2 between weeks 1 and 2, 0.14 cm2 between weeks 2 and 3, and 1.1 cm2 between weeks 3 and 4. We constructed two separate auto-regressive time series model to examine the changes in distributions of area and centroid distance over time, adjusting for autocorrelations in the data. We found a significant decrease in area over time across all weeks, (β = -0.201, $p < 0.01$). For centroid migration, there was a decrease during weeks 2 (β = -23.224, $p < 0.05$) and 3 (β = -40.585, $p < 0.01$).

4.4 Discussion

In this work, we show that epidural SCS has the potential to be an effective and stable approach for restoring sensation in people with upper-limb amputations. Further, we believe that percutaneous SCS can be used as an effective platform for development of somatosensory neuroprostheses, especially for labs that focus on advanced prosthetic control but have not developed their own stimulation technologies. The electrodes used in this study are commercially available and were implanted using standard surgical techniques under local anesthesia during a procedure spanning 3-4 hours. In all subjects, we were able to evoke sensory percepts that were focal and localized to the distal missing limb. Critically, this included people with amputations ranging from trans-radial through shoulder disarticulation. The repertoire of sensory percepts elicited varied across subjects and thus, this approach would require user-dependent characterization, which is similar to the results reported by other studies of peripheral somatosensory neuroprostheses [32, 44, 42, 43]. While most of the stimulation parameters evoked paresthesias, some of the percepts were more naturalistic.

The intensity of the evoked sensations could be modulated by varying stimulation amplitude with little or no increase in the perceived area of the evoked sensations. Below we summarize these results and discuss their implications for the design of a somatosensory neuroprosthesis.

4.4.1 Epidural SCS Evokes Sensations Localized to the Missing Hand and Arm

SCS-evoked sensory percepts were perceived to emanate from the missing limb in all subjects. Some percepts were highly localized to a single finger or focal region of the palm, while others were diffuse, covering large regions of the limb. In our second and third subjects, distal sensations were often accompanied by a secondary sensation at the residual limb. It is unclear whether these secondary sensations are a result of neuroplastic changes in the representation of the amputated hand in the cortex or are a limitation of the selectivity of the SCS electrodes used in this study. Future studies in people with intact limbs undergoing lateral SCS may help to differentiate these effects, since those subjects would not have similar neuroplastic changes. Factors that may limit stimulation selectivity with our approach include the thickness of the cerebrospinal fluid in the subdural space and the relatively large size of the contacts on the SCS leads. Consequently, the sensory percepts evoked in this study were sometimes more diffuse than those reported in other studies using peripheral neurostimulation approaches [32, 36, 34, 43]. Importantly though, they are comparable in focality to those used to effectively deliver sensory feedback during recent long-term take-home studies of bidirectional prosthesis using peripheral nerve stimulation (Cuberovic et al., 2019) or targeted reinnervation [205].

In all except Subject 4, monopolar stimulation primarily evoked sensations in the forearm and upper arm, whereas multipolar stimulation allowed us to evoke sensations that were localized to distal regions of the missing hand and wrist. We could not identify any difference (e.g. in surgical technique) that led to this difference in focality of monopolar stimulation for Subject 4 as compared to all other subjects. In all subjects, the leads were steered toward the lateral spinal cord and spinal roots, ipsilateral to the amputation. At this location, the dorsal rootlets fan out under the dura before entering the spinal cord at the dorsal root entry zone. In the cervical spinal cord, the rootlets are each approximately 0.4–1.3

mm in diameter and densely packed with few spaces between them [206, 207, 208]. This arrangement, superficially resembling the flattened peripheral nerve cross-section achieved by the flat interface nerve electrode [32, 43], may lend itself to a higher degree of selective activation than could be achieved with stimulation of more traditional SCS targets such as the dorsal columns or the dorsal root ganglia, although this may require development of new SCS devices with more optimal electrode sizing and spacing.

The relationship between the locations of the electrodes and that of the evoked percepts showed marked inter-subject variability and deviation from expected dermatomes. For example, all electrodes in Subject 1 were in the T1 region, but the reported sensations were in the missing hand, a region covered by the C6–C8 dermatomes. Recently, it has been recognized that dermatomes inadequately reflect inter-individual variability in dermatome coverage and overlap, suggesting that the variability observed in our study may reflect natural inter-subject differences [201]. However, a limitation of this study is that we did not directly image the spinal cord or dorsal roots. As such, we could not determine the exact spatial arrangement of the implanted SCS electrodes relative to target neural structures. Several research groups have developed highly detailed computational modeling techniques to study how the electric fields generated in SCS interact with neural structures [183, 209]. These techniques could potentially help illuminate the specific neural targets and pathways that were activated in this study. These observations combined with simulation studies could also inform the design of stimulation schemes and novel electrodes to improve the selectivity of our somatosensory neuroprosthesis.

4.4.2 Stimulation Parameters Primarily Modulate Intensity of Sensation

With respect to the perceptual qualities of evoked sensations in this study, we observed a robust relationship between stimulus amplitude and percept intensity. Every electrode tested across all four subjects demonstrated a statistically significant linear relationship between stimulation amplitude and perceived intensity. This is similar to what has been observed with peripheral nerve stimulation [44, 41]. Interestingly, we observed JNDs to be proportional to the stimulation amplitude with higher stimulation amplitudes resulting in larger JNDs.

Such a relationship between JNDs and stimulus amplitude is consistent with Weber's law which governs the behavior of most peripheral sensory receptors [210]. We also observed that subject responses could accurately be separated into three, but not five, separate intensity categories (i.e. low, medium, and high) based on the stimulation amplitude, which suggests that they would be able to successfully perform a 3-level discrimination task, based only on perceived intensity, such as identifying three different force levels exerted by objects of different stiffnesses. These expected performance levels are similar to those demonstrated by others using peripheral nerve stimulation to restore somatosensation [34], and it is possible that they could improve with time and training, continuous (rather than discrete) modulation of amplitude, and the addition of active efferent control of a prosthesis. Future work should focus on demonstration of such closed-loop control with sensory feedback using lateral SCS.

An increase in stimulus amplitude is thought to increase perceived intensity by recruiting a larger volume of somatosensory afferent neurons [31]. An increase in the volume of recruited neurons could also result in an increase in percept area. However, we observed little to no effect of increasing stimulation amplitude on percept area. It is possible that the anatomical distance between adjacent spinal roots reduces this effect [211]. Additionally, it is currently unknown whether there is strong somatotopic organization of the fanned-out dorsal rootlets where they enter the spinal cord (i.e. whether neighboring rootlets innervate neighboring patches of skin). The minor changes in focality of sensation as amplitude increases may be due to the presence of this somatotopic organization and recruitment of neurons in adjacent rootlets.

A primary aim of providing artificial somatosensory feedback has been to evoke naturalistic sensations, particularly those described as touch or pressure. Most of the percepts reported in this and previous studies of somatosensory neuroprostheses have been described as paresthesias. Most of the percepts evoked by our stimulation paradigm were described as paresthesias. However, for Subjects 2 and 3, we report that 8.25% and 19.5% of all evoked percepts were described as touch or pressure alone. Studies that relied on peripheral nerve stimulation to restore somatosensory feedback have reported similar proportions of naturalistic percepts, e.g. 8-30% as touch-like percepts [41, 212, 30] and 2-29% as pressure-like percepts [48, 37, 41, 212]. Continuous modulation of stimulus parameters, such as modu-

lating pulse width [32, 30] or varying charge density [32] have been proposed to evoke more naturalistic cutaneous or proprioceptive sensations. However, a recent study demonstrated that patterned stimulation did not reliably change paresthetic sensations to more naturalistic ones [47]. Additionally, biomimetic stimulus trains [213, 35] have been proposed to evoke more naturalistic sensations, though none of these approaches have established a stimulation paradigm that reliably elicits naturalistic sensations across subjects. We too, did not uncover a reliable way to evoke naturalistic sensation during the course of this study. Thus, the choice of electrodes and stimulation parameters would have to be optimized for each individual user to evoke percepts with the desired modalities.

Only one subject (Subject 4, trans-radial amputation) reported proprioceptive percepts that were repeatedly evoked over more than a few minutes. This result aligns with other studies, which often report only limited examples of proprioceptive percepts [37], or which describe proprioceptive sensations that result directly from muscle contractions in the residual limb [41]. While SCS did not evoke overt reflexive movements of the residual limb in any subject at the stimulation amplitudes used in this study, it is possible that these proprioceptive percepts result from small reflexive contractions of residual limb muscles which themselves activate muscle spindle afferents. Complex coordination of activation of muscle spindle and cutaneous (e.g. slowly adapting type II) afferents may be required for directly evoking realistic kinesthetic percepts. Future work should explore the downstream effects of stimulation of proprioceptive and cutaneous afferents on perception of kinesthesia. Regardless, we propose that even though we evoked primarily paresthetic sensations, the ability to evoke these percepts via a clinically translatable approach in individuals with high-level amputations establishes the promise of this approach towards restoring sensation.

4.4.3 Percutaneous SCS Electrodes and Evoked Percepts are Stable Over One Month

The location of the implanted SCS electrodes and the corresponding evoked percepts showed only minor migration across the duration of implantation. In clinical practice, SCS lead migration is a common complication, occurring in as many as 15–20% of cases [202, 55,

203, 204], and is typically classified by a complete loss of paresthetic coverage of the region of interest. Repeated monitoring of both the physical location of the SCS leads and the evoked sensations demonstrated that there was some migration immediately after implantation, but minimal movement thereafter. As a preemptive measure against loss of coverage due to the initial migration, we opted to use 16-contact leads in Subjects 2–4. By placing the leads such that the most rostral contacts were above the target spinal levels, we ensured continued coverage even in the case of caudal migration. It is worth noting that we did not anchor these leads to any bony structures or nearby tissue. Future permanently implanted systems for restoring sensation using SCS can utilize these anchoring techniques and thereby reduce or eliminate lead migration [203]. The stability in the electrodes is reflected in the stability of the evoked percepts. In the hand region, we observed a migration of evoked percepts of 10–25 mm, which is similar to the shift reported in peripheral stimulation approaches [43]. Moreover, given that the spatial acuity in the palm region is approximately 8–10 mm [214, 215, 216, 217], the scale of migration observed is within the range that would not likely be detectable by the user.

4.4.4 Comparison to Alternative Approaches

The techniques described in this study have both important advantages and disadvantages that should be considered when selecting an approach for restoring sensation after upper-limb amputation. A major advantage of the percutaneous approach described here is that there is a relatively low barrier to initiating clinical studies because the electrodes are commercially available from multiple manufacturers and the surgical procedures are commonly performed at most major medical centers. However, this reliance on commercially available electrodes also likely limited selectivity and focality. Regardless, a great deal of technical and scientific development can be achieved with this approach before moving on to more complex studies involving custom electrodes and implantable stimulators.

Another major advantage of the approach is its viability for people with high-level amputations, in which the peripheral nerve has been amputated. In this population, the spinal cord and roots typically remain intact, and we have demonstrated that stimulation of those

structures can produce focal sensations in the missing hand. Currently, the only other viable neuroprosthetic techniques for restoring sensation after proximal amputation are invasive approaches such as targeted reinnervation or stimulation of structures in the central nervous system.

As compared to other techniques that focus on peripheral nerve stimulation, such as epineural stimulation with cuff electrodes or penetrating stimulation with Utah arrays or longitudinal intrafascicular electrodes, our results demonstrate substantially less focal percepts and less consistent coverage of each individual digit across subjects. Further, sensations in the hand were often accompanied by a sensation on the residual limb. It is currently unclear to what degree this is a limitation of the relatively large size of the electrodes we used here, as opposed to a fundamental limitation of the selectivity of epidural SCS. Future work will focus on computational studies to explore this question and design new electrodes that can more selectively target the sensory afferents in the dorsal rootlets to maximize the selectivity and focality of our approach. With respect to clinical applications, the 3-fold dynamic range afforded by the stimulus amplitude is similar to those reported previously [41]. Though the absolute current values we used are an order of magnitude higher than those required for peripheral nerve stimulation, epidural stimulation systems are widely used in a clinical setting and also in patient homes. This suggests that a neuroprosthetic device based on this approach can be effectively utilized in clinical or home setting.

An important limitation of this study is that we focused on characterizing the sensations evoked by SCS but did not demonstrate that those sensations could be used as part of a closed-loop neuroprosthetic system. While we demonstrate that many of the qualities of the evoked sensations are similar to those reported by others (e.g. sensation intensity modulates linearly with stimulation amplitude), it will be critical to demonstrate that sensations remain stable and are useful during closed-loop prosthetic applications. For example, while we did not control subject posture during any of our experiments, it will be important to demonstrate that sensations remain stable during intentional movements of the neck, shoulders, and arms. Certainly, future work will focus on achieving these demonstrations and characterizing the effects of sensory restoration via SCS on dexterous control of prosthetic limbs.

4.5 Conclusions

Since this approach targets proximal neural pathways, SCS-mediated sensory restoration lends itself to use for a wide range of populations, such as individuals with proximal amputations and those with peripheral neuropathies in which stimulation of peripheral nerves may be difficult or impossible. Provided that the injury does not affect the dorsal roots and spinal cord, our results suggest that these techniques can be effective in restoring sensation, regardless of the level of limb loss. Moreover, the widespread clinical use of SCS and the well-understood risk profile provide a potential pathway towards clinical adoption of these techniques for a somatosensory neuroprosthesis.

5.0 Closed-loop stimulation of cervical spinal cord and dorsal roots in upper-limb amputees to enable sensory discrimination

The contents of this chapter are in preparation for submission as a journal article by: *Chandrasekaran S*, Nanivadekar AC*, Helm ER, Boninger ML, Collinger JL, Gaunt RG, Fisher LE.* * These authors contributed equally to this work.

5.1 Introduction

People with upper-limb amputation rely heavily on sustained visual attention when performing everyday activities with a prosthesis [10, 11]. This reliance on visual cues leads to sub-optimal motor control in various situations such as attempting to grasp an object that is out of the line of sight, or rapidly modulating grip force to prevent object slipping [218]. Surveys of users of upper-limb prostheses have reported somatosensory feedback as a top unmet need [172, 10].

Normal haptic perception requires an interplay between tactile and proprioceptive modalities of sensory information [17]. Broadly, tactile information conveys contact with the object, the optimal pressure required to interact with the object to prevent slip, and the surface features of the object [17]. Meanwhile, proprioceptive information conveys the state and orientation of the hand and fingers which enables inference of object location, shape, and size [17]. Several studies have demonstrated the effectiveness of artificial somatosensory feedback in conveying these multiple modalities of information during use of a prosthesis. When tactile information was delivered by electrical stimulation of peripheral nerves in the residual limb, study participants demonstrated improvements manipulating objects [219], controlling grip force [220, 221, 37], and identifying object compliance [34, 33, 48, 222]. Further, electrical stimulation designed to mimic mechanoreceptor firing patterns can enable amputees to discriminate naturalistic textures [223, 224].

Proprioceptive sensations have been far more challenging to evoke reliably with electrical stimulation of peripheral nerves. Instead, prior studies have typically conveyed proprioceptive information by remapping the intensity of an evoked tactile sensation based on a signal such as grasp aperture or finger joint angle. With these techniques, participants could discriminate sizes of objects with a success rate better than chance [33, 48, 222].

We have previously shown that stimulation of the lateral cervical spinal cord can evoke focal sensations in the missing fingers and hand, even in people with high level amputations, such as at the proximal humerus or shoulder. The goals of this study were to provide functionally relevant sensory feedback in real-time via lateral spinal cord stimulation (SCS) and to identify factors affecting the utility of this feedback to an amputee using a prosthesis. We used FDA-approved, commercially available SCS leads to provide somatosensory feedback to two subjects with upper-limb amputation. Subjects were asked to interact with an object using a sensorized DEKA [225, 226] hand or a virtual representation of that hand, rendered in MuJoCo [227, 228]. Subject 1 used a DataGlove worn on her contralateral, intact hand to proportionally control the aperture of the prosthesis, and Subject 2 used EMG signals from the residual limb to trigger threshold-based constant velocity closing of the prosthetic hand. Tactile sensory feedback was provided by varying the stimulus amplitude in real-time to modulate the intensity of the evoked percept. Subjects were asked to determine the size or compliance of the object based on this feedback. With less than an hour of training, both subjects were able to use the sensory feedback to perform the discrimination tasks at a success level above chance. Additionally, specific features of the control system such as the peak stimulus amplitude, the rate of change of stimulation, and the aperture of the prosthetic hand at object contact encoded size and compliance of the presented objects. Each subjects' ability to attend to these features determined their performance on the object discrimination task. These results demonstrate that percepts evoked via SCS can be modulated to provide meaningful, functionally relevant sensory feedback to amputees in real-time. However, the design of the control system determines what sensory information is available to the subjects.

5.2 Methods

5.2.1 Study Design

We have previously demonstrated that the intensity of percepts evoked via SCS is linearly related to the amplitude of stimulation. The aim of this study was to modulate the intensity of the percept in real-time while subjects used a sensorized prosthetic hand to interact with objects of different size and compliance. Subjects were asked to identify each object and the utility of sensory feedback via SCS was measured in terms of their overall performance on this task. To characterize the factors affecting the utility of sensory feedback, subjects performed the object discrimination task using two separate sensor-stimulation mappings (linear and exponential), and two different control environments (real and virtual prosthetic hand).

Two subjects with upper-limb amputations were recruited for this study. Subject 1 had a transhumeral amputation on the right arm while Subject 2 had a transradial amputation on the right arm. Neither subject had experience using a prosthetic limb before participating in these experiments. The time since amputation was greater than 2 years for both subjects. All procedures and experiments were approved by the University of Pittsburgh and Army Research Labs Institutional Review Boards and Subjects provided informed consent before participation.

5.2.2 Electrode Implantation

SCS leads were implanted through a minimally invasive, outpatient procedure performed under local anesthesia. With the subject in a prone position, three 16-contact SCS leads (Infinion, Boston Scientific) were percutaneously inserted into the epidural space on the lateral aspect of the C5–C8 spinal cord (Figure 5.1) through a 14-gauge Tuohy needle. Contacts were 3 mm long, with 1 mm inter-contact spacing. Leads were steered via a stylet under fluoroscopic guidance, and electrode placement was iteratively adjusted based on the subjects' verbal report of the location of sensations evoked by intraoperative stimulation. The entire procedure took approximately 3–4 hours. The leads were maintained for up to

29 days and subsequently explanted by gently pulling on the external portion of the lead. subjects attended testing sessions 3–4 days per week during the implantation period. The testing sessions lasted up to a maximum of 8 hours.

5.2.3 Neural Stimulation

During testing sessions, stimulation was delivered using three 32-channel stimulators (Nano 2+Stim; Ripple, Inc.). The maximum current output for these stimulators was 1.5 mA per channel. In order to achieve the higher current amplitudes required for SCS, a custom-built circuit board was used to connect together the output of groups of four channels, thereby increasing the maximum possible output to 6 mA per channel. Custom software in MATLAB was used to trigger and control stimulation.

Stimulation pulse trains were charge-balanced, cathodic-first square pulses, with symmetric cathodic and anodic phases. Stimulation was performed either in a monopolar configuration, with the ground electrode placed at a distant location such as on the skin at the shoulder or hip, or in a multipolar configuration with one or more local SCS contacts acting as the return path. Stimulation frequencies and pulse widths ranged 1–300 Hz and 50–1000 μs, respectively. The interphase interval was 60 μs. All stimulus amplitudes reported in this manuscript refer to the first phase amplitude.

5.2.4 Recording Perceptual Responses

The methodology for recording perceptual responses, characterizing their psychophysical properties, and determining their stability at threshold have been detailed elsewhere [111]. Briefly, at the offset of each stimulation train, subjects used a touchscreen interface [229] developed in Python to document the location and perceptual quality of the evoked sensation. The location of the sensory percept was recorded using a free-hand drawing indicating the outline of the evoked percept on an image of the appropriate body segment, i.e., hand, arm or torso. The percept quality was recorded using several descriptors that have been used previously to characterize evoked percepts [184, 135].

5.2.5 Motor Control of Prosthetic Hand

Subjects performed an object discrimination task using a sensorized DEKA hand (Mobius Bionics) or a virtual representation of that hand, rendered in MuJoCo. Neither subject was a regular prosthesis user, so implementing a complex control scheme to achieve dexterous handling of objects would have required considerable training. Instead, each subject controlled the aperture of the prosthetic hand using a customized control signal. Subject 1 wore a Data Glove (Fifth Dimension Technologies, 5DT) on her contralateral, intact hand. The grasp aperture from the Data Glove was used to proportionally control the aperture of the real and virtual DEKA hand. Subject 2 had stroke-induced paralysis in her contralateral arm and could not use the Data Glove to control the DEKA hand. Therefore, bipolar surface EMG was recorded from the residual muscle in the ipsilateral forearm. EMG data were recorded at 2000 Hz, high-pass filtered at 10 Hz, downsampled to 50 Hz and rectified. This rectified EMG signal was normalized to the peak EMG recorded during a maximum voluntary contraction prior to each session. When this signal crossed a manually defined threshold (upon elbow flexion), the DEKA hand was commanded to close at a constant velocity of 15 degrees/s. Any time the processed EMG signal was below threshold, the hand was commanded to open at a constant velocity of 30 degrees/s.

5.2.6 Real-time Somatosensory Feedback via SCS

A subset of SCS electrodes that evoked focal percepts localized to the phantom hand and fingertips were used to provide real-time somatotopically matched feedback during the object discrimination task. Sensors embedded in the fingertips of the DEKA hand or virtual sensors in MuJoCo measured the force generated upon contact with the presented object. Each sensor was mapped to specific SCS electrodes such that the receptive field of the evoked percept overlapped with the location of the sensors in the hand. Custom software was written in MATLAB (Mathworks, Natick, MA) to process the contact force and control stimulation in real-time with an update rate of 50 Hz. Sensor signals were low-pass filtered using a 4th order Butterworth filter with a cutoff at 4 Hz. We implemented a linear and an exponential transformation between contact force and stimulus amplitude. For a linear transformation,

the contact force was first normalized to a scale ranging from 0 to 1 as shown in equation 5.1,

$$F_n = \frac{(F - F_{min})}{(F_{max} - F_{min})} \tag{5.1}$$

where, F_n is the normalized contact force, $F$is the instantaneous contact force, F_{max} and F_{min} are the upper and lower limits of the contact force measured by the sensor, respectively. The instantaneous amplitude of stimulation A was determined as shown in equation 5.2,

$$A = F_n \cdot (A_{max} - A_{min}) + A_{min} \tag{5.2}$$

where, A_{max} and A_{min} are the upper and lower limits of the stimulus amplitude. For an exponential transformation, the instantaneous amplitude of stimulation A, was determined as shown in equation 5.3

$$A = \begin{cases} A_{min} \cdot e^{\omega F} & \text{if } F > 1 \\ 0 & \text{if } F \leq 1 \end{cases} \tag{5.3}$$

where, F the instantaneous contact force measured by the sensor, ω is an empirically assigned scaling factor (0.005 to 0.025), and A_{min} is the lower limit of the stimulus amplitude. Subject 1 performed the object discrimination task using both sensor-stimulus transformations. Her performance using each transformation is reported separately. Subject 2 performed the object discrimination task using the linear transformation only.

5.2.7 Object Discrimination Task Design

Table 5.1 provides a summary of the control scheme and number of object presentations for the physical and virtual object discrimination task for Subjects 1 and 2.

5.2.7.1 Virtual DEKA hand in MuJoCo Both subjects used a virtual representation of the DEKA hand to perform the object discrimination task in a virtual environment designed using MuJoCo. For Subject 1, spheres of three different sizes (small, medium, and large) and compliances (soft, medium, and hard) were presented (Figure 5.2A). For the size discrimination task, objects of three different sizes were presented 36 times in random order resulting in a total of 108 object presentations. A linear transform between sensor force and

Table 5.1: Summary of object discrimination trials and control scheme per subject

Subject	Control Scheme	Control Environment	Object presentations per task				
			Size task		Compliance task		
			linear	exponential	linear	exponential	control
1	Contralateral Data Glove	virtual DEKA	36	72	18	90	-
		real DEKA	55	21	-	-	-
2	ipsilateral EMG	virtual DEKA	15	-	75	-	30
		real DEKA	30	-	60	-	15

stimulation was used for 36 of these presentations and an exponential transform was used for 72 presentations. For the compliance discrimination task, three different compliances were presented 36 times in random order resulting in a total of 108 object presentations. A linear transform between sensor force and stimulation was used for 18 of these presentations and an exponential transform was used for 90 presentations.

For Subject 2, cylinders of three different sizes and compliance levels were presented (Figure 5.4A). For each presentation, the subject had 10 seconds to explore the object. For the size discrimination task, objects of three different sizes (and hard compliance) were presented 5 times in random order resulting in a total of 15 object presentations. For the compliance discrimination task, three different compliances (and large size) were presented 25 times in random order resulting in a total of 75 object presentations. A linear transform between sensor force and stimulation was used for all trials. Subject 2 also performed control trials for compliance discrimination wherein somatosensory feedback via SCS was not provided. For these trials, objects of three different compliances were presented 10 times in random order resulting in a total of 30 object presentations.

5.2.7.2 Physical DEKA hand Subject 1 was presented with cubes of four different sizes (extra small, small, medium, and large) and identical compliance (Figure 5.2C). The order of presentation was randomized and the subject performed the task without visual feedback. A timeout for object exploration was not enforced, however the subject never

explored an object for more than 10 seconds. The number of presentations for each object during a session was variable. A linear transform between sensor force and stimulation was used for 9, 18, 12, and 16 presentations of the four sizes, respectively. An exponential transform was used for 6, 7, 4, and 4 presentations of the four sizes, respectively (Table 5.1).

Subject 2 was presented with cylinders of three different sizes (small, medium, and large) or compliances (soft, medium, and hard) (Figure 5.4C). The design of these objects was changed from cubes to cylinders to reduce the slippage between the fingers and the corners of objects observed in Subject 1. The subject was given 20 seconds to explore each object. For the size discrimination task, objects of three different sizes (all with hard compliance) were presented 10 times in random order resulting in a total of 30 object presentations. For the compliance discrimination task, three different compliances (all with medium size) were presented 20 times in random order resulting in a total of 60 object presentations. The subject performed the task without visual and audio feedback. A linear transform between sensor force and stimulation was used for all object presentations. Subject 2 also performed control trials for compliance discrimination wherein somatosensory feedback via SCS was not provided. For these trials objects of three different sizes were presented 5 times in random order resulting in a total of 15 object presentations.

5.2.7.3 Statistical Analysis We characterized the relationship between hand aperture, contact force, and stimulation amplitude for each object presentation to identify how size and compliance were encoded through stimulation. This also allows us to postulate on the strategy employed by each subject during the object discrimination task. For each subject, separate multivariate analyses of variance (MANOVA) were performed for object discrimination tasks involving the real and virtual DEKA hand. Size and compliance were the independent variables and hand aperture at stimulation onset, peak amplitude of stimulation and rate of the change of stimulation were the dependent variables. Subsequent univariate analysis (ANOVA) was carried out for each independent variable and follow up *post-hoc* (Tukey-HSD) tests were carried out for dependent variables that displayed a significant effect.

5.3 Results

5.3.1 SCS Evokes Sensory Percepts Localized to the Missing Limb

Three SCS leads were implanted in the cervical epidural space in each of two individuals with upper-limb amputation (Subjects 3 and 4 in Table 4.1 are referred to as Subjects 1 and 2 here). In both subjects, epidural SCS evoked sensory percepts in focal regions of the missing limb including the fingers, palm, and forearm. In this study, we used a subset of electrodes (n=3 in Subject 1, and n=1 in Subject 2) to provide somatotopically-

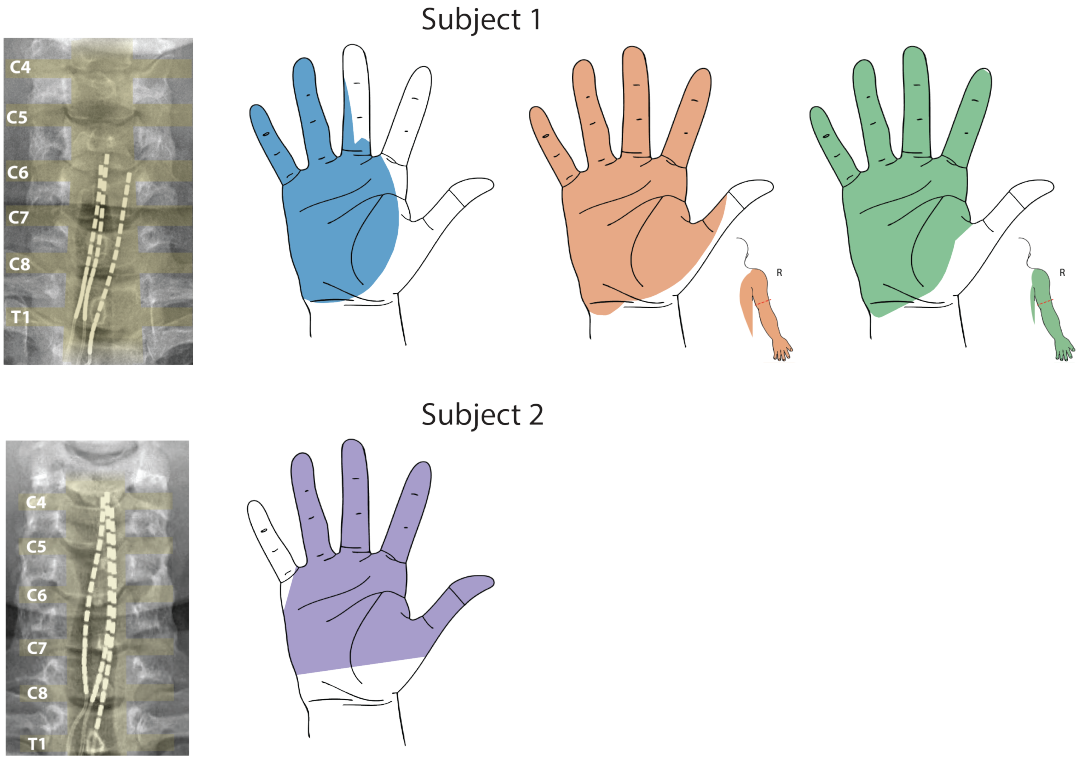

Figure 5.1: Representative sensory percepts for Subjects 1-2. Colored areas represent the stable projected fields of the electrodes that were used during closed loop object discrimination tasks. Each color represents a unique stimulation electrode per subject. Simultaneously evoked percepts in the residual forearm are shown inset for the respective electrodes.

Table 5.2: Comparison of performance on object discrimination task for each sensor-stimulation transform

Subject	Control Environment	Accuracy (%)				
		Size task		Compliance task		
		linear	exponential	linear	exponential	control
1	virtual DEKA	63	74	27	46	-
	real DEKA	58	42	-	-	-
2	virtual DEKA	27	-	51	-	37
	real DEKA	27	-	60	-	47

matched sensory feedback in real-time as subjects interacted with objects of varying size or compliance. Figure 5.1 shows representative sensory percepts evoked by these electrodes that were localized to the missing hand in each subject. A complete overview of the perceptual quality, stability and psychophysical properties of percepts evoked via SCS has been detailed in chapter 4.

5.3.2 SCS Provides Functionally Relevant Somatosensory Feedback

Table 5.2 provides a summary of each subject's performance on the physical and virtual object discrimination task.

5.3.2.1 Subject 1: Size discrimination using the virtual DEKA hand in MuJoCo

Optimal performance using exponential sensor-stimulus transform

To assess the functional utility of somatosensory feedback via SCS, we asked Subject 1 to explore objects of three different sizes and compliances in a virtual environment (MuJoCo) (Figure 5.2A). The subject was most successful in determining the size of the objects using an exponential transformation between sensor force and stimulation amplitude, (Figure 5.2B), with an overall accuracy of 74%. The highest overall accuracy within a single session wherein

objects were presented in random order was 94%. Across multiple sessions, the subject correctly identified large and small objects (92% and 79% accuracy respectively) more often than medium objects (50%). Interestingly, when the subject misidentified medium-sized objects, they were always incorrectly identified as large-sized objects.

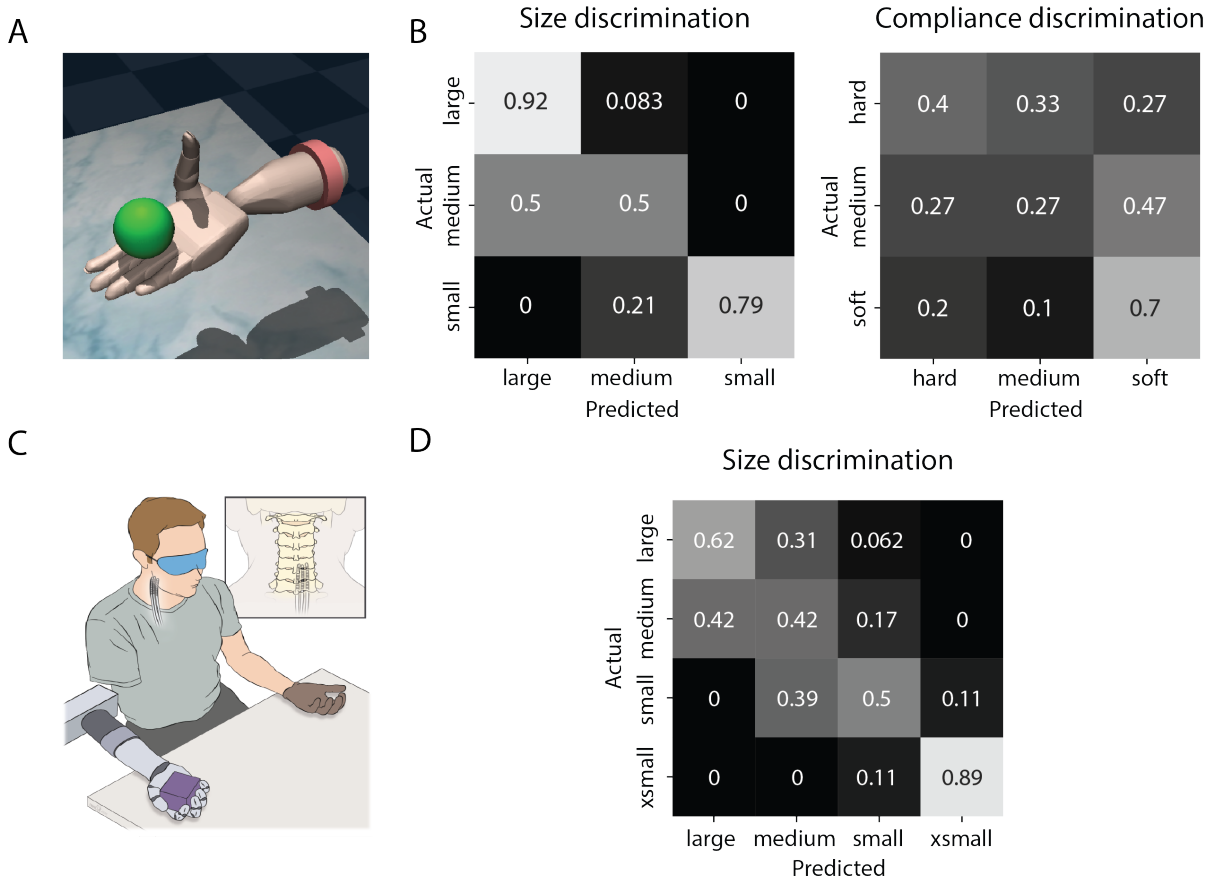

Figure 5.2: Object discrimination results for Subject 1. A) Representation of DEKA hand in MuJoCo virtual environment with spherical object. B) Confusion matrices for object discrimination task using virtual DEKA hand and exponential sensor-stimulus transform. C) Experimental setup for object discrimination task with physical DEKA hand and DataGlove. D) Confusion matrix for object size discrimination task using a linear sensor-stimulus transform.

When performance on the size discrimination task was analyzed for each object compliance (Supplementary Figure C.1A), Subject 1 had the highest accuracy when presented with soft objects (95%) as opposed to medium and hard objects (71% and 54%). Objects with stiffer compliance were frequently misidentified as larger sizes.

Linear Transformation

When a linear transformation between sensor force and stimulation amplitude was used the overall performance on the size detection task decreased to 63% (Figure 5.3A). Moreover, there was greater misidentification between objects of adjacent size when a linear transform was used. Anecdotally, the subject reported that the perceived intensity of stimulation for medium and large objects was very similar. These results indicate that the exponential transform provided optimal separation between the three object sizes.

5.3.2.2 Subject 1: Compliance discrimination using the virtual DEKA hand in MuJoCo

Optimal performance using exponential sensor-stimulus transform

The subject was less accurate when determining object compliance with an overall accuracy of 46% across all sessions and object sizes, and with a peak performance of 50% for a single session when all three compliances were presented in random order. However, the subject was consistently more successful in identifying the soft object (70% accuracy). Furthermore, when identifying object compliance for different object sizes (Supplementary Figure C.1B), the subject performed below chance levels when presented with small objects (overall accuracy 13%) but performance improved as object size increased (27% and 67% for medium and large objects, respectively). Interestingly, for medium and large objects the subject correctly identified soft objects with a high accuracy (100% and 80%) but she could only correctly identify all three compliances at above chance levels for the large object (70%, 50% and 80% for soft, medium and hard respectively).

Linear Transform

Similar to size discrimination when a linear transformation between sensor force and stimulation amplitude was used the overall performance on the compliance detection task decreased to below chance levels (27%).

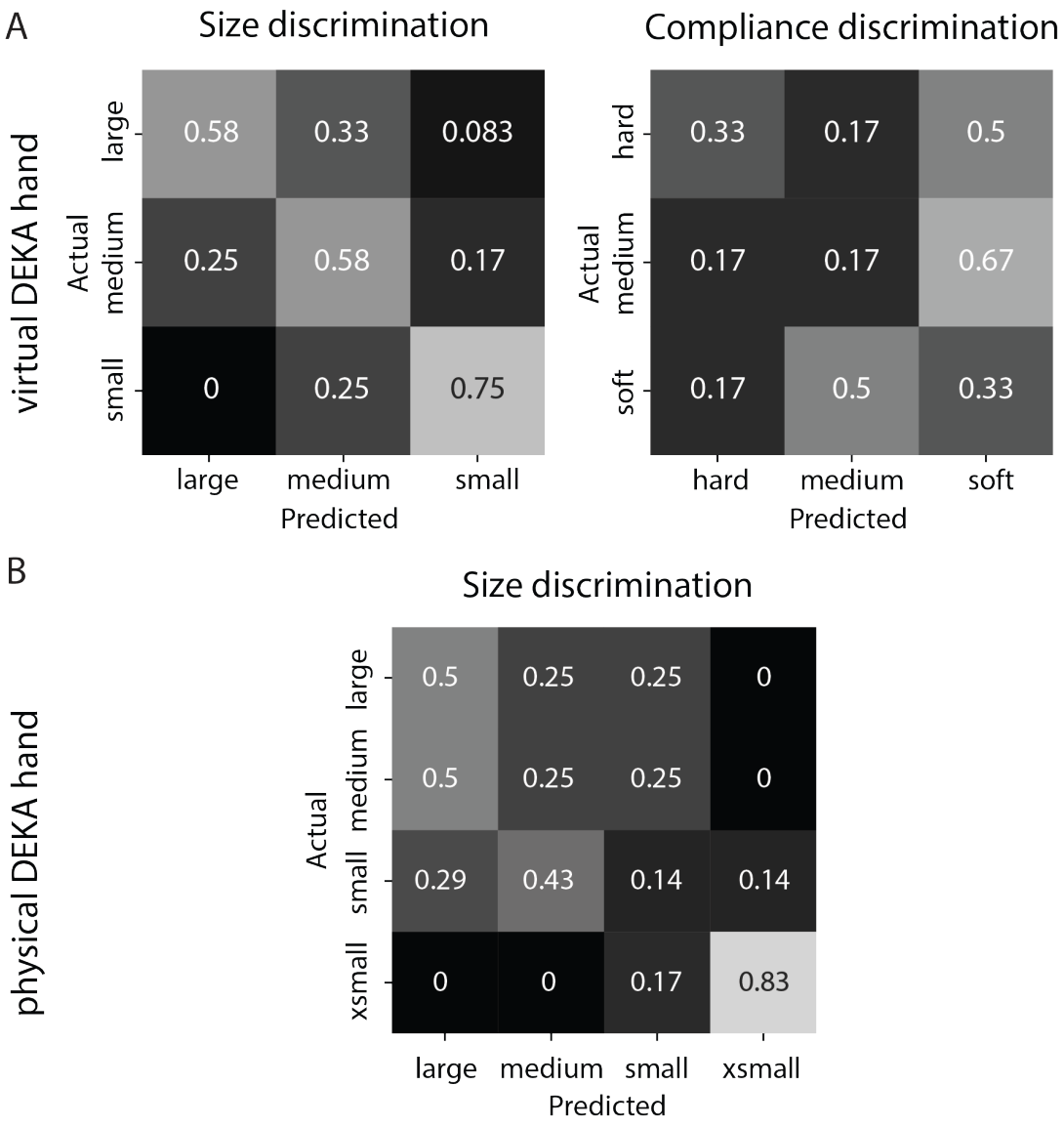

Figure 5.3: A) Comparison of the performance of Subject 1 on the object discrimination task using the virtual DEKA hand and a linear mapping between sensor force and stimulation amplitude. B) Comparison of the performance of Subject 1 on the object discrimination task using the physical DEKA hand and an exponential mapping between sensor force and stimulation amplitude.

5.3.2.3 Subject 1: Size discrimination using the DEKA hand

Optimal performance using using linear sensor-stimulus transform

The subject also used a physical DEKA hand to explore and identify objects of four different sizes with an overall accuracy of 58% (Figure 5.2C). The subject achieved accuracy rates of 89% and 62% with the largest and smallest objects (chance level = 25%), respectively. The confusion matrix (Figure 5.2D) shows that, for the two intermediate sizes, the subject commonly misidentified them as objects of adjacent sizes. Moreover, 52% of all errors were misidentifications of these intermediate objects as the next larger size. This trend was similar to the misidentification of intermediate objects observed with in the virtual environment.

Exponential transform

When an exponential transformation between sensor force and stimulation amplitude was used the overall performance on the size detection task decreased to 42% (Figure 5.3B). For both transforms the extra-small objects were identified with high accuracy (89% and 83% respectively), however, the exponential transform resulted in greater misidentification of all other objects.

5.3.2.4 Subject 2: Size discrimination using the virtual DEKA hand in MuJoCo

Subject 2 also used the virtual DEKA hand to identify object size for hard objects using a linear transformation between sensor force and stimulation amplitude only. The overall accuracy on this task was 27% (below chance levels) (Figure 5.4B). The subject never correctly identified small objects and frequently misidentified medium objects as small objects

.

5.3.2.5 Subject 2: Compliance discrimination using the virtual DEKA hand in MuJoCo

The subject performed the compliance discrimination task for medium-sized objects with an overall accuracy of 51%. The highest overall accuracy within a single session wherein objects were presented in random order was 60%. However, objects of adjacent compliance were frequently misidentified and only the soft objects were identified with an accuracy greater than 50%. Additionally, when sensory feedback was removed during control trials, the overall accuracy decreased to 36% (Supplementary Figure C.3A).

5.3.2.6 Subject 2: Size discrimination using the DEKA hand Subject 2 used the physical DEKA hand to identify three different sizesof cylindrical objects. The overall accuracy on this task was 27% (below chance levels) and was comparable to the performance with the virtual DEKA hand. Accuracy for the size identification task was below chance levels (i.e. 33%) for all sessions of testing.

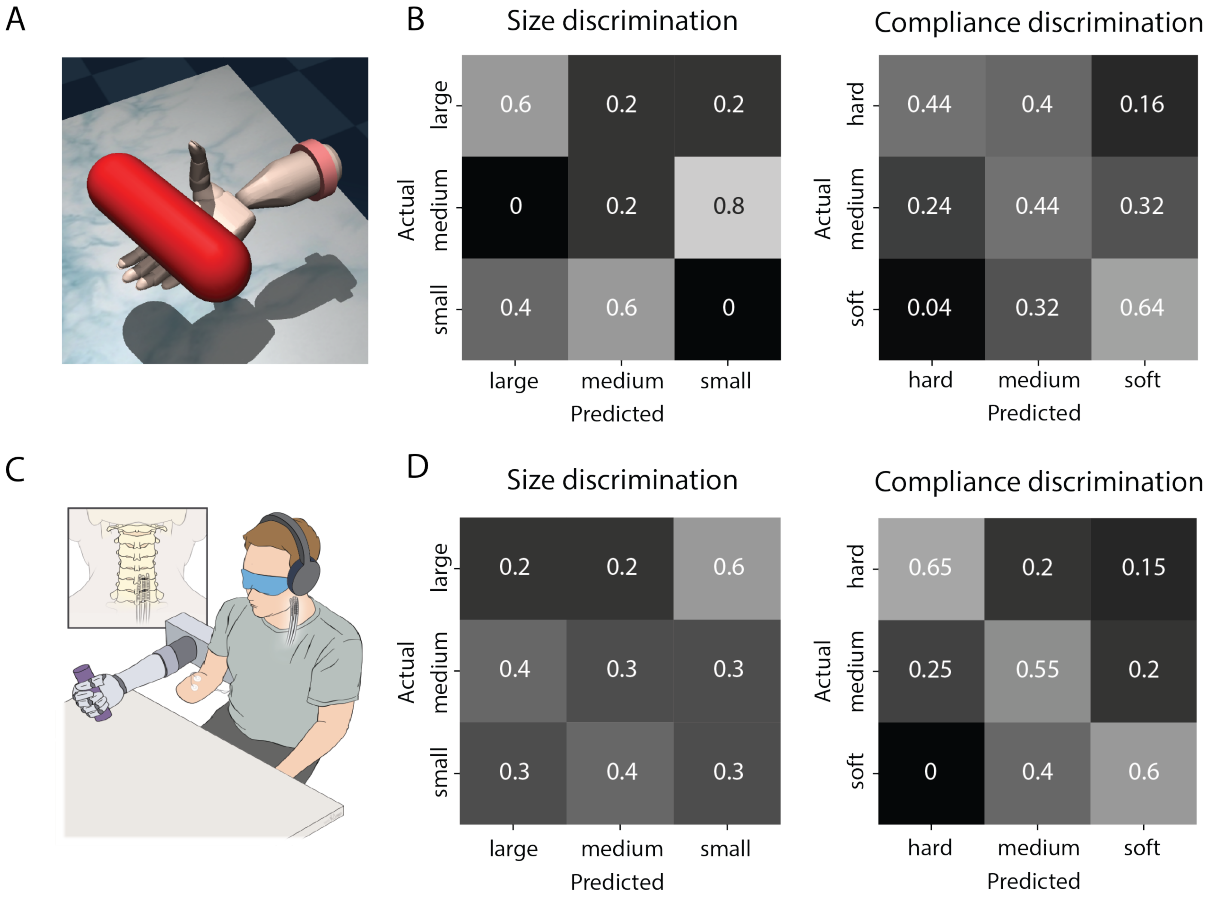

Figure 5.4: A) Representation of DEKA hand in MuJoCo virtual environment with cylindrical object. B) Confusion matrices for object discrimination task performance with virtual DEKA hand using linear sensor-stimulus transform. C) Experimental setup for object discrimination task with physical DEKA hand and ipsilateral EMG electrodes. D) Confusion matrices for object discrimination task using linear sensor-stimulus transform.

5.3.2.7 Subject 2: Compliance discrimination using the DEKA hand Compared to size discrimination, the subject identified the object compliance with a higher overall accuracy (60%). The confusion matrix in Figure 5.4D shows that for compliance detection tasks, the Subject was able to identify the soft, medium, and hard objects with accuracies of 60%, 55%, and 65%, respectively. Similar to the trend observed in Subject 1, 54% of all errors were misidentifications of the object as the next less compliant object. Performance on the compliance discrimination task was similar for small (67%), medium (60%) and large (54%) sized objects (Supplementary Figure C.2). Additionally, when sensory feedback was removed during control trials, the overall accuracy decreased to 46% (Supplementary Figure C.3B).

5.3.3 Object Size and Compliance are Encoded by Independent Features of Stimulation

To understand which features of sensory feedback were used by each subject to determine object size or compliance, we characterized the relationship between hand aperture at stimulation onset, peak amplitude of stimulation, and the rate of change of stimulation for each object presentation (Figures 5.5 and 5.6). For objects with the same size, stimulation onset occurred at the same aperture across multiple trials. Furthermore, for objects with the same size the rate of change of stimulation after object contact and the maximum stimulation amplitude were both dependent on the compliance of the object.

5.3.3.1 Subject 1: virtual DEKA hand in MuJoCo For Subject 1, when using the virtual DEKA hand and an exponential sensor-stimulus transform, size and compliance of the object showed a significant multivariate effect on the contact aperture, peak stimulation amplitude, and rate of change of stimulation as a group. Univariate analysis showed that there was a statistically significant relationship between object size and both contact aperture and peak stimulation amplitude ($p < 0.01$). Post-hoc tests showed that the contact aperture was significantly different ($p < 0.01$) for all object sizes. A separate univariate analysis showed that there was a statistically significant relationship between object compliance and

both the rate of change of stimulation and the peak stimulation amplitude ($p < 0.01$). Post-hoc tests showed that the rate of change of stimulation was significantly different ($p < 0.01$) between hard-medium and hard-soft objects. The peak stimulation amplitude was significantly different for hard and soft objects only ($p < 0.01$).

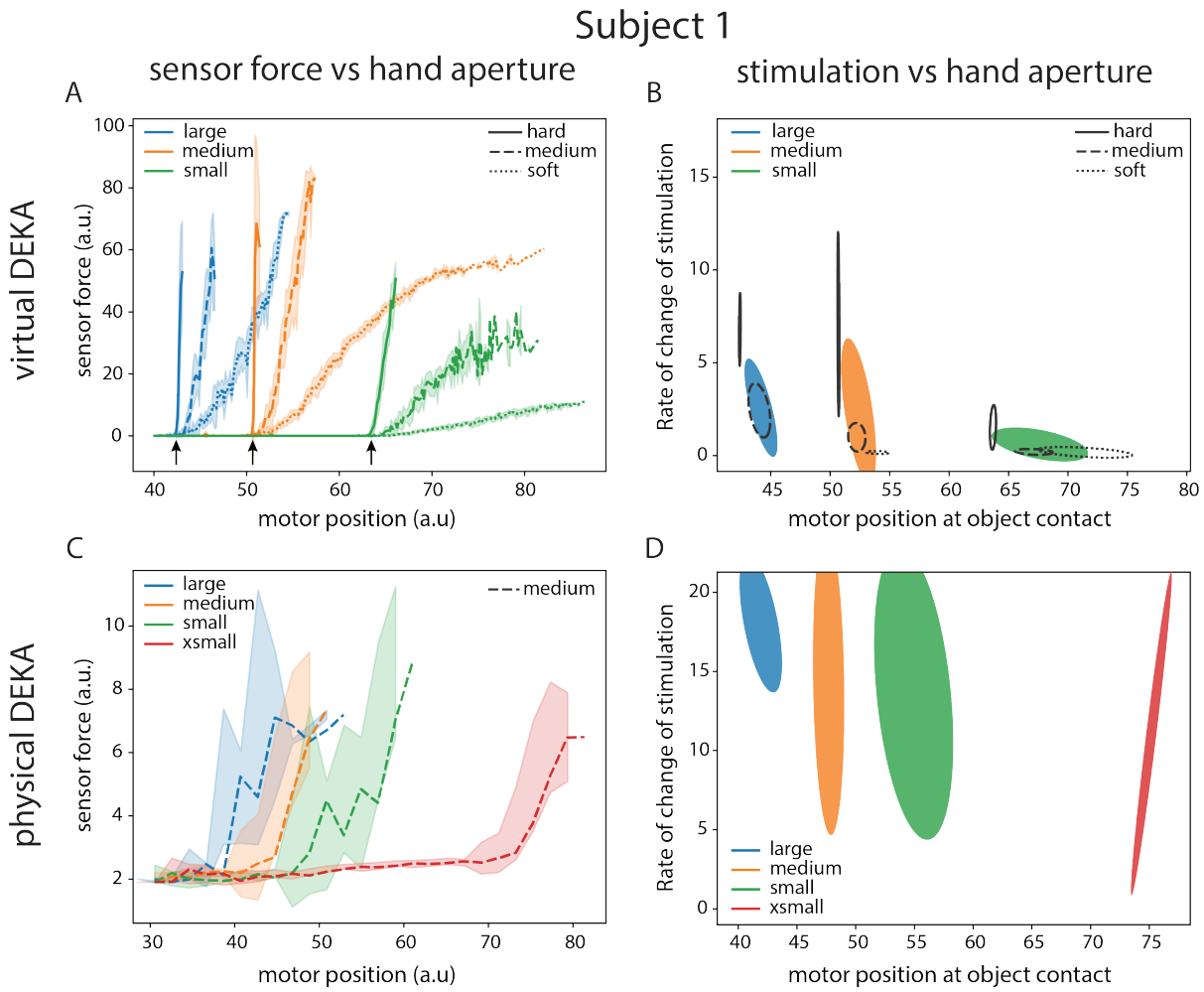

Figure 5.5: Relationship between sensor force and prosthetic hand aperture using the A) virtual DEKA and C) physical DEKA for Subject 1. Standard deviational ellipses for the rate of change of stimulation amplitude and motor position at stimulation onset for each object using the B) virtual DEKA and D) physical DEKA for Subject 1. The color of the lines and ellipses represent object size and the line style represents the compliance of the object. Arrows in panel A represent the approximate motor position at object contact.

These results indicate that for Subject 1 contact aperture contained reliable information regarding object size (Figure 5.5B). The significant difference in contact aperture for all sizes may also explain the subject's high overall accuracy on the size discrimination task (74% accuracy). Conversely, peak stimulation amplitude and the rate of change of stimulation reliably encoded hard and soft objects only resulting in greater misidentification of medium objects and an overall lower accuracy. Supplementary table C.1 summarizes the distribution of stimulation onset times and rate of change of stimulation for each object.

5.3.3.2 Subject 1: physical DEKA hand With the physical DEKA hand and a linear sensor-stimulus transform, object size was the only independent variable since all objects had a medium compliance. Univariate analysis showed that there was a statistically significant relationship between object size and the contact aperture for all sizes and a post-hoc analysis confirmed that the contact aperture was significantly different for each pair of object sizes. This result indicates that the subject could identify object size reliably from contact aperture alone (Figure 5.5D).

5.3.3.3 Subject 2: virtual DEKA hand in MuJoCo For Subject 2, when using the virtual DEKA hand, size and compliance of the object showed a significant multivariate effect on the contact aperture, peak stimulation amplitude, and rate of change of stimulation as a group. Univariate analysis showed that there was a statistically significant relationship between object size and contact aperture ($p < 0.01$) only. Post-hoc tests showed that the contact aperture was significantly different ($p < 0.01$) for all object sizes. A separate univariate analysis also showed that there was a statistically significant relationship between object compliance and contact aperture ($p < 0.01$). Post-hoc tests showed that the contact aperture was significantly different ($p < 0.01$) between hard-medium and hard-soft objects only ($p < 0.01$).

These results indicate that both object size and compliance were encoded in the contact aperture alone. However, this subject was better at identifying object compliance (51%) than size (27%). Additionally, only medium-sized objects were used during the compliance detection task. A one-way ANOVA and subsequent post-hoc analysis confirmed that for

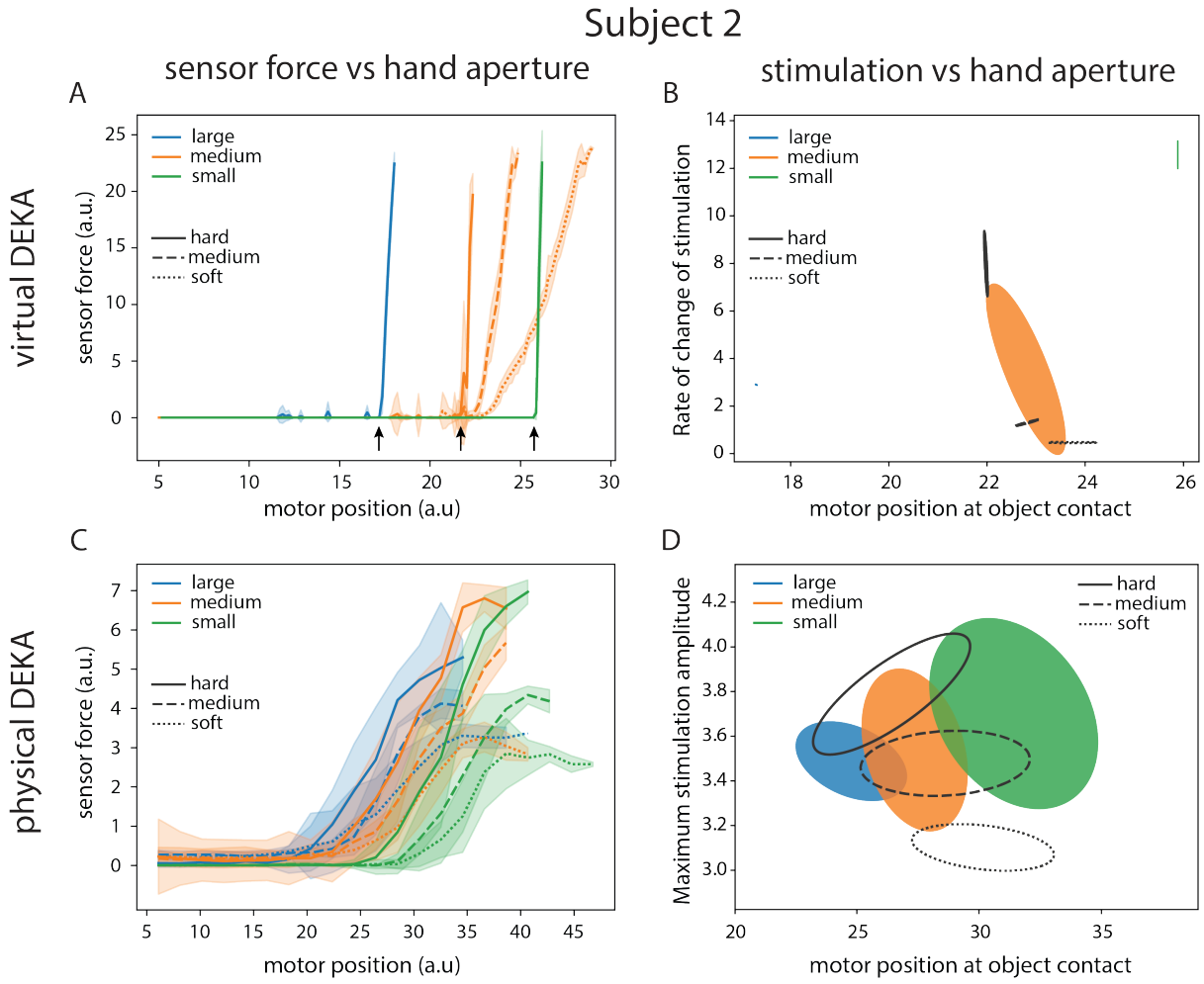

Figure 5.6: Relationship between sensor force and prosthetic hand aperture using the A) virtual DEKA and C) physical DEKA hand for Subject 2. B) Standard deviational ellipses for the rate of change of stimulation amplitude and motor position at stimulation onset for each object using the virtual DEKA hand for Subject 2. D) Standard deviational ellipses for the maximum stimulation amplitude and motor position for each object using the physical DEKA for Subject 2. The color of the lines and ellipses represent object size and the line style represents the compliance of the object. Arrows in panel A represent the approximate motor position at object contact.

medium sized objects there was a significant difference in the rate of change of stimulation for each compliance. Therefore, it is possible that the subject relied on the rate of change of stimulation in addition to the contact aperture, to determined object compliance (Figure 5.6B).

5.3.3.4 Subject 2: physical DEKA hand For the object discrimination task with the physical DEKA hand, size and compliance of the object showed a significant multivariate effect on the contact aperture, peak stimulation amplitude, and rate of change of stimulation as a group. Univariate analysis showed that there was a statistically significant relationship between object size and contact aperture ($p < 0.01$). Post-hoc tests showed that the contact aperture was significantly different ($p < 0.01$) for all object sizes. A separate univariate analysis showed that there was a statistically significant relationship between object compliance and both the contact aperture and the peak stimulation amplitude ($p < 0.01$). Post-hoc tests showed that the peak stimulation amplitude was significantly different for all object compliances ($p < 0.01$). The contact aperture was significantly different ($p < 0.01$) between hard-medium and hard-soft objects only.

These results again indicate that contact aperture encodes the object size and compliance. However, the peak stimulation amplitude conveys additional information regarding the compliance of the object (Figure 5.6D), which may explain the subjects improved performance on the compliance detection task.

5.4 Discussion

5.4.1 Subjects can use Somatosensory Feedback via SCS during an Object Discrimination Task

In this study, we demonstrate that somatotopically-matched real-time feedback provided by SCS can be used by subjects to determine object size or compliance. Subject 1 was consistently more adept at determining object size (up to 74% accuracy) while Subject 2

achieved a higher accuracy level in determining object compliance (up to 60% accuracy). Both subjects could readily use the sensory feedback with minimal training and acclimatization. However, performance varied based on the control strategy (real or virtual DEKA hand) and the sensor-stimulation transformation (linear or exponential).

5.4.2 Task Performance is Dependent on Detection of Features in Stimulation

5.4.2.1 Subject 1 For Subject 1, when using the virtual DEKA hand, an exponential sensor-stimulus transform resulted in highest accuracy on the size discrimination tasks (exponential: 74%, linear: 63%). Whereas with the physical DEKA hand, a linear transformation resulted in highest accuracy for size discrimination (linear: 58%; exponential: 42%). Additionally, for the compliance discrimination task with the virtual DEKA hand an exponential transform resulted in highest accuracy as compared to a linear transform (46% and 27% respectively). For the same SCS electrodes and identical range of stimulation amplitude this observation implies that optimal delivery of somatosensory feedback is dependent on the dynamics of the control system.

Providing true proprioceptive information through artificial somatosensory feedback has consistently been a difficult challenge for somatosensory neuroprostheses. Most studies have provided grasp aperture information by remapping it to a tactile sensation [48] or to a sensation of movement of a specific finger or joint [222]. Recently, it has been shown that grasp aperture information is key to determining object size [48]. Subject 1 had proportional control of the DEKA hand through a DataGlove on her contralateral intact hand. This control strategy provided the subject with information about hand aperture through the intact sensory pathways of proprioception on the contralateral limb. Combined with the onset of stimulation upon object contact, this proprioceptive information could provide a reliable estimate of object size. However, this subject misidentified the medium object in at least 50% of the trials. Our results indicate a significant relationship between grasp aperture and object size. However, the difference in grasp aperture between large, medium, and small objects was 6-8 angular degrees. It is possible that Subject 1 could reliably detect larger changes in angular degrees and therefore performed better when identifying large and

small objects. This suggests that even with natural proprioception, it can be difficult to determine object size without any reference to the adjacent object sizes. Additionally, grasp aperture inferred from the contralateral hand did not provide any information regarding object compliance. The subject's poorer performance on the compliance detection task may be attributed to the inability to reliably detect the rate of change of stimulation after object contact.

5.4.2.2 Subject 2 Subject 2 used an EMG signal to achieve constant velocity control of hand aperture. This method constrained the trajectory of the prosthetic fingers and provided a reliable measure of the stimulation dynamics upon object contact. Additionally, there was no proprioceptive feedback to infer the grasp aperture and the subject had to rely entirely on the rate of change of stimulation and peak stimulation amplitude. Previous studies have shown subjects potentially using this information to discriminate between objects of different compliances [34]. In this study, Subject 2 also showed an improvement (up to 60% accuracy) over Subject 1 in determining object compliance. Our results indicate that object compliance has a strong relationship with stimulation dynamics upon object contact. It is possible that Subject 2 was inherently better at discriminating the rate of change of stimulation (using the virtual DEKA) and the peak stimulus amplitude (using the real DEKA). Her decreased performance in the absence of any stimulation also indicate that she was utilizing feedback delivered via SCS.

Additionally, grasping the object required a sustained elbow flexion (i.e. suprathreshold EMG signal). In the absence of proprioceptive feedback, Subject 2 may have attended to the time delay between the onset of elbow flexion and the onset of stimulation to infer the grasp aperture at object contact. However, the subject was not provided any feedback regarding the state of the EMG signal. Therefore, for each trial the time delay between the onset of elbow flexion and the onset of grasp was variable. The subject could not have reliably estimated grasp aperture from the time delay, and this may explain her decreased accuracy on the size discrimination task.

5.4.3 Considerations for Closed-Loop Prosthesis Design

In this study we have demonstrated that SCS provides somatosensory feedback that subjects can use to identify the size and compliance of objects. However, there are a few shortcomings that could be addressed in future work. The percutaneous SCS study described herein lasted for 29 days in both subjects. Initial experiments focused on mapping evoked percepts and studying their psychophysics. This information is vital to determining the electrodes and stimulation parameters to use during the object discrimination task. However, this also constrained the number of repetitions of the object discrimination task that could administered. Neither subjects had prior experience using a prosthesis, and these tasks were performed without extensive prior training. It is possible that over time subjects can learn to attend to specific changes in the stimulation and improve their performance on the object discrimination tasks. Future work should focus on tracking subject performance across multiple days of using this feedback to interact with objects.

Previously reported psychophysics data showed that both subjects could discriminate three specific intensity levels (72% accuracy) based on trains of stimulation that had three discrete amplitudes. In this study, somatosensory feedback was modulated in real-time. Therefore, subjects had to attend to the dynamics of stimulation (rate of change, peak amplitude) instead of the instantaneous intensity of the evoked percept. However, our psychophysics testing did not quantify subjects' ability to detect changes in stimulation dynamics. In fact, identifying the sensor-stimulus transform that provided optimal separation for different objects was a major challenge. Future work should focus on characterizing the threshold and just-noticeable difference for dynamic properties of stimulation to identify the optimal sensor-stimulus transform.

Additionally, it is worth noting that the object discrimination task used in this study and several other studies is essentially a modified magnitude estimation task. When all other object properties are held constant a single feature of stimulation (e.g. peak amplitude) can encode a distinct property of an object (e.g. compliance). Subjects that can perceive gradation in this feature will demonstrate higher accuracy. However, these results may not generalize to a potential somatosensory neuroprosthesis. When presented with a novel object,

the same features of stimulation may encode multiple object properties and the utility of this feedback may be limited. Studies that monitor subject performance during activities of daily living and novel interactions are necessary to characterize the functional utility of artificial somatosensory feedback.

6.0 Summary of results and Future work

This dissertation chronicles work done towards evaluating a potential somatosensory neural interface at the dorsal roots and the dorsal root ganglia. Specifically, we evaluated the performance of epineural stimulation at the DRG in a feline model, developed a computational model to identify the mechanism of action for DRG stimulation and carried out first-in-human experiments to restore sensation via epidural stimulation in individuals with amputation. There still remains a significant amount of work towards developing a clinically viable somatosensory neuroprosthesis. However, we have established an approach to iterate on the design and efficacy of novel neural interfaces in pre-clinical studies and validate the functional utility of these interfaces in clinical studies.

6.1 Selective Recruitment at the DRG

Selectivity is an important requirement for a somatosensory neural interface to deliver focal feedback. We have shown previously that microstimulation of the lumbar dorsal root ganglia (L5-L7 DRG) using penetrating microelectrodes selectively recruits distal branches of the sciatic and femoral nerves in an acute preparation. However, a variety of challenges limit the clinical translatability of DRG microstimulation via penetrating electrodes. For clinical translation of a DRG somatosensory neural interface, electrodes placed on the epineural surface of the DRG may be a viable path forward.

In chapter 2, we evaluated the recruitment properties of epineural electrodes and compared their performance with that of penetrating electrodes. Specifically, we compared the number of selectively recruited distal nerve branches and the threshold stimulus intensities between penetrating and epineural electrode arrays. Given the diffuse nature of epineural stimulation, we expected less selective recruitment and frequent coactivation of the sciatic and femoral branches. Surprisingly, a majority (67%) of epineural electrodes selectively re-

cruited a single distal branch of the sciatic or femoral nerve at threshold. Overall, epineural stimulation yielded at least one instance of selective recruitment for all instrumented nerves and functionally agonist muscles.

The epineural electrodes we used had a large contact area (∼375 μm), and were placed far (∼1-2 mm) from the neural targets in the DRG, separated by a thick epineurium. As anticipated, epineural stimulation had a higher threshold for selective recruitment however, the dynamic range of selectivity was also significantly higher than that for penetrating electrodes. In the context of clinical translation, a higher dynamic range within which the same population of afferents can be recruited is desirable. It provides a larger parameter space to modulate the subjective quality of percepts and also serves to counter the effect of increased thresholds due to electrode encapsulation or migration.

The pattern of recruitment via epineural stimulation was also consistent with known hindlimb dermatomes such that stimulation at the L5 DRG recruited nerves projecting to the quadriceps and stimulation at the L6 and L7 DRG recruited nerves projecting to distal regions of the foot and ankle. Our results showed that the epineural stimulation at the caudal lumbar DRG provides access to the entire sensory representation of the foot. Despite higher recruitment thresholds, epineural stimulation provides comparable selectivity and superior dynamic range to penetrating electrodes. These results suggest that it may be possible to achieve a highly selective neural interface with the DRG without penetrating the epineurium. An epineural somatosensory interface at the DRG may be sufficient to evoke relevant percepts that are localized to the missing limb in a somatosensory neuroprosthesis for people with an amputation.

Future improvements to these epineural arrays should include a higher number of electrodes with smaller contacts. An array of epineural electrodes with a low pitch may have multiple electrodes recruiting the same nerve or sensory modality. This built-in redundancy is important to compensate for the potential effects of array migration. Furthermore, an increased number of electrodes allows for a larger parameter space within which to vary stimulation. Current steering techniques can be used to fine tune the population of afferents recruited based on their receptive field and modality. In this study all stimulation was delivered in a monopolar configuration with a constant frequency. However, evidence from our

clinical studies with epidural SCS suggests that multipolar stimulation where the frequency is varied, changes the modality of the evoked percept. It is possible that selective recruitment of afferents based on their modality may be independent of the stimulation amplitude. Establishing the relationship between the modality of recruited afferents and specific parameters of stimulation (amplitude, frequency, pulse width) may improve recruitment selectivity and optimize navigation of the parameter space.

Another consideration for the design of epineural arrays is the implant procedure for future clinical studies. For the pre-clinical study described in chapter 2, we performed a laminectomy to expose the DRG and place the electrode arrays. However, we also performed studies in human cadavers to identify less invasive, clinically viable alternatives to a laminectomy. These studies indicated that a small (8-10 mm diameter) foraminotomy at the joint between the vertebrae may expose the spinal root and allow optimal electrode placement at the DRG. While a foraminotomy is a fairly common, minimally invasive, outpatient procedure, significant modifications will be required to steer the electrode array into the foramen and ensure fixation at the DRG. Furthermore, the flexibility of the silicone substrate of the array and adhesion to the surrounding tissue are a challenge that preclude the use of these arrays clinically.

6.2 Mechanism of Afferent Recruitment at the DRG

In addition to selectively recruiting afferents, being able to modulate their response and provide graded feedback is critical for a somatosensory neuroprosthesis. Additionally, since afferents at the DRG do not display any consistent somatotopy, designing electrodes that provide sufficient coverage of the DRG is also necessary. An understanding of the mechanism of recruitment via DRG stimulation and the neural structures that play a role in epineural stimulation are crucial to optimize the delivery of stimulation.

In chapter 3, we developed a computational model of the DRG and sensory afferents to study the mechanism of recruitment via DRG stimulation. We showed that epineural stimulation primarily activated neural structures arranged near the periphery. A majority of

these structures were the excitable initial segment or axon hillocks of afferents at the DRG. In some instances, the large t-junction of pseudounipolar neurons was also recruited. Due to the high stimulation amplitudes and proximity to the electrodes, recruitment of neurons was invariant to the diameter of the axon branches, unlike the reverse recruitment seen in peripheral nerves. Furthermore, this model indicated that the superior dynamic range of epineural stimulation observed in chapter 2 may be due to densely packed large soma and sparse axons at the periphery. This suggests that the neural targets of stimulation via epineural and penetrating electrodes may be different. The comparable selectivity between epineural and penetrating stimulation is due to a combination of anatomical differences and inherent differences in the electrical properties of the neural targets being activated.

A majority of the effort on this project was spent validating the model of the DRG to explain the selectivity results seen in chapter 2. However, future work should use this model and the methodology described herein to optimize the design of novel electrodes. Specifically, this model can be used to perform simulations in which the electrode size, spacing, and location are varied to examine the effects of these geometric properties on neural activation. The overlap in afferent populations recruited for neighboring electrodes and the dynamic range of stimulation for each arrangement of electrodes, can be used to design epineural electrodes that allow for increased selectivity.

Future revisions to this model should also include the diverse modality of afferents present at the DRG. Specifically, including multi-compartment models of Aα, Aδ and C-fibers may help identify the differences in recruitment across fiber types. Additionally, several studies have documented changes in non-nociceptive sensory neurons that may contribute to neuropathic pain post-injury or amputation [230, 231, 232]. Modeling these changes in channel expression and membrane excitability along with novel electrode interfaces may lead to innovations in DRG and spinal cord stimulation that improves patient outcomes.

6.3 Epidural Stimulation to Restore Sensation in Amputees

6.3.1 Upper-Limb Amputees

Restoring somatosensory feedback to people with limb amputations is crucial to improve prosthetic control. Multiple studies have demonstrated that peripheral nerve stimulation and targeted reinnervation can provide somatotopically relevant sensory feedback. While effective, the surgical procedures required for these techniques remain a major barrier to translatability.

In chapter 4, we demonstrated in four people with upper-limb amputation that epidural spinal cord stimulation (SCS), a common clinical technique to treat pain, evoked somatosensory percepts that were perceived as emanating from the missing arm and hand. Over up to 29 days, stimulation evoked sensory percepts in consistent locations in the missing hand regardless of time since amputation or level of amputation. Evoked sensations were occasionally described as naturalistic (e.g. touch or pressure), but were often paresthesias. Increasing stimulus amplitude increased the perceived intensity linearly, without increasing area of the sensations.

We also demonstrated that somatotopically-matched tactile feedback delivered via SCS could be used to discriminate object size and compliance. We observed that one participant performed best in discriminating objects while the other participant performed best in discriminating object compliance. At the same time, discrimination of the other object property in both participants respectively was only slightly above or at chance level. We also showed that the task design and control schema dictated which object property could be reliably determined by the participant using the somatosensory feedback. Our observations suggest that while artificial somatosensory feedback provided via spinal cord stimulation can be readily used to infer information about the real-world with minimal training, the control schema of prosthetic devices dictates the efficacy of this feedback.

6.3.2 Lower-Limb amputees

Lower-limb prostheses provide significant capabilities to lower-limb amputees (LLAs), and have a higher adoption rate than upper-limb prostheses [233]. There are however several deficiencies in the current technology of lower-limb prostheses. A primary concern for LLAs using prostheses is a lowered confidence in maintaining balance and a fear of falling. An important factor in this reduced balance may be the loss of proprioceptive and somatosensory feedback from the amputated limb. In fact, multiple research groups have developed both non-invasive [50] and invasive approaches [32, 234, 235, 41, 42] to restore sensation in the lower limb by stimulating the residual sciatic and tibial nerves. These studies demonstrated that sensory feedback localized to the phantom limb significantly improved the postural stability of LLAs and improved mobility, decreased incidents of falling, and enhanced embodiment of the prosthesis.

A major advantage of using SCS for sensory restoration is that we can target specific dermatomes (or spinal levels) based on the nature of the amputation, with minimal modifications to our electrode implant procedure. Our study described in chapters 4 and 5 demonstrated that cervical SCS can evoke meaningful percepts localized to the amputated limb in upper-limb amputees. We recently extended this study to include lower limb amputees and deliver sensory feedback via lumbosacral (L4-S1) SCS. In two individuals with trans-tibial amputation, we showed that stimulation can evoke percepts in the phantom limb at the calf, ankle, toes and sole of the foot (Figure 6.1). While these are frequently accompanied by sensations in the residual limb, both subjects were able to discriminate them from sensations in the phantom limb. Similar to the observation in upper-limb amputees, we were also able to evoke a variety of sensory modalities with Subject 1 reporting more naturalistic percepts than Subject 2 (Figure 6.2).

Considering these results along with the extensive clinical use of SCS, this approach to somatosensory restoration may be beneficial to a diverse population of amputees, including those with proximal amputations. However, future work should focus on the chronic stability of both the implanted electrodes and the evoked percepts. The study described in chapter 4 utilized commercially available SCS electrodes because of the low barrier to initiating clinical

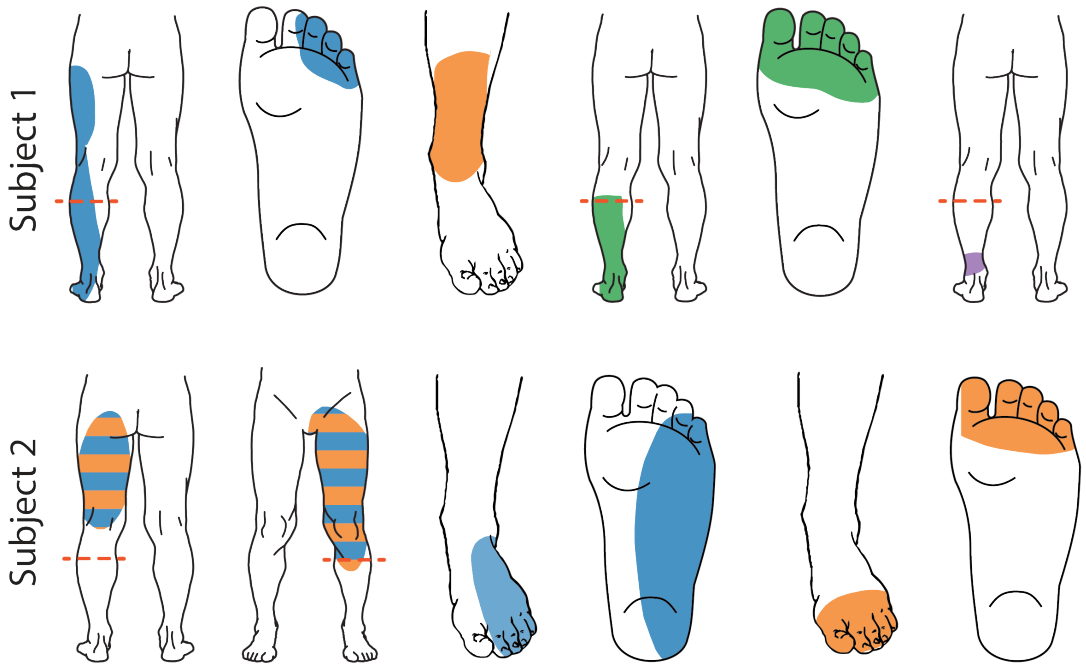

Figure 6.1: Representative sensory percept locations in lower limb amputee subjects. Colored areas represent selected projected fields that were reported for more than two testing sessions and remained stable for at least two weeks. Each color represents a unique stimulation electrode per subject.

studies. These electrodes were not designed for chronic percutaneous implant and mitigating lead migration through surgical techniques (e.g. strain relief loop, securing the electrode to the fascia) or design modifications is critical. A future somatosensory neural interface at the spinal cord will likely require custom electrodes and implantable stimulators that remain stable while the user performs activities of daily living.

Additionally, it is possible that the SCS electrodes we used limited the selectivity and focality of evoked percepts. Smaller electrode contacts that approximate the size and angle of dorsal rootlets as they enter the spinal cord may provide a better interface to target individual rootlets and generate more focal percepts. This approach may also avoid the large residual limb sensations that were evoked in our subjects.

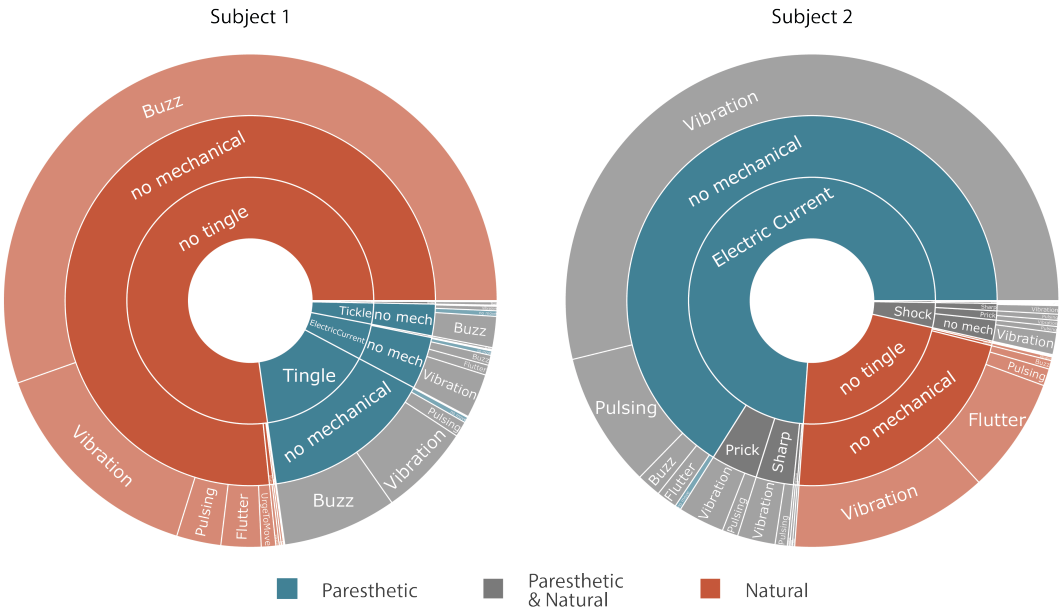

Figure 6.2: Sunburst plot showing the combination of paresthetic (teal), naturalistic (red), and mixed (grey) percept descriptors used by each subject. Subject 1, predominantly reported naturalistic sensations (77.4%) with most of those percepts described as having a low frequency (vibration) or high frequency (buzz) oscillatory component to them. For Subject 2 most sensory percepts were either paresthetic or of mixed modality (73.8%)

Lastly, a thorough investigation of the functional and psychosocial consequences of using a sensory-enabled prosthesis is important. Our study focusing on object discrimination using closed-loop stimulation is a proof-of-concept for how stimulation may be delivered in real-time. However, it is important to monitor and observe how subjects use this feedback in their homes and communities, unconstrained to specific tasks [44]. This will help develop rigorous outcome measures for prosthetic embodiment, self-image, social interaction, and overall quality of life and also highlight user priorities with regards to naturalistic feedback, sensory discrimination, and prosthetic control.

6.4 Understanding Phantom Limb Pain

Beyond the functional deficits that result from amputation, up to 85% of amputees have pain that appears to emanate from their missing limb, known as phantom limb pain (PLP) [236, 237, 238]. PLP has many different presentations, ranging from mild to severe, intermittent to constant, and can have physical, psychological and functional impacts on amputees who experience it. The varying presentations and mechanisms of PLP make it difficult to effectively provide long-term pain relief. Studies have shown that improving sensory discrimination through residual limb stimulation and improving usage of a traditional prosthetic can reduce PLP [239, 240, 241].

In our studies, we administered the McGill Pain questionnaire (MPQ) once before implantation, weekly during the 29-day study, and one month after explant and saw a decrease in MPQ scores over the course of the implant period 6.3. In some subjects this decrease was clinically significant (greater than 5 points) and lasted up to one month after the study was completed. These observations suggest that a neuroprosthetic approach to treatment of PLP via a somatosensory neural interface at the spinal cord may be possible. The primary hypothesis for treatment of pain using SCS is that stimulation activates Aβ fibers, leveraging pain gating mechanisms in the spinal cord [242]. Aβ fibers typically relay information from cutaneous mechanoreceptors that convey touch and pressure-like sensations. It is plausible therefore that the reduction in PLP observed in our subjects was a consequence of evoking percepts in the phantom limb.

Studies have shown that physical activity and psychological factors modulate PLP [243, 244]. By virtue of being enrolled in our study, subjects experience a change in their daily routine. This may confound the reduction in PLP that we observe in these subjects. Nevertheless, characterizing the sensory modality of evoked percepts, and stimulation parameters that are associated with adequate pain control may provide insight in to the mechanism of acute and chronic changes in PLP.

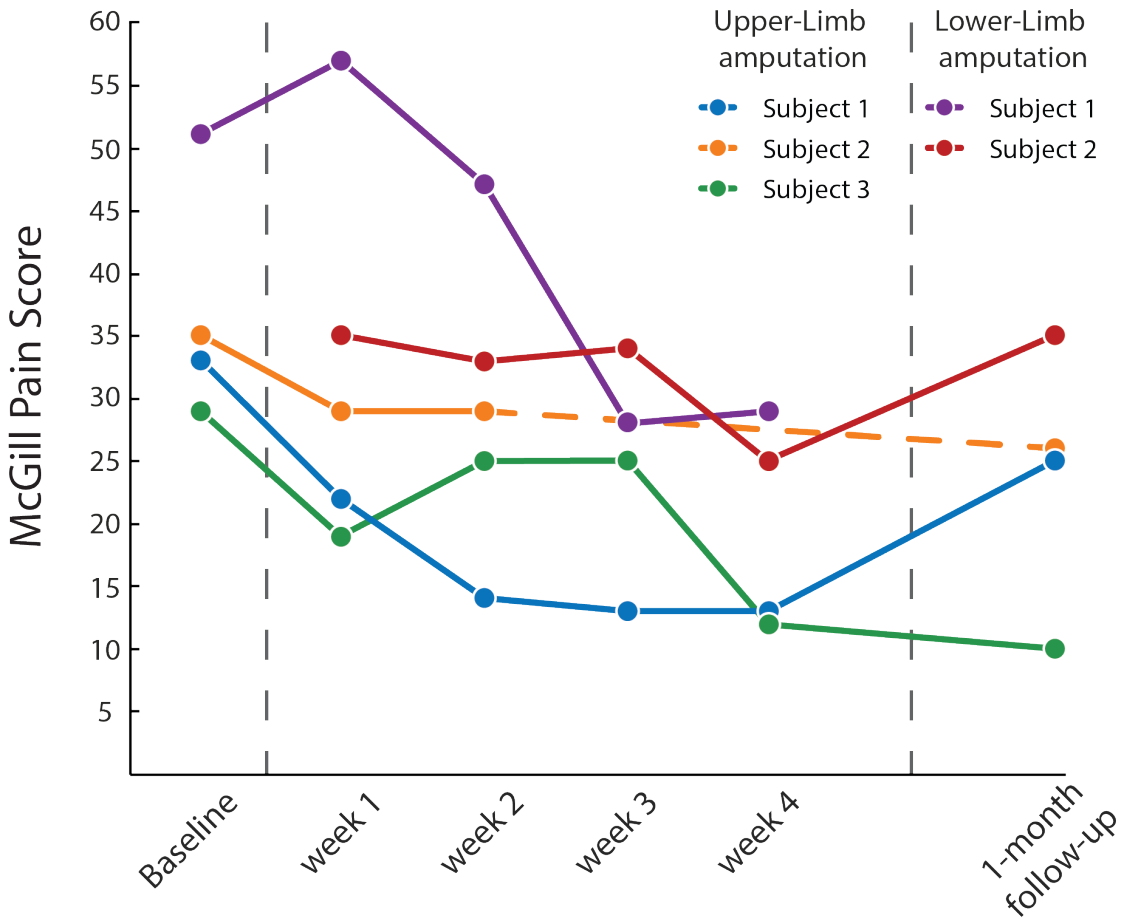

Figure 6.3: McGill Pain Questionnaire (MPQ) scores for phantom limb pain across all amputee subjects. The questionnaire was administered prior to the study to measure baseline PLP and once every week throughout the duration of the study. All subjects showed a clinically significant decrease in their MPQ scores. For two subjects this decrease in PLP lasted up to one month after explant

Additionally, a phenomenon known as proprioceptive memory is thought to contribute to PLP in amputees [245, 246, 247]. The phantom limb is perceived to be in a contorted position and no amount of attempted movement relieves this sensation. In such cases, it is possible that evoking proprioceptive sensations may reduce PLP as well.

6.5 Exploring Proprioception

Proprioception relies on the dynamic activity of a distributed network of afferents and is dependent on higher order processing. The activity of a variety of muscular and cutaneous afferents encodes specific information about the kinematic state of the limb [97]. This activity is integrated in the somatosensory cortex to generate a perception of movement or limb position [248].

Prior studies have shown that single muscle spindle afferents encode joint position but do not produce conscious percepts of joint movement [249]. However, activating an ensemble of cutaneous [250, 251, 252, 253], or muscular [254, 255, 256, 257, 258] afferents can produce illusory movements of the fingers and hand. Additionally, proprioceptive afferents are large diameter fibers with low recruitment thresholds. This suggests that we should be able to readily recruit these afferents and evoke proprioceptive percepts via electrical stimulation. An early study focusing on peripheral nerve stimulation to restore sensory feedback showed that evoked proprioceptive sensations were subtle and subjects had to focus on the stimulation to perceive these sensations [39]. Subsequent studies, including ours (Figure 6.4) have reported occasional movement (or proprioceptive) sensations. However, evoking stable proprioceptive percepts has been far more challenging as compared to tactile or cutaneous sensations.

One possible explanation for the absence of proprioceptive percepts may be the nature of recruitment of these afferents. Cutaneous afferents inhibit pre-synaptic inhibition of proprioceptive afferents [259, 260, 261, 262, 263, 264]. We would expect therefore, that cutaneous and proprioceptive percepts would frequently co-occur. However, it is possible that this circuitry is interrupted when cutaneous afferents are recruited via electrical stimulation. Pre-synaptic inhibition may prevent the recruitment of enough afferents to be generate a conscious percept. This mechanism may also explain why proprioceptive percepts appear vague and subtle. Future work should focus on identifying the mechanism of inhibition of proprioceptive afferents and devise stimulation paradigms to activate proprioceptive and cutaneous afferents selectively.

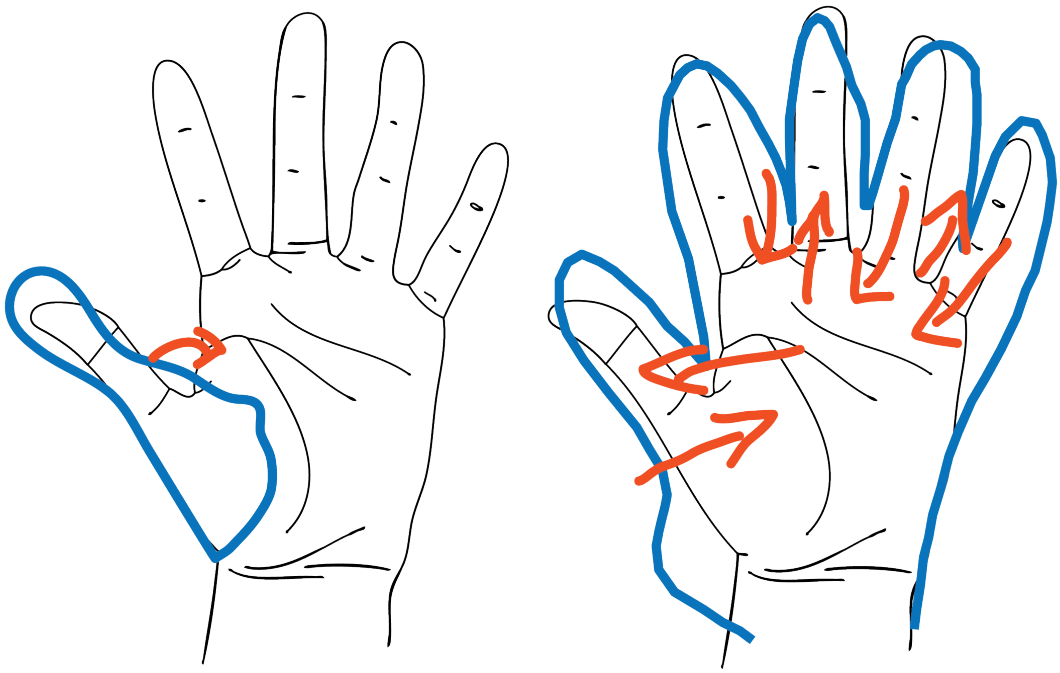

Figure 6.4: Example of a proprioceptive percept evoked in one subject. The subject described feeling his hand opening and closing. On a separate occasion for the same stimulating electrode, he described feeling his thumb flexing and extending

Another possible avenue for evoking proprioceptive percepts may involve replicating the dynamic activity of afferent via stimulation. For our study focused on mapping the location and modality of evoked percepts, we primarily delivered trains of stimulation with constant parameters (amplitude, frequency and pulse width). Instead, delivering time-variable electrical stimulation may replicate the dynamic activity of afferents that convey proprioceptive information. Specifically, using biomimetic stimulus patterns based on muscle spindle firing rates may produce more naturalistic and proprioceptive percepts.

Another factor that may impact artificial proprioception may be higher order processing. While the cortical mechanisms of proprioception and sensory feedback are outside the scope of this thesis, several studies have shown that embodiment and cognitive integration improves prosthesis control and sensory acuity [265, 41]. It is possible that increasingly immersive

experimental paradigms may help subjects focus on their phantom limb and improve the perception of evoked proprioceptive percepts. Advancements in virtual reality (VR) and augmented reality technologies can be used to deliver visuotactile feedback while subjects perform a task in a virtual environment. Future work should focus on developing similar testing paradigms that may improve the embodiment and naturalness of evoked percepts and improve detection of subtle proprioceptive percepts.

Appendix A

Motor Thresholds, ENG Detection Performance and Dynamic Range Statistics

Table A.1: Post-implant nerve cuff motor thresholds. Nerve identities were determined using known anatomical landmarks and verified by finding coarse motor thresholds using a voltage-controlled stimulator.

	Nerve cuff	Motor Threshold (V)			
		G	**H**	**I**	**J**
Femoral branch	Femoral contact 2	0.24	0.36	0.32	0.25
	Femoral contact 4	0.24	0.36	0.48	0.38
	Saphenous	20	6	40	30
	Vastus Medialis	15	0.28	0.27	<0.1
	Vastus Lateralis	0.22	1	-	-
	Sartorius	24	50	0.23	0.4
Sciatic branch	Sciatic contact 2	0.5	0.33	0.3	0.31
	Sciatic contact 4	0.65	0.28	0.36	0.26
	Tibial	0.29	12	0.1	0.18
	Medial Gastrocnemius	0.25	0.14	0.12	0.12
	Lateral Gastrocnemius	0.18	0.15	0.1	0.8
	Distal Tibial	0.18	0.17	0.16	0.28
	Common Peroneal	0.15	18	1	0.21
	Distal Common Peroneal	16	21	0.26	0.32
	Biceps Femoris	27	18	-	-
	Sural	NR	0.26	3.5	4.1

Table A.2: Accuracy of the automated ENG detection algorithm per nerve cuff per epineural stimulation subject. Accuracy was calculated from true positive (TP), true negative (TN), false positive (FP), and false negative (FN) rates using the formula: (TP+TN)/(TP+TN+FP+FN) where an expert reviewer's manual annotations were used as ground truth for detection of ENG responses.

	Nerve cuff	**Detection Accuracy (%)**			
		G	**H**	**I**	**J**
Femoral branch	Femoral Nerve	52.34	76.96	73.94	95.32
	Saphenous	42.02	89.77	89.94	62.79
	Vastus Medialis	45.60	92.34	86.23	77.47
	Vastus Lateralis	46.39	85.36	-	-
	Sartorius	37.71	82.50	90.17	93.79
Sciatic branch	Sciatic Nerve	94.27	96.99	100.00	99.19
	Tibial	97.12	97.76	97.62	76.97
	Lateral Gastrocnemius	93.67	96.79	100.00	97.49
	Medial Gastrocnemius	96.30	95.80	99.40	93.82
	Distal Tibial	96.40	98.23	100.00	92.44
	Common Peroneal	93.33	97.17	91.43	54.84
	Distal Common Peroneal	88.52	98.11	88.22	79.88
	Sural	100.00	-	-	92.90
	Lateral Cutaneous	-	94.50	99.42	74.86
	Medial Cutaneous	-	94.56	99.43	-

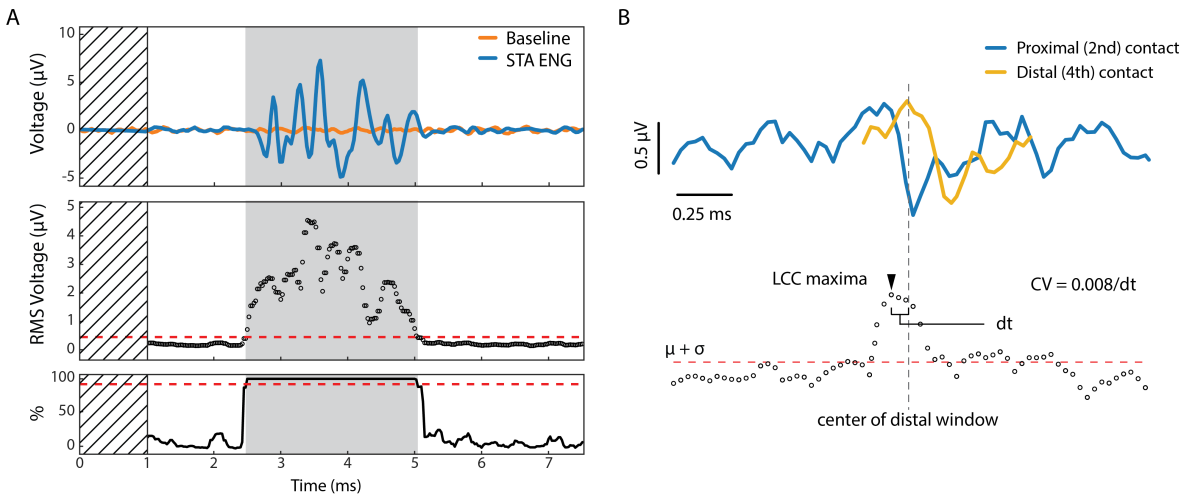

Figure A.1: A) Example of automated ENG detection for a single trial. Top panel shows the stimulus triggered average ENG from the common peroneal nerve (blue) compared to the baseline ENG. Hatched section denotes 1 ms blanking period for stimulation artifact. Middle panel displays the average windowed RMS calculated using a 250 μs sliding window with 25 μs overlap between consecutive windows. Red dashed line indicates 99% confidence interval. Bottom panel shows the percentage of the subsampled averages that were supra-threshold (95%). B) Example of the local cross correlation calculated between ENG recorded on the 2^{nd} (blue) and 4^{th} (yellow) contact of the sciatic nerve cuff. Maximum of LCC is used to calculate the conduction velocity.

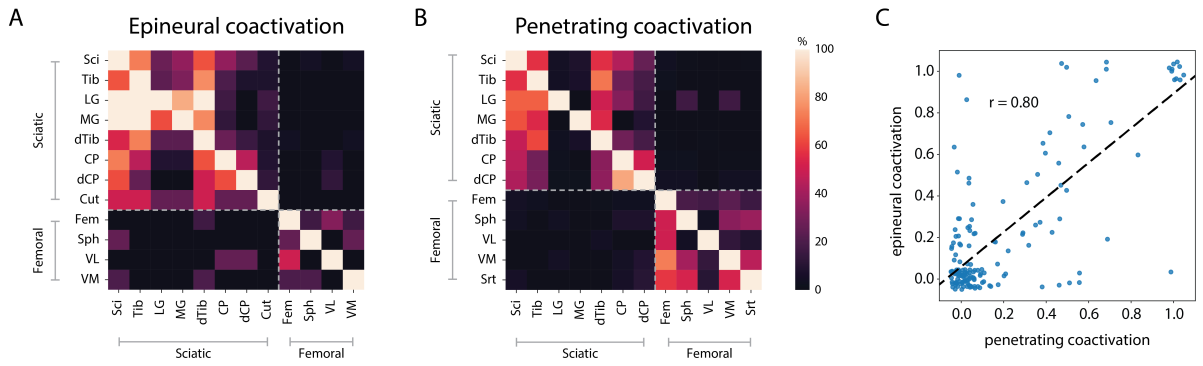

Figure A.2: Normalized coactivation matrix for A) epineural and B) penetrating stimulation calculated by adding the coactivation matrix at each DRG and normalizing the counts in each row by dividing by the total number of times that a given nerve was recruited. C) Relationship between epineural and penetrating coactivation where each dot in the scatter plot represents one active-coactive nerve pair

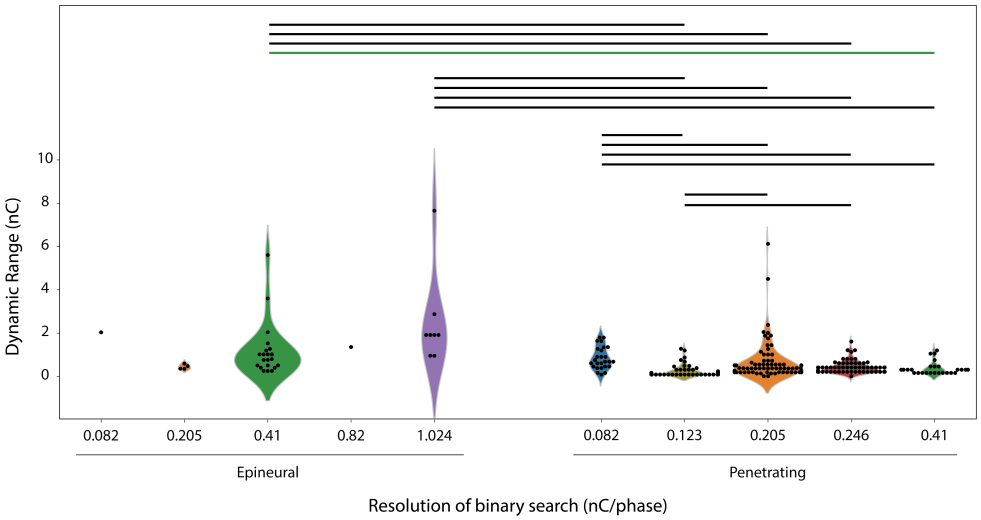

Figure A.3: Distribution of dynamic ranges for each resolution of binary search and electrode type. Horizontal lines indicate distributions with significant differences using Dunn's nonparametric comparisons for post hoc Kruskal-Wallis testing

Appendix B

Receptive Fields and Psychophysics for SCS Electrodes

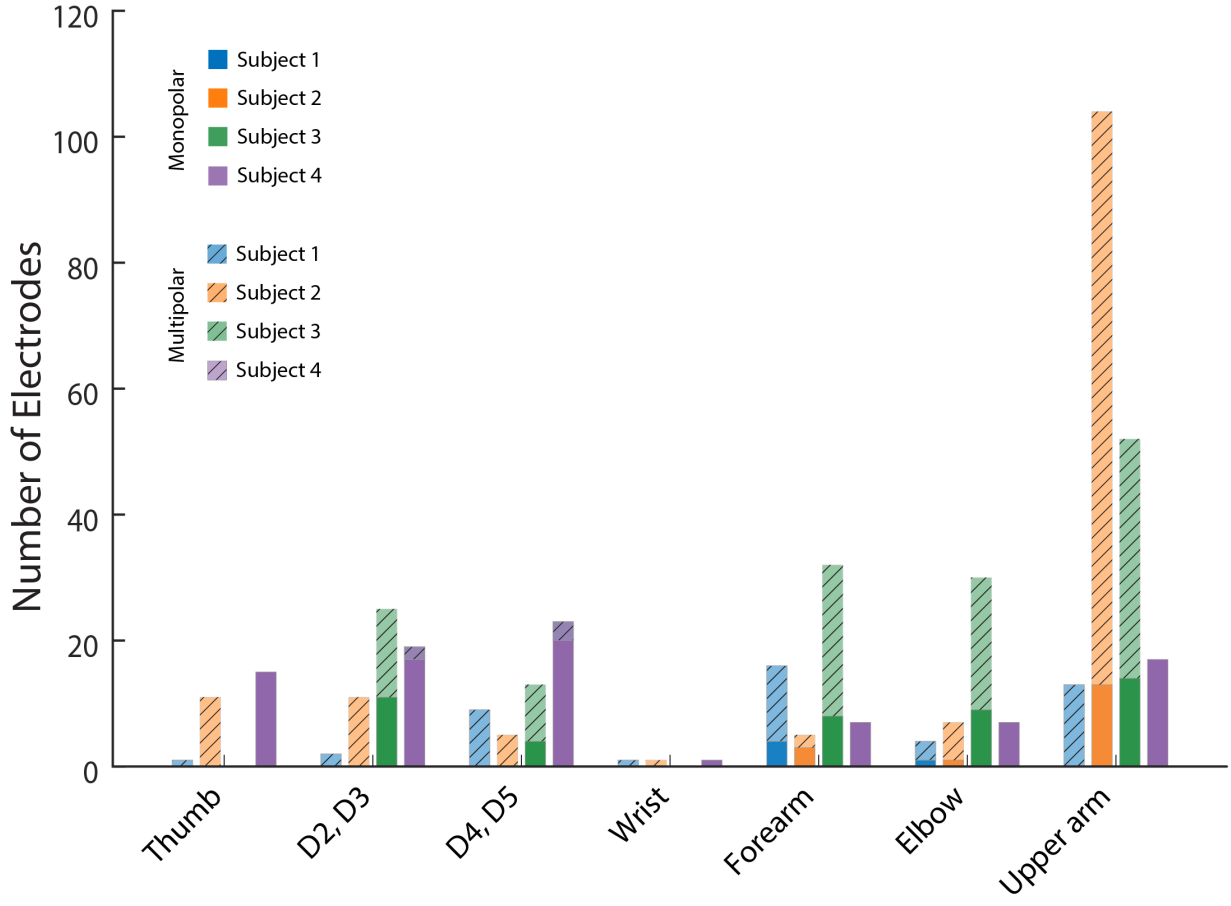

Figure B.1: The number of electrodes that evoked a sensory percept at a specific anatomical location. Lighter, hatched colored bars indicate multipolar electrodes and darker colored bars indicate monopolar electrodes.

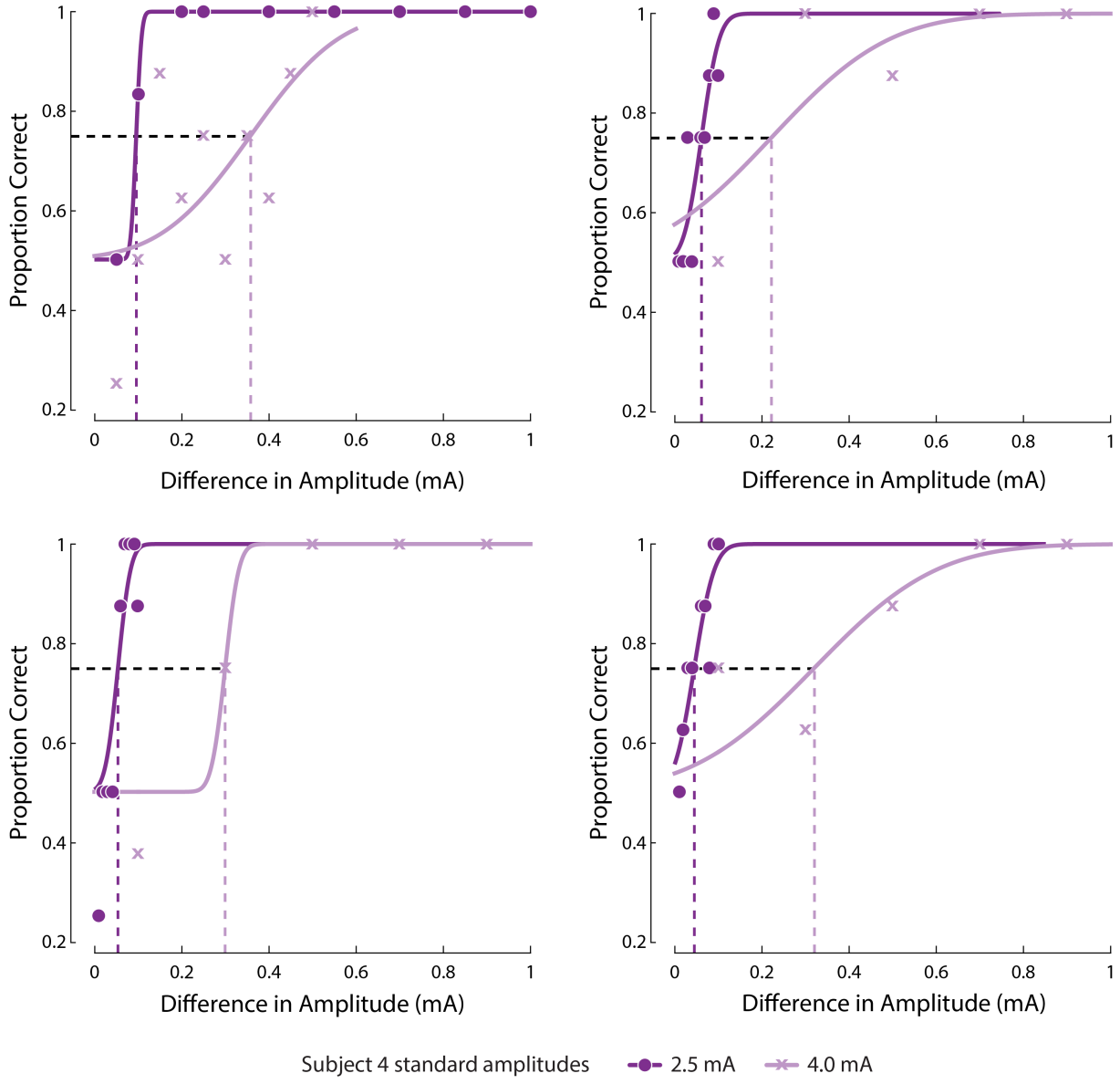

Figure B.2: Psychometric curves fit to response of Subject 4 to JND tasks on 4 electrodes as shown in Figure 4D.

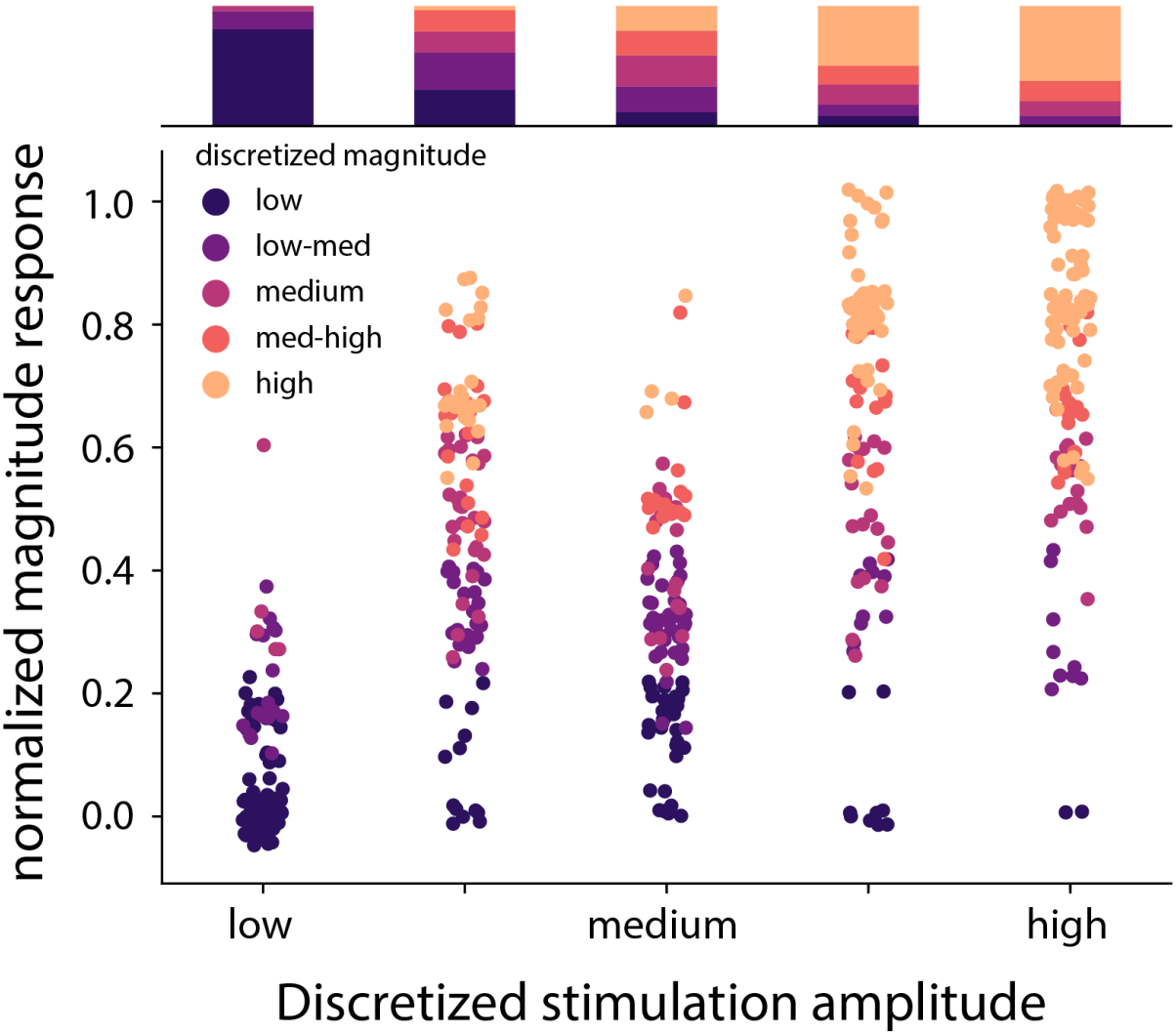

Figure B.3: Confusion matrix for stimulation amplitude and the reported intensity of the evoked percept for all subjects. Stimulation amplitude and reported intensity were independently discretized into five linearly spaced bins. Overall accuracy of predicting stimulation bins from subject ratings of sensation intensity was lower than the three-target task shown in Figure 4F.

Appendix C

Closed-Loop Object Discrimination Task Performance

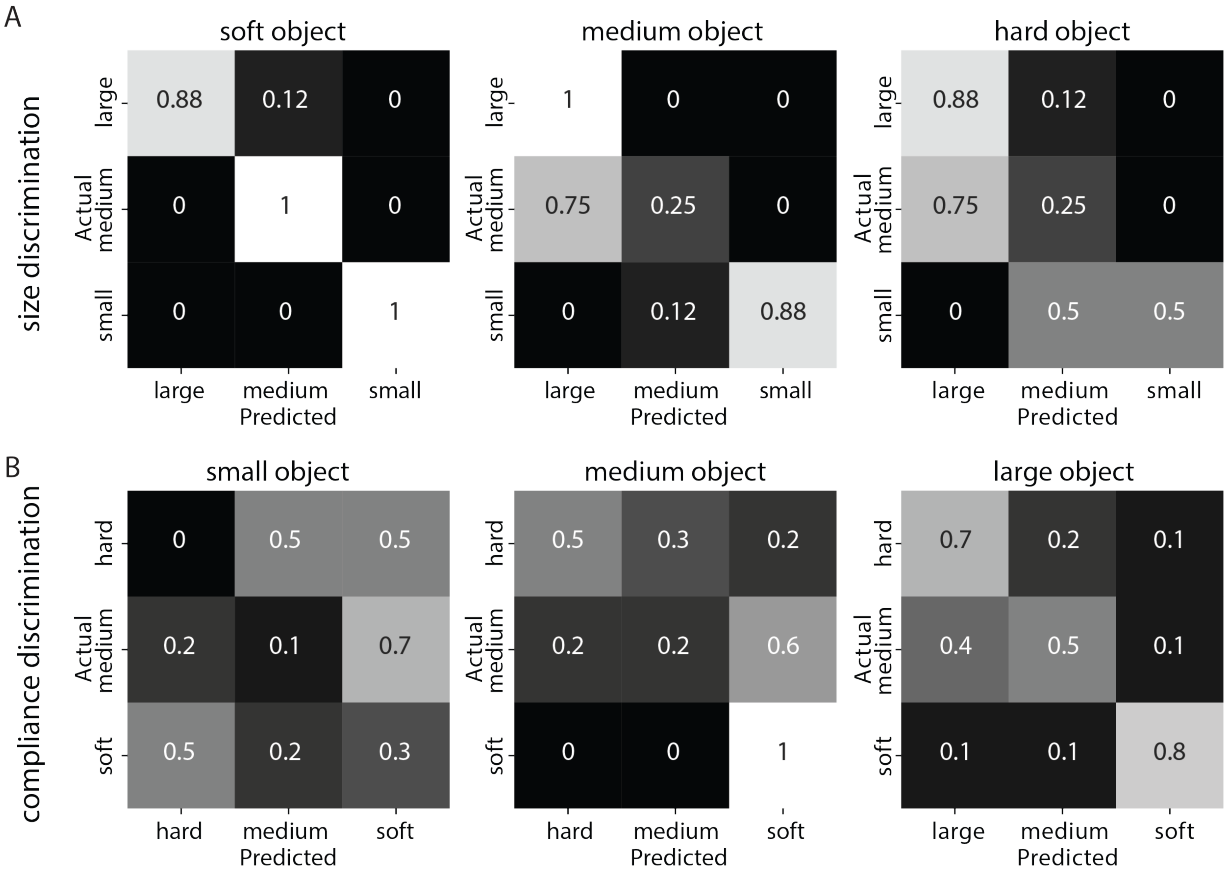

Figure C.1: Confusion matrices for the performance of Subject 1 on the A) compliance discrimination task for each object size and the B) size discrimination task for each object compliance using the virtual DEKA hand.

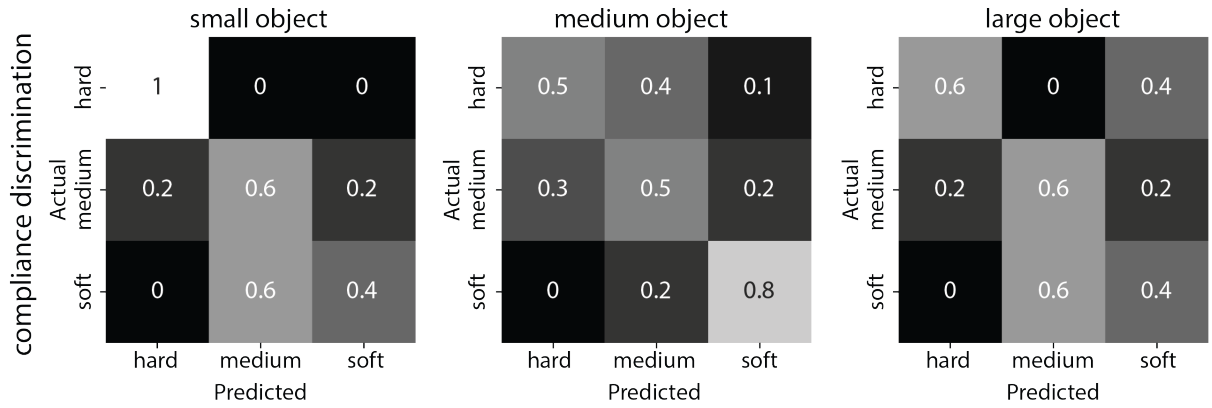

Figure C.2: Confusion matrices for the performance of Subject 2 on the compliance discrimination task for each object size using the physical DEKA hand.

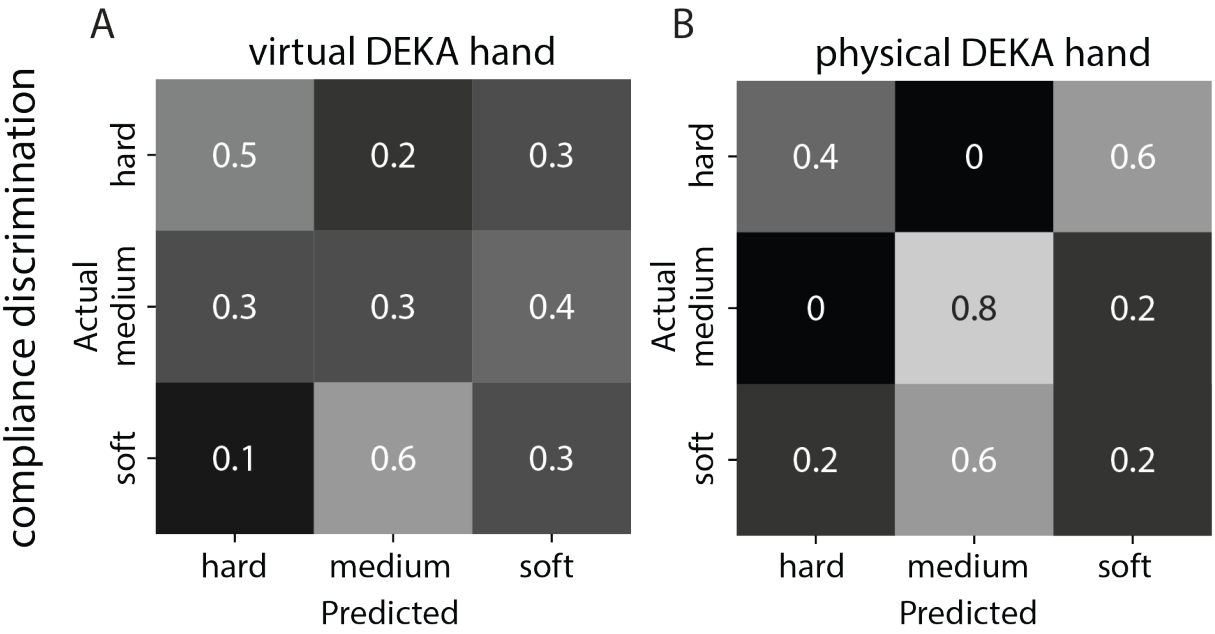

Figure C.3: Confusion matrices for the performance of Subject 2 on the compliance discrimination task in the absence of any somatosensory feedback via SCS using the A) virtual DEKA and B) physical DEKA hand

Table C.1: Summary of hand aperture and stimulation dynamics for each object when using the virtual (MuJoCo) and physical DEKA hand

Subject	Control Environment	Object size	Maximum stimulation amplitude (mA)			Rate of change of stimulation (mA.au-1)			Hand aperture at stim onset (au)		
			hard	medium	soft	hard	medium	soft	hard	medium	soft
1	MuJoCo	large	5.38±0.15	4.6±1.33	4.21±1.5	6.8±1.96	2.44±1.46	0.6±0.35	42.41±0.07	44.05±0.92	45.19±1.14
		medium	4.92±1.4	4.14±1.62	3.2±0.85	7.08±4.96	0.99±0.77	0.17±0.08	50.7±0.08	52.24±0.73	53.98±0.95
		small	3.34±0.87	2.4±0.4	1.9±0.16	1.52±1.2	0.2±0.16	0.18±0.29	63.7±0.26	67.14±1.58	71.46±3.93
	DEKA	large		2.29±0.11			18.04±4.38			41.92±1.81	
		medium		2.32±0.05			14.33±9.68			47.7±1.34	
		small		2.31±0.08			13.6±9.24			54.93±3.37	
		extra small		2.28±0.06			11.16±10.2			75.1±1.9	
2	MuJoCo	large	4.5±0.0			2.9±0.02			17.3±0.02		
		medium	4.5±0.0	4.5±0.01	4.46±0.1	7.99±1.37	1.3±0.15	0.47±0.03	21.98±0.04	22.82±0.27	23.74±0.49
		small	4.5±0.0			12.57±0.58			25.88±0.0		
	DEKA	large	3.58±0.13	3.46±0.07	3.2±0.05	3.28±6.95	2.15±4.12	0.11±0.02	23.6±1.9	25.76±1.49	27.45±1.48
		medium	3.79±0.24	3.53±0.19	3.07±0.12	3.42±5.91	1.61±3.83	0.12±0.06	26.1±1.97	27.69±1.55	29.48±0.72
		small	4.0±0.27	3.42±0.1	3.09±0.05	0.39±0.25	0.29±0.18	0.12±0.01	29.76±2.85	32.96±2.97	34.93±2.74

Bibliography

[1] M. S. Maurer, J. Burcham, and H. Cheng, "Diabetes mellitus is associated with an increased risk of falls in elderly residents of a long-term care facility," *The Journals of Gerontology. Series A, Biological Sciences and Medical Sciences*, vol. 60, pp. 1157–1162, Sept. 2005.

[2] J. N. Sanes, K. H. Mauritz, E. V. Evarts, M. C. Dalakas, and A. Chu, "Motor deficits in patients with large-fiber sensory neuropathy.," *Proceedings of the National Academy of Sciences of the United States of America*, vol. 81, pp. 979–982, Feb. 1984.

[3] R. L. Sainburg, H. Poizner, and C. Ghez, "Loss of proprioception produces deficits in interjoint coordination," *Journal of Neurophysiology*, vol. 70, pp. 2136–2147, Nov. 1993.

[4] J. D. Cole and E. M. Sedgwick, "The perceptions of force and of movement in a man without large myelinated sensory afferents below the neck.," *The Journal of Physiology*, vol. 449, pp. 503–515, Apr. 1992.

[5] P. X. Ku, N. A. Abu Osman, and W. A. B. Wan Abas, "Balance control in lower extremity amputees during quiet standing: a systematic review," *Gait & Posture*, vol. 39, pp. 672–682, Feb. 2014.

[6] N. Vanicek, S. Strike, L. McNaughton, and R. Polman, "Postural Responses to Dynamic Perturbations in Amputee Fallers Versus Nonfallers: A Comparative Study With Able-Bodied Subjects," *Archives of Physical Medicine and Rehabilitation*, vol. 90, pp. 1018–1025, June 2009.

[7] G. Fernie and P. Holliday, "Postural sway in amputees and normal subjects.," *The Journal of Bone & Joint Surgery*, vol. 60, pp. 895–898, Oct. 1978.

[8] T. M. Quai, S. G. Brauer, and J. C. Nitz, "Somatosensation, circulation and stance balance in elderly dysvascular transtibial amputees:," *Clinical Rehabilitation*, July 2016. Publisher: SAGE PublicationsSage CA: Thousand Oaks, CA.

[9] L. J. Kozak and M. F. Owings, "Ambulatory and inpatient procedures in the United States, 1995," *Vital and Health Statistics. Series 13, Data from the National Health Survey*, vol. 13, pp. 1–116, Mar. 1998.

[10] E. Biddiss, D. Beaton, and T. Chau, "Consumer design priorities for upper limb prosthetics," *Disability and Rehabilitation: Assistive Technology*, vol. 2, pp. 346–357, Jan. 2007. Publisher: Taylor & Francis _eprint: https://doi.org/10.1080/17483100701714733.

[11] F. Cordella, A. L. Ciancio, R. Sacchetti, A. Davalli, A. G. Cutti, E. Guglielmelli, and L. Zollo, "Literature review on needs of upper limb prosthesis users," *Frontiers in Neuroscience*, vol. 10, no. MAY, pp. 1–14, 2016.

[12] E. A. Biddiss and T. T. Chau, "Upper limb prosthesis use and abandonment: A survey of the last 25 years," *Prosthetics and Orthotics International*, vol. 31, no. 3, pp. 236–257, 2007.

[13] T. R. Dillingham, L. E. Pezzin, E. J. MacKenzie, and A. R. Burgess, "Use and Satisfaction with Prosthetic Devices Among Persons with Trauma-Related Amputations: A Long-Term Outcome Study," *American Journal of Physical Medicine & Rehabilitation*, vol. 80, pp. 563–571, Aug. 2001.

[14] R. Gailey, L. V. McFarland, R. A. Cooper, J. Czerniecki, J. M. Gambel, S. Hubbard, C. Maynard, D. G. . Smith, M. Raya, and G. E. Reiber, "Unilateral lower-limb loss: Prosthetic device use and functional outcomes in servicemembers from Vietnam war and OIF/OEF conflicts," *The Journal of Rehabilitation Research and Development*, vol. 47, no. 4, p. 317, 2010.

[15] I. Cuberovic, A. Gill, L. J. Resnik, D. J. Tyler, and E. L. Graczyk, "Learning of Artificial Sensation Through Long-Term Home Use of a Sensory-Enabled Prosthesis," *Frontiers in Neuroscience*, vol. 13, 2019.

[16] P. D. Marasco, K. Kim, J. E. Colgate, M. A. Peshkin, and T. A. Kuiken, "Robotic touch shifts perception of embodiment to a prosthesis in targeted reinnervation amputees," *Brain*, vol. 134, pp. 747–758, Mar. 2011.

[17] H. P. Saal and S. J. Bensmaia, "Touch is a team effort: interplay of submodalities in cutaneous sensibility," *Trends in Neurosciences*, vol. 37, pp. 689–697, Dec. 2014.

[18] R. W. Mann, "Paper 15: Efferent and Afferent Control of an Electromyographic, Proportional-Rate, Force Sensing Artificial Elbow with Cutaneous Display of Joint Angle," *Proceedings of the Institution of Mechanical Engineers, Conference Proceedings*, vol. 183, pp. 86–92, Sept. 1968. Publisher: IMECHE.

[19] R. W. Mann and S. D. Reimers, "Kinesthetic Sensing for the EMG Controlled "Boston Arm"," *IEEE Transactions on Man-Machine Systems*, vol. 11, pp. 110–115, Mar. 1970. Conference Name: IEEE Transactions on Man-Machine Systems.

[20] G. K. Patel, S. Dosen, C. Castellini, and D. Farina, "Multichannel electrotactile feedback for simultaneous and proportional myoelectric control," *Journal of Neural Engineering*, vol. 13, no. 5, p. 056015, 2016.

[21] M. Štrbac, M. Belić, M. Isaković, V. Kojić, G. Bijelić, I. Popović, M. Radotić, S. Došen, M. Marković, D. Farina, and T. Keller, "Integrated and flexible multichannel interface for electrotactile stimulation," *Journal of Neural Engineering*, vol. 13, no. 4, p. 046014, 2016.

[22] M. Strbac, M. Isakovic, M. Belic, I. Popovic, I. Simanic, D. Farina, T. Keller, and S. Dosen, "Short- and Long-Term Learning of Feedforward Control of a Myoelectric Prosthesis with Sensory Feedback by Amputees," *IEEE transactions on neural systems and rehabilitation engineering: a publication of the IEEE Engineering in Medicine and Biology Society*, vol. 25, no. 11, pp. 2133–2145, 2017.

[23] H. J. B. Witteveen, E. A. Droog, J. S. Rietman, and P. H. Veltink, "Vibro- and electrotactile user feedback on hand opening for myoelectric forearm prostheses," *IEEE transactions on bio-medical engineering*, vol. 59, pp. 2219–2226, Aug. 2012.

[24] E. Raveh, S. Portnoy, and J. Friedman, "Myoelectric Prosthesis Users Improve Performance Time and Accuracy Using Vibrotactile Feedback When Visual Feedback Is Disturbed," *Archives of Physical Medicine and Rehabilitation*, vol. 99, no. 11, pp. 2263–2270, 2018.

[25] P. B. Shull and D. D. Damian, "Haptic wearables as sensory replacement, sensory augmentation and trainer – a review," *Journal of NeuroEngineering and Rehabilitation*, vol. 12, p. 59, July 2015.

[26] C. E. Stepp, Q. An, and Y. Matsuoka, "Repeated Training with Augmentative Vibrotactile Feedback Increases Object Manipulation Performance," *PLOS ONE*, vol. 7, p. e32743, Feb. 2012. Publisher: Public Library of Science.

[27] C. Antfolk, M. D'Alonzo, M. Controzzi, G. Lundborg, B. Rosén, F. Sebelius, and C. Cipriani, "Artificial redirection of sensation from prosthetic fingers to the phantom hand map on transradial amputees: vibrotactile versus mechanotactile sensory feedback," *IEEE transactions on neural systems and rehabilitation engineering: a publication of the IEEE Engineering in Medicine and Biology Society*, vol. 21, pp. 112–120, Jan. 2013.

[28] D. Zhang, H. Xu, P. B. Shull, J. Liu, and X. Zhu, "Somatotopical feedback versus non-somatotopical feedback for phantom digit sensation on amputees using electrotactile stimulation," *Journal of NeuroEngineering and Rehabilitation*, vol. 12, May 2015.

[29] G. Chai, D. Zhang, and X. Zhu, "Developing Non-Somatotopic Phantom Finger Sensation to Comparable Levels of Somatotopic Sensation through User Training With Electrotactile Stimulation," *IEEE transactions on neural systems and rehabilitation engineering: a publication of the IEEE Engineering in Medicine and Biology Society*, vol. 25, no. 5, pp. 469–480, 2017.

[30] D. W. Tan, M. A. Schiefer, M. W. Keith, J. R. Anderson, J. Tyler, and D. J. Tyler, "A neural interface provides long-term stable natural touch perception," *Science Translational Medicine*, vol. 6, pp. 257ra138–257ra138, Oct. 2014. Publisher: American Association for the Advancement of Science Section: Research Article.

[31] E. L. Graczyk, M. A. Schiefer, H. P. Saal, B. P. Delhaye, S. J. Bensmaia, and D. J. Tyler, "The neural basis of perceived intensity in natural and artificial touch," *Science Translational Medicine*, vol. 8, pp. 362ra142–362ra142, Oct. 2016.

[32] H. Charkhkar, C. E. Shell, P. D. Marasco, G. J. Pinault, D. J. Tyler, and R. J. Triolo, "High-density peripheral nerve cuffs restore natural sensation to individuals with lower-limb amputations," *Journal of Neural Engineering*, vol. 15, p. 056002, July 2018. Publisher: IOP Publishing.

[33] K. Horch, S. Meek, T. G. Taylor, and D. T. Hutchinson, "Object discrimination with an artificial hand using electrical stimulation of peripheral tactile and proprioceptive pathways with intrafascicular electrodes," *IEEE Transactions on Neural Systems and Rehabilitation Engineering*, vol. 19, no. 5, pp. 483–489, 2011.

[34] S. Raspopovic, M. Capogrosso, F. M. Petrini, M. Bonizzato, J. Rigosa, G. D. Pino, J. Carpaneto, M. Controzzi, T. Boretius, E. Fernandez, G. Granata, C. M. Oddo, L. Citi, A. L. Ciancio, C. Cipriani, M. C. Carrozza, W. Jensen, E. Guglielmelli, T. Stieglitz, P. M. Rossini, and S. Micera, "Restoring Natural Sensory Feedback in

Real-Time Bidirectional Hand Prostheses," *Science Translational Medicine*, vol. 6, pp. 222ra19–222ra19, Feb. 2014. Publisher: American Association for the Advancement of Science Section: Research Article.

[35] G. Valle, A. Mazzoni, F. Iberite, E. D'Anna, I. Strauss, G. Granata, M. Controzzi, F. Clemente, G. Rognini, C. Cipriani, T. Stieglitz, F. M. Petrini, P. M. Rossini, and S. Micera, "Biomimetic Intraneural Sensory Feedback Enhances Sensation Naturalness, Tactile Sensitivity, and Manual Dexterity in a Bidirectional Prosthesis Case Study Biomimetic Intraneural Sensory Feedback Enhances Sensation Naturalness, Tactile Sensitivity, and Man," *Neuron*, vol. 100, pp. 1–9, 2018.

[36] T. S. Davis, H. A. C. Wark, D. T. Hutchinson, D. J. Warren, K. O'Neill, T. Scheinblum, G. A. Clark, R. A. Normann, and B. Greger, "Restoring motor control and sensory feedback in people with upper extremity amputations using arrays of 96 microelectrodes implanted in the median and ulnar nerves," *Journal of Neural Engineering*, vol. 13, p. 036001, Mar. 2016. Publisher: IOP Publishing.

[37] J. A. George, D. T. Kluger, T. S. Davis, S. M. Wendelken, V. E. Okorokova, Q. He, C. C. Duncan, D. T. Hutchinson, Z. C. Thumser, D. T. Beckler, P. D. Marasco, S. J. Bensmaia, and G. A. Clark, "Biomimetic sensory feedback through peripheral nerve stimulation improves dexterous use of a bionic hand," *Science Robotics*, vol. 4, no. 32, p. eaax2352, 2019.

[38] P. M. Rossini, S. Micera, A. Benvenuto, J. Carpaneto, G. Cavallo, L. Citi, C. Cipriani, L. Denaro, V. Denaro, G. Di Pino, F. Ferreri, E. Guglielmelli, K.-P. Hoffmann, S. Raspopovic, J. Rigosa, L. Rossini, M. Tombini, and P. Dario, "Double nerve intraneural interface implant on a human amputee for robotic hand control," *Clinical Neurophysiology*, vol. 121, pp. 777–783, May 2010.

[39] G. S. Dhillon, S. M. Lawrence, D. T. Hutchinson, and K. W. Horch, "Residual function in peripheral nerve stumps of amputees: implications for neural control of artificial limbs," *The Journal of Hand Surgery*, vol. 29, pp. 605–615, July 2004.

[40] G. S. Dhillon, T. B. Krüger, J. S. Sandhu, and K. W. Horch, "Effects of Short-Term Training on Sensory and Motor Function in Severed Nerves of Long-Term Human Amputees," *Journal of Neurophysiology*, vol. 93, pp. 2625–2633, May 2005. Publisher: American Physiological Society.

[41] F. M. Petrini, M. Bumbasirevic, G. Valle, V. Ilic, P. Mijović, P. Čvančara, F. Barberi, N. Katic, D. Bortolotti, D. Andreu, K. Lechler, A. Lesic, S. Mazic, B. Mijović, D. Guiraud, T. Stieglitz, A. Alexandersson, S. Micera, and S. Raspopovic, "Sensory feedback restoration in leg amputees improves walking speed, metabolic cost and phantom pain," *Nature Medicine*, vol. 25, no. 9, pp. 1356–1363, 2019.

[42] F. M. Petrini, G. Valle, I. Strauss, G. Granata, R. D. Iorio, E. D'Anna, P. Čvančara, M. Mueller, J. Carpaneto, F. Clemente, M. Controzzi, L. Bisoni, C. Carboni, M. Barbaro, F. Iodice, D. Andreu, A. Hiairrassary, J.-L. Divoux, C. Cipriani, D. Guiraud, L. Raffo, E. Fernandez, T. Stieglitz, S. Raspopovic, P. M. Rossini, and S. Micera, "Six-Month Assessment of a Hand Prosthesis with Intraneural Tactile Feedback," *Annals of Neurology*, vol. 85, no. 1, pp. 137–154, 2019.

[43] D. W. Tan, M. A. Schiefer, M. W. Keith, J. R. Anderson, and D. J. Tyler, "Stability and selectivity of a chronic, multi-contact cuff electrode for sensory stimulation in human amputees," *Journal of Neural Engineering*, vol. 12, p. 026002, Jan. 2015. Publisher: IOP Publishing.

[44] E. L. Graczyk, L. Resnik, M. A. Schiefer, M. S. Schmitt, and D. J. Tyler, "Home use of a neural-connected sensory prosthesis provides the functional and psychosocial experience of having a hand again," *Scientific Reports*, vol. 8, no. 1, pp. 1–17, 2018.

[45] M. Ortiz-Catalan, B. Hakansson, and R. Branemark, "An osseointegrated human-machine gateway for long-term sensory feedback and motor control of artificial limbs," *Science Translational Medicine*, vol. 6, pp. 257re6–257re6, Oct. 2014.

[46] M. Ortiz-Catalan, E. Mastinu, P. Sassu, O. Aszmann, and R. Brånemark, "Self-Contained Neuromusculoskeletal Arm Prostheses," *New England Journal of Medicine*, vol. 382, pp. 1732–1738, Apr. 2020.

[47] M. Ortiz-Catalan, J. Wessberg, E. Mastinu, A. Naber, and R. Brånemark, "Patterned Stimulation of Peripheral Nerves Produces Natural Sensations With Regards to Location but Not Quality," *IEEE Transactions on Medical Robotics and Bionics*, vol. 1, pp. 199–203, Aug. 2019.

[48] E. D'Anna, G. Valle, A. Mazzoni, I. Strauss, F. Iberite, J. Patton, F. M. Petrini, S. Raspopovic, G. Granata, R. Di Iorio, M. Controzzi, C. Cipriani, T. Stieglitz, P. M. Rossini, and S. Micera, "A closed-loop hand prosthesis with simultaneous intraneural tactile and position feedback," *Science Robotics*, vol. 4, no. 27, p. eaau8892, 2019.

[49] H. Shin, Z. Watkins, H. H. Huang, Y. Zhu, and X. Hu, "Evoked haptic sensations in the hand via non-invasive proximal nerve stimulation," *Journal of Neural Engineering*, vol. 15, p. 046005, Aug. 2018.

[50] L. Pan, L. Vargas, A. Fleming, X. Hu, Y. Zhu, and H. H. Huang, "Evoking haptic sensations in the foot through high-density transcutaneous electrical nerve stimulations," *Journal of Neural Engineering*, vol. 17, p. 036020, June 2020.

[51] P. D. Marasco, A. E. Schultz, and T. A. Kuiken, "Sensory capacity of reinnervated skin after redirection of amputated upper limb nerves to the chest," *Brain*, vol. 132, pp. 1441–1448, June 2009.

[52] T. A. Kuiken, L. A. Miller, R. D. Lipschutz, B. A. Lock, K. Stubblefield, P. D. Marasco, P. Zhou, and G. A. Dumanian, "Targeted reinnervation for enhanced prosthetic arm function in a woman with a proximal amputation: a case study," *Lancet*, vol. 369, no. 9559, pp. 371–380, 2007.

[53] T. A. Kuiken, P. D. Marasco, B. A. Lock, R. N. Harden, and J. P. A. Dewald, "Redirection of cutaneous sensation from the hand to the chest skin of human amputees with targeted reinnervation," *Proceedings of the National Academy of Sciences*, vol. 104, no. 50, p. 20061, 2007.

[54] K. Kumar and S. Rizvi, "Historical and Present State of Neuromodulation in Chronic Pain," *Current Pain and Headache Reports*, vol. 18, no. 1, p. 387, 2014.

[55] T. Kinfe, F. Quack, C. Wille, S. Schu, and J. Vesper, "Paddle Versus Cylindrical Leads for Percutaneous Implantation in Spinal Cord Stimulation for Failed Back Surgery Syndrome: A Single-Center Trial," *Journal of Neurological Surgery Part A: Central European Neurosurgery*, vol. 75, no. 06, pp. 467–473, 2014.

[56] P. J. Lynch, T. McJunkin, E. Eross, S. Gooch, and J. Maloney, "Case Report: Successful Epiradicular Peripheral Nerve Stimulation of the C2 Dorsal Root Ganglion for Postherpetic Neuralgia," *Neuromodulation: Technology at the Neural Interface*, vol. 14, no. 1, pp. 58–61, 2011. _eprint: https://onlinelibrary.wiley.com/doi/pdf/10.1111/j.1525-1403.2010.00307.x.

[57] L. Liem, M. Russo, F. J. P. M. Huygen, J.-P. V. Buyten, I. Smet, P. Verrills, M. Cousins, C. Brooker, R. Levy, T. Deer, and J. Kramer, "A Multicenter, Prospective Trial to Assess the Safety and Performance of the Spinal Modulation Dorsal Root

Ganglion Neurostimulator System in the Treatment of Chronic Pain," *Neuromodulation: Technology at the Neural Interface*, vol. 16, no. 5, pp. 471–482, 2013. _eprint: https://onlinelibrary.wiley.com/doi/pdf/10.1111/ner.12072.

[58] T. R. Deer, E. Grigsby, R. L. Weiner, B. Wilcosky, and J. M. Kramer, "A prospective study of dorsal root ganglion stimulation for the relief of chronic pain," *Neuromodulation*, vol. 16, no. 1, pp. 67–72, 2013.

[59] C. Harrison, S. Epton, S. Bojanic, A. L. Green, and J. J. FitzGerald, "The Efficacy and Safety of Dorsal Root Ganglion Stimulation as a Treatment for Neuropathic Pain: A Literature Review," *Neuromodulation: Technology at the Neural Interface*, vol. 2017, 2017.

[60] S. Schmidt, K. Horch, and R. Normann, "Biocompatibility of silicon-based electrode arrays implanted in feline cortical tissue," *Journal of Biomedical Materials Research*, vol. 27, no. 11, pp. 1393–1399, 1993. _eprint: https://onlinelibrary.wiley.com/doi/pdf/10.1002/jbm.820271106.

[61] V. S. Polikov, P. A. Tresco, and W. M. Reichert, "Response of brain tissue to chronically implanted neural electrodes," *Journal of Neuroscience Methods*, vol. 148, pp. 1–18, Oct. 2005.

[62] D. McCreery, W. Agnew, T. Yuen, and L. Bullara, "Charge density and charge per phase as cofactors in neural injury induced by electrical stimulation," *IEEE Transactions on Biomedical Engineering*, vol. 37, pp. 996–1001, Oct. 1990. Conference Name: IEEE Transactions on Biomedical Engineering.

[63] M. R. MacEwan, E. R. Zellmer, J. J. Wheeler, H. Burton, and D. W. Moran, "Regenerated Sciatic Nerve Axons Stimulated through a Chronically Implanted Macro-Sieve Electrode," *Frontiers in Neuroscience*, vol. 10, Dec. 2016.

[64] I. Delgado-Martínez, M. Righi, D. Santos, A. Cutrone, S. Bossi, S. D'Amico, J. Del Valle, S. Micera, and X. Navarro, "Fascicular nerve stimulation and recording using a novel double-aisle regenerative electrode," *Journal of Neural Engineering*, vol. 14, no. 4, p. 046003, 2017.

[65] K. Garde, E. Keefer, B. Botterman, P. Galvan, and M. I. Romero, "Early interfaced neural activity from chronic amputated nerves," *Frontiers in Neuroengineering*, vol. 2, p. 5, 2009.

[66] I. P. Clements, V. J. Mukhatyar, A. Srinivasan, J. T. Bentley, D. S. Andreasen, and R. V. Bellamkonda, "Regenerative scaffold electrodes for peripheral nerve interfacing," *IEEE transactions on neural systems and rehabilitation engineering: a publication of the IEEE Engineering in Medicine and Biology Society*, vol. 21, pp. 554–566, July 2013.

[67] S. L. Woo, T. A. Kung, D. L. Brown, J. A. Leonard, B. M. Kelly, and P. S. Cederna, "Regenerative Peripheral Nerve Interfaces for the Treatment of Postamputation Neuroma Pain: A Pilot Study," *Plastic and Reconstructive Surgery – Global Open*, vol. 4, p. e1038, Dec. 2016.

[68] Z. T. Irwin, K. E. Schroeder, P. P. Vu, D. M. Tat, A. J. Bullard, S. L. Woo, I. C. Sando, M. G. Urbanchek, P. S. Cederna, and C. A. Chestek, "Chronic recording of hand prosthesis control signals via a regenerative peripheral nerve interface in a rhesus macaque," *Journal of Neural Engineering*, vol. 13, no. 4, p. 046007, 2016.

[69] S. L. Woo, M. G. Urbanchek, P. S. Cederna, and N. B. Langhals, "Revisiting non-vascularized partial muscle grafts: a novel use for prosthetic control," *Plastic and Reconstructive Surgery*, vol. 134, pp. 344e–346e, Aug. 2014.

[70] T. A. Kung, R. A. Bueno, G. K. Alkhalefah, N. B. Langhals, M. G. Urbanchek, and P. S. Cederna, "Innovations in prosthetic interfaces for the upper extremity," *Plastic and Reconstructive Surgery*, vol. 132, pp. 1515–1523, Dec. 2013.

[71] P. P. Vu, A. K. Vaskov, Z. T. Irwin, P. T. Henning, D. R. Lueders, A. T. Laidlaw, A. J. Davis, C. S. Nu, D. H. Gates, R. B. Gillespie, S. W. P. Kemp, T. A. Kung, C. A. Chestek, and P. S. Cederna, "A regenerative peripheral nerve interface allows real-time control of an artificial hand in upper limb amputees," *Science Translational Medicine*, vol. 12, Mar. 2020. Publisher: American Association for the Advancement of Science Section: Research Article.

[72] S. M. Iyer, K. L. Montgomery, C. Towne, S. Y. Lee, C. Ramakrishnan, K. Deisseroth, and S. L. Delp, "Virally mediated optogenetic excitation and inhibition of pain in freely moving nontransgenic mice," *Nature Biotechnology*, vol. 32, pp. 274–278, Mar. 2014.

[73] P.-H. Tsui, S.-H. Wang, and C.-C. Huang, "In vitro effects of ultrasound with different energies on the conduction properties of neural tissue," *Ultrasonics*, vol. 43, pp. 560–565, June 2005.

[74] Y.-F. Lee, C.-C. Lin, J.-S. Cheng, and G.-S. Chen, "Nerve conduction block in diabetic rats using high-intensity focused ultrasound for analgesic applications," *British Journal of Anaesthesia*, vol. 114, pp. 840–846, May 2015.

[75] E. J. Juan, R. González, G. Albors, M. P. Ward, and P. Irazoqui, "Vagus Nerve Modulation Using Focused Pulsed Ultrasound: Potential Applications and Preliminary Observations in a Rat," *International journal of imaging systems and technology*, vol. 24, pp. 67–71, Mar. 2014.

[76] J. L. Foley, J. W. Little, and S. Vaezy, "Image-guided high-intensity focused ultrasound for conduction block of peripheral nerves," *Annals of Biomedical Engineering*, vol. 35, pp. 109–119, Jan. 2007.

[77] A. R. Duke, E. Peterson, M. A. Mackanos, J. Atkinson, D. Tyler, and E. D. Jansen, "Hybrid electro-optical stimulation of the rat sciatic nerve induces force generation in the plantarflexor muscles," *Journal of Neural Engineering*, vol. 9, p. 066006, Dec. 2012.

[78] E. H. Lothet, K. M. Shaw, H. Lu, J. Zhuo, Y. T. Wang, S. Gu, D. B. Stolz, E. D. Jansen, C. C. Horn, H. J. Chiel, and M. W. Jenkins, "Selective inhibition of small-diameter axons using infrared light," *Scientific Reports*, vol. 7, June 2017.

[79] R. D. Graham, T. M. Bruns, B. Duan, and S. F. Lempka, "Dorsal root ganglion stimulation for chronic pain modulates AB-fiber activity but not C-fiber activity: A computational modeling study," *Clinical Neurophysiology*, vol. 130, pp. 941–951, June 2019.

[80] U. Proske and S. C. Gandevia, "The Proprioceptive Senses: Their Roles in Signaling Body Shape, Body Position and Movement, and Muscle Force," *Physiological Reviews*, vol. 92, pp. 1651–1697, Oct. 2012. Publisher: American Physiological Society.

[81] M. Devor, "Unexplained peculiarities of the dorsal root ganglion," *Pain*, vol. 82, Aug. 1999.

[82] E. Matsumoto and J. Rosenbluth, "Plasma membrane structure at the axon hillock, initial segment and cell body of frog dorsal root ganglion cells," *Journal of Neurocytology*, vol. 14, pp. 731–747, Oct. 1985.

[83] A. K. Ostrowski, Z. J. Sperry, G. Kulik, and T. M. Bruns, "Quantitative models of feline lumbosacral dorsal root ganglia neuronal cell density," *Journal of Neuroscience Methods*, vol. 290, pp. 116–124, Oct. 2017.

[84] A. I. Kashkoush, R. A. Gaunt, L. E. Fisher, T. M. Bruns, and D. J. Weber, "Recording single- and multi-unit neuronal action potentials from the surface of the dorsal root ganglion," *Scientific Reports*, vol. 9, p. 2786, Feb. 2019. Number: 1 Publisher: Nature Publishing Group.

[85] G. E. Goslow, R. M. Reinking, and D. G. Stuart, "The cat step cycle: Hind limb joint angles and muscle lengths during unrestrained locomotion," *Journal of Morphology*, vol. 141, no. 1, pp. 1–41, 1973. _eprint: https://onlinelibrary.wiley.com/doi/pdf/10.1002/jmor.1051410102.

[86] Z. Hasan, "A model of spindle afferent response to muscle stretch," *Journal of Neurophysiology*, vol. 49, pp. 989–1006, Apr. 1983.

[87] J. Houk and W. Simon, "Responses of Golgi tendon organs to forces applied to muscle tendon," *Journal of Neurophysiology*, vol. 30, pp. 1466–1481, Nov. 1967.

[88] M. G. Maltenfort and R. E. Burke, "Spindle model responsive to mixed fusimotor inputs and testable predictions of beta feedback effects," *Journal of Neurophysiology*, vol. 89, pp. 2797–2809, May 2003.

[89] M. P. Mileusnic, I. E. Brown, N. Lan, and G. E. Loeb, "Mathematical models of proprioceptors. I. Control and transduction in the muscle spindle," *Journal of Neurophysiology*, vol. 96, pp. 1772–1788, Oct. 2006.

[90] M. P. Mileusnic and G. E. Loeb, "Mathematical models of proprioceptors. II. Structure and function of the Golgi tendon organ," *Journal of Neurophysiology*, vol. 96, pp. 1789–1802, Oct. 2006.

[91] M. P. Mileusnic and G. E. Loeb, "Force estimation from ensembles of Golgi tendon organs," *Journal of Neural Engineering*, vol. 6, p. 036001, Apr. 2009. Publisher: IOP Publishing.

[92] A. Prochazka, "Quantifying proprioception," *Progress in Brain Research*, vol. 123, pp. 133–142, 1999.

[93] A. Prochazka and M. Gorassini, "Ensemble firing of muscle afferents recorded during normal locomotion in cats," *The Journal of Physiology*, vol. 507, pp. 293–304, Feb. 1998.

[94] A. Prochazka, R. A. Westerman, and S. P. Ziccone, "Ia afferent activity during a variety of voluntary movements in the cat," *The Journal of Physiology*, vol. 268, pp. 423–448, June 1977.

[95] A. Schaafsma, E. Otten, and J. D. Van Willigen, "A muscle spindle model for primary afferent firing based on a simulation of intrafusal mechanical events," *Journal of Neurophysiology*, vol. 65, pp. 1297–1312, June 1991.

[96] T. Umeda, H. Watanabe, M.-a. Sato, M. Kawato, T. Isa, and Y. Nishimura, "Decoding of the spike timing of primary afferents during voluntary arm movements in monkeys," *Frontiers in Neuroscience*, vol. 8, 2014. Publisher: Frontiers.

[97] J. B. Wagenaar, V. Ventura, and D. J. Weber, "State-space decoding of primary afferent neuron firing rates," *Journal of Neural Engineering*, vol. 8, p. 016002, Feb. 2011.

[98] P. B. Brown and H. R. Koerber, "Cat hindlimb tactile dermatomes determined with single-unit recordings," *Journal of Neurophysiology*, vol. 41, pp. 260–267, Mar. 1978. Publisher: American Physiological Society.

[99] Y. Aoyagi, R. B. Stein, A. Branner, K. G. Pearson, and R. A. Normann, "Capabilities of a penetrating microelectrode array for recording single units in dorsal root ganglia of the cat," *Journal of Neuroscience Methods*, vol. 128, pp. 9–20, Sept. 2003.

[100] M. Kausz and M. Réthelyi, "Lamellar Arrangement of Neuronal Somata in the Dorsal Root Ganglion of the Cat," *Somatosensory Research*, vol. 2, pp. 193–204, Jan. 1985. Publisher: Taylor & Francis _eprint: https://doi.org/10.3109/07367228509144563.

[101] K. Ziegler-Graham, E. J. MacKenzie, P. L. Ephraim, T. G. Travison, and R. Brookmeyer, "Estimating the Prevalence of Limb Loss in the United States: 2005 to 2050," *Archives of Physical Medicine and Rehabilitation*, vol. 89, pp. 422–429, Mar. 2008.

[102] W. C. Miller, A. B. Deathe, M. Speechley, and J. Koval, "The influence of falling, fear of falling, and balance confidence on prosthetic mobility and social activity among individuals with a lower extremity amputation," *Archives of Physical Medicine and Rehabilitation*, vol. 82, pp. 1238–1244, Sept. 2001.

[103] M. J. Cole, S. Durham, and D. D. Ewins, "An evaluation of patient perceptions to the value of the gait laboratory as part of the rehabilitation of primary lower limb amputees:," *Prosthetics and Orthotics International*, Jan. 2008. Publisher: SAGE PublicationsSage UK: London, England.

[104] G. Dhillon and K. Horch, "Direct neural sensory feedback and control of a prosthetic arm," *IEEE Transactions on Neural Systems and Rehabilitation Engineering*, vol. 13, pp. 468–472, Dec. 2005. Conference Name: IEEE Transactions on Neural Systems and Rehabilitation Engineering.

[105] J. Holsheimer and W. A. Wesselink, "Optimum electrode geometry for spinal cord stimulation: The narrow bipole and tripole," *Medical and Biological Engineering and Computing*, vol. 35, pp. 493–497, Sept. 1997.

[106] Foster K R and Schwan H P, "Dielectric properties of tissues and biological materials: a critical review," *Crit. Rev. Biomed. Eng.*, vol. 17, p. 25, 1989.

[107] M. B. Christensen, S. M. Pearce, N. M. Ledbetter, D. J. Warren, G. A. Clark, and P. A. Tresco, "The foreign body response to the Utah Slant Electrode Array in the cat sciatic nerve," *Acta Biomaterialia*, vol. 10, pp. 4650–4660, Nov. 2014.

[108] V. V. Patel, F. P. Heidenreich, R. R. Bindra, K. Yamaguchi, and R. H. Gelberman, "Morphologic changes in the ulnar nerve at the elbow with flexion and extension: A magnetic resonance imaging study with 3-dimensional reconstruction," *Journal of Shoulder and Elbow Surgery*, vol. 7, pp. 368–374, July 1998.

[109] C. B. Novak, H. Mehdian, and H. P. von Schroeder, "Laxity of the Ulnar Nerve During Elbow Flexion and Extension," *The Journal of Hand Surgery*, vol. 37, pp. 1163–1167, June 2012.

[110] H. Gray and W. H. Lewis, *Anatomy of the human body*. Philadelphia,: Lea & Febiger,, 20th ed., by warren h. lewis ed., 1918. Pages: 1-1396.

[111] S. Chandrasekaran, A. C. Nanivadekar, G. McKernan, E. R. Helm, M. L. Boninger, J. L. Collinger, R. A. Gaunt, and L. E. Fisher, "Sensory restoration by epidural stimulation of the lateral spinal cord in upper-limb amputees," *eLife*, vol. 9, p. e54349, July 2020. Publisher: eLife Sciences Publications, Ltd.

[112] C. A. Ayers, L. E. Fisher, R. A. Gaunt, and D. J. Weber, "Microstimulation of the lumbar DRG recruits primary afferent neurons in localized regions of lower limb," *Journal of Neurophysiology*, vol. 116, pp. 51–60, Apr. 2016. Publisher: American Physiological Society.

[113] L. E. Fisher, C. A. Ayers, M. Ciollaro, V. Ventura, D. J. Weber, and R. A. Gaunt, "Chronic recruitment of primary afferent neurons by microstimulation in the feline dorsal root ganglia," *Journal of Neural Engineering*, vol. 11, p. 036007, Apr. 2014. Publisher: IOP Publishing.

[114] S. M. Pirris, S. Dhall, P. V. Mummaneni, and A. S. Kanter, "Minimally invasive approach to extraforaminal disc herniations at the lumbosacral junction using an operating microscope: case series and review of the literature," *Neurosurgical Focus*, vol. 25, p. E10, Aug. 2008. Publisher: American Association of Neurological Surgeons Section: Neurosurgical Focus.

[115] Kohli N and Patterson D, "InterStim therapy: a contemporary approach to overactive bladder," *Rev. Obstet. Gynecol.*, vol. 2, p. 8, 2009.

[116] T. R. Deer, R. M. Levy, J. Kramer, L. Poree, K. Amirdelfan, E. Grigsby, P. Staats, A. W. Burton, A. H. Burgher, J. Obray, J. Scowcroft, S. Golovac, L. Kapural, R. Paicius, C. Kim, J. Pope, T. Yearwood, S. Samuel, W. P. McRoberts, H. Cassim, M. Netherton, N. Miller, M. Schaufele, E. Tavel, T. Davis, K. Davis, L. Johnson, and N. Mekhail, "Dorsal root ganglion stimulation yielded higher treatment success rate for complex regional pain syndrome and causalgia at 3 and 12 months: a randomized comparative trial," *PAIN*, vol. 158, pp. 669–681, Apr. 2017.

[117] R. L. Weiner, A. Yeung, C. Montes Garcia, L. Tyler Perryman, and B. Speck, "Treatment of FBSS Low Back Pain with a Novel Percutaneous DRG Wireless Stimulator: Pilot and Feasibility Study," *Pain Medicine*, vol. 17, pp. 1911–1916, Oct. 2016. Publisher: Oxford Academic.

[118] R. Levy, T. R. Deer, L. Poree, S. M. Rosen, L. Kapural, K. Amirdelfan, N. Soliday, A. Leitner, and N. Mekhail, "Multicenter, Randomized, Double-Blind Study Protocol Using Human Spinal Cord Recording Comparing Safety, Efficacy, and Neurophysiological Responses Between Patients Being Treated With Evoked Compound Action Potential–Controlled Closed-Loop Spinal Cord Stimulation or Open-Loop Spinal Cord Stimulation (the Evoke Study)," *Neuromodulation: Technology at the Neural Interface*, vol. 22, no. 3, pp. 317–326, 2019. _eprint: https://onlinelibrary.wiley.com/doi/pdf/10.1111/ner.12932.

[119] P. B. Yoo, M. Sahin, and D. M. Durand, "Selective Stimulation of the Canine Hypoglossal Nerve Using a Multi-contact Cuff Electrode," *Annals of Biomedical Engineering*, vol. 32, pp. 511–519, Apr. 2004.

[120] R. A. Gaunt, J. A. Hokanson, and D. J. Weber, "Microstimulation of primary afferent neurons in the L7 dorsal root ganglia using multielectrode arrays in anesthetized cats: thresholds and recruitment properties," *Journal of Neural Engineering*, vol. 6, p. 055009, Sept. 2009. Publisher: IOP Publishing.

[121] K. W. Altman and R. Plonsey, "Analysis of the longitudinal and radial resistivity measurements of the nerve trunk," *Annals of Biomedical Engineering*, vol. 17, pp. 313–324, July 1989.

[122] J. B. Nielsen and T. Sinkjaer, "Afferent feedback in the control of human gait," *Journal of Electromyography and Kinesiology*, vol. 12, pp. 213–217, June 2002.

[123] K. G. Pearson, "Generating the walking gait: role of sensory feedback," in *Progress in Brain Research*, vol. 143 of *Brain Mechanisms for the Integration of Posture and Movement*, pp. 123–129, Elsevier, Jan. 2004.

[124] J. M. Donelan and K. G. Pearson, "Contribution of sensory feedback to ongoing ankle extensor activity during the stance phase of walking," *Canadian Journal of Physiology and Pharmacology*, vol. 82, pp. 589–598, July 2004. Publisher: NRC Research Press.

[125] M. J. Grey, J. B. Nielsen, N. Mazzaro, and T. Sinkjær, "Positive force feedback in human walking," *The Journal of Physiology*, vol. 581, no. 1, pp. 99–105, 2007. _eprint: https://physoc.onlinelibrary.wiley.com/doi/pdf/10.1113/jphysiol.2007.130088.

[126] G. W. Hiebert, P. J. Whelan, A. Prochazka, and K. G. Pearson, "Contribution of hind limb flexor muscle afferents to the timing of phase transitions in the cat step cycle," *Journal of Neurophysiology*, vol. 75, pp. 1126–1137, Mar. 1996. Publisher: American Physiological Society.

[127] G. W. Hiebert and K. G. Pearson, "Contribution of Sensory Feedback to the Generation of Extensor Activity During Walking in the Decerebrate Cat," *Journal of Neurophysiology*, vol. 81, pp. 758–770, Feb. 1999. Publisher: American Physiological Society.

[128] R. Amir and M. Devor, "Electrical Excitability of the Soma of Sensory Neurons Is Required for Spike Invasion of the Soma, but Not for Through-Conduction," *Biophysical Journal*, vol. 84, pp. 2181–2191, Apr. 2003.

[129] K. Ollivier-Lanvin, A. J. Krupka, N. AuYong, K. Miller, B. I. Prilutsky, and M. A. Lemay, "Electrical stimulation of the sural cutaneous afferent nerve controls the amplitude and onset of the swing phase of locomotion in the spinal cat," *Journal of Neurophysiology*, vol. 105, pp. 2297–2308, Mar. 2011. Publisher: American Physiological Society.

[130] D. P. C. Lloyd and H. T. Chang, "Afferent fibers in muscle nerves," *Journal of Neurophysiology*, vol. 11, pp. 199–207, May 1948. Publisher: American Physiological Society.

[131] C. C. Hunt and A. K. McIntyre, "An analysis of fibre diameter and receptor characteristics of myelinated cutaneous afferent fibres in cat," *The Journal of Physiology*, vol. 153, no. 1, pp. 99–112, 1960. _eprint: https://physoc.onlinelibrary.wiley.com/doi/pdf/10.1113/jphysiol.1960.sp006521.

[132] D. J. Bourbeau, J. A. Hokanson, J. E. Rubin, and D. J. Weber, "A computational model for estimating recruitment of primary afferent fibers by intraneural stimulation in the dorsal root ganglia," *Journal of Neural Engineering*, vol. 8, p. 056009, Aug. 2011. Publisher: IOP Publishing.

[133] M. Risling, H. Aldskogius, C. Hildebrand, and S. Remahl, "Effects of sciatic nerve resection on L7 spinal roots and dorsal root ganglia in adult cats," *Experimental Neurology*, vol. 82, pp. 568–580, Dec. 1983.

[134] G. A. Tabot, S. S. Kim, J. E. Winberry, and S. J. Bensmaia, "Restoring tactile and proprioceptive sensation through a brain interface," *Neurobiology of Disease*, vol. 83, pp. 191–198, Nov. 2015.

[135] S. N. Flesher, J. L. Collinger, S. T. Foldes, J. M. Weiss, J. E. Downey, E. C. Tyler-Kabara, S. J. Bensmaia, A. B. Schwartz, M. L. Boninger, and R. A. Gaunt, "Intracortical microstimulation of human somatosensory cortex," *Science Translational Medicine*, vol. 8, pp. 361ra141–361ra141, Oct. 2016. Publisher: American Association for the Advancement of Science Section: Research Article.

[136] D. C. Bradley, P. R. Troyk, J. A. Berg, M. Bak, S. Cogan, R. Erickson, C. Kufta, M. Mascaro, D. McCreery, E. M. Schmidt, V. L. Towle, and H. Xu, "Visuotopic Mapping Through a Multichannel Stimulating Implant in Primate V1," *Journal of Neurophysiology*, vol. 93, pp. 1659–1670, Mar. 2005. Publisher: American Physiological Society.

[137] Y. H.-L. Luo and L. da Cruz, "The Argus® II Retinal Prosthesis System," *Progress in Retinal and Eye Research*, vol. 50, pp. 89–107, Jan. 2016.

[138] B. S. Wilson and M. F. Dorman, "Cochlear implants: A remarkable past and a brilliant future," *Hearing Research*, vol. 242, pp. 3–21, Aug. 2008.

[139] K. H. Lee, K. Chung, J. M. Chung, and R. E. Coggeshall, "Correlation of cell body size, axon size, and signal conduction velocity for individually labelled dorsal root ganglion cells in the cat," *Journal of Comparative Neurology*, vol. 243, no. 3, pp. 335–346, 1986. _eprint: https://onlinelibrary.wiley.com/doi/pdf/10.1002/cne.902430305.

[140] M. Capogrosso and S. F. Lempka, "A computational outlook on neurostimulation," *Bioelectronic Medicine*, vol. 6, May 2020.

[141] N. A. Pelot, C. E. Behrend, and W. M. Grill, "On the parameters used in finite element modeling of compound peripheral nerves," *Journal of Neural Engineering*, vol. 16, p. 016007, Dec. 2018. Publisher: IOP Publishing.

[142] C. C. McIntyre and T. J. Foutz, "Computational modeling of deep brain stimulation," *Handbook of clinical neurology*, vol. 116, pp. 55–61, 2013.

[143] S. F. Lempka, H. J. Zander, C. J. Anaya, A. Wyant, J. G. Ozinga, and A. G. Machado, "Patient-Specific Analysis of Neural Activation During Spinal Cord Stimulation for Pain," *Neuromodulation: Technology at the Neural Interface*, vol. 23, no. 5, pp. 572–581, 2020. _eprint: https://onlinelibrary.wiley.com/doi/pdf/10.1111/ner.13037.

[144] B. Coburn, "A theoretical study of epidural electrical stimulation of the spinal cord–Part II: Effects on long myelinated fibers," *IEEE transactions on bio-medical engineering*, vol. 32, pp. 978–986, Nov. 1985.

[145] B. Coburn and W. K. Sin, "A theoretical study of epidural electrical stimulation of the spinal cord–Part I: Finite element analysis of stimulus fields," *IEEE transactions on bio-medical engineering*, vol. 32, pp. 971–977, Nov. 1985.

[146] J. Holsheimer, "Which Neuronal Elements are Activated Directly by Spinal Cord Stimulation," *Neuromodulation: Technology at the Neural Interface*, vol. 5, no. 1, pp. 25–31, 2002. _eprint: https://onlinelibrary.wiley.com/doi/pdf/10.1046/j.1525-1403.2002._2005.x.

[147] C. C. McIntyre, A. G. Richardson, and W. M. Grill, "Modeling the Excitability of Mammalian Nerve Fibers: Influence of Afterpotentials on the Recovery Cycle," *Journal of Neurophysiology*, vol. 87, pp. 995–1006, Feb. 2002. Publisher: American Physiological Society.

[148] N. Khadka, X. Liu, H. Zander, J. Swami, E. Rogers, S. F. Lempka, and M. Bikson, "Realistic anatomically detailed open-source spinal cord stimulation (RADO-SCS) model," *Journal of Neural Engineering*, vol. 17, p. 026033, Apr. 2020. Publisher: IOP Publishing.

[149] T. R. Deer and J. E. Pope, "Dorsal root ganglion stimulation approval by the Food and Drug Administration: advice on evolving the process," *Expert Review of Neurotherapeutics*, vol. 16, pp. 1123–1125, Oct. 2016. Publisher: Taylor & Francis _eprint: https://doi.org/10.1080/14737175.2016.1206817.

[150] S. Schu, A. Gulve, S. ElDabe, G. Baranidharan, K. Wolf, W. Demmel, D. Rasche, M. Sharma, D. Klase, G. Jahnichen, A. Wahlstedt, H. Nijhuis, and L. Liem, "Spinal Cord Stimulation of the Dorsal Root Ganglion for Groin Pain—A Retrospective Review," *Pain Practice*, vol. 15, no. 4, pp. 293–299, 2015. _eprint: https://onlinelibrary.wiley.com/doi/pdf/10.1111/papr.12194.

[151] S. Eldabe, K. Burger, H. Moser, D. Klase, S. Schu, A. Wahlstedt, B. Vanderick, E. Francois, J. Kramer, and J. Subbaroyan, "Dorsal Root Ganglion (DRG) Stimulation in the Treatment of Phantom Limb Pain (PLP)," *Neuromodulation: Technology at the Neural Interface*, vol. 18, no. 7, pp. 610–617, 2015. _eprint: https://onlinelibrary.wiley.com/doi/pdf/10.1111/ner.12338.

[152] S. Eldabe, A. Espinet, A. Wahlstedt, P. Kang, L. Liem, N. K. Patel, J. Vesper, A. Kimber, W. Cusack, and J. Kramer, "Retrospective Case Series on the Treatment of Painful Diabetic Peripheral Neuropathy With Dorsal Root Ganglion Stimulation," *Neuromodulation: Technology at the Neural Interface*, vol. 21, no. 8, pp. 787–792, 2018. _eprint: https://onlinelibrary.wiley.com/doi/pdf/10.1111/ner.12767.

[153] F. M. U. Mol and R. M. H. Roumen, "DRG Spinal Cord Stimulation as Solution for Patients With Severe Pain Due to Anterior Cutaneous Nerve Entrapment Syndrome: A Case Series," *Neuromodulation: Technology at the Neural Interface*, vol. 21, no. 3, pp. 317–319, 2018. _eprint: https://onlinelibrary.wiley.com/doi/pdf/10.1111/ner.12692.

[154] R. D. Graham, T. M. Bruns, B. Duan, and S. F. Lempka, "The Effect of Clinically Controllable Factors on Neural Activation During Dorsal Root Ganglion Stimulation," *Neuromodulation: Technology at the Neural Interface*, vol. n/a, no. n/a, 2020. _eprint: https://onlinelibrary.wiley.com/doi/pdf/10.1111/ner.13211.

[155] M. A. Schiefer, R. J. Triolo, and D. J. Tyler, "A Model of Selective Activation of the Femoral Nerve With a Flat Interface Nerve Electrode for a Lower Extremity Neuroprosthesis," *IEEE transactions on neural systems and rehabilitation engineering : a publication of the IEEE Engineering in Medicine and Biology Society*, vol. 16, pp. 195–204, Apr. 2008.

[156] K. S. Frahm, K. Hennings, L. Vera-Portocarrero, P. W. Wacnik, and C. D. Mørch, "Nerve Fiber Activation During Peripheral Nerve Field Stimulation: Importance of Electrode Orientation and Estimation of Area of Paresthesia," *Neuromodulation: Technology at the Neural Interface*, vol. 19, no. 3, pp. 311–318, 2016. _eprint: https://onlinelibrary.wiley.com/doi/pdf/10.1111/ner.12371.

[157] M. Zelechowski, G. Valle, and S. Raspopovic, "A computational model to design neural interfaces for lower-limb sensory neuroprostheses," *Journal of NeuroEngineering and Rehabilitation*, vol. 17, p. 24, Feb. 2020.

[158] M. L. Hines and N. T. Carnevale, "Neuron: A Tool for Neuroscientists," *The Neuroscientist*, vol. 7, pp. 123–135, Apr. 2001. Publisher: SAGE Publications Inc STM.

[159] M. L. Hines, A. P. Davison, and E. Muller, "NEURON and Python," *Frontiers in Neuroinformatics*, vol. 3, Jan. 2009.

[160] G. v. Rossum, F. L. Drake, and G. Van Rossum, *The Python language reference*. No. Guido van Rossum; Fred L. Drake [ed.] ; Pt. 2 in Python documentation manual, Hampton, NH: Python Software Foundation, release 3.0.1 [repr.] ed., 2010. OCLC: 837611997.

[161] M. Ito and Takahashi, I, "Impulse conduction through spinal ganglion," *Tokyo: Igaku Shoin*, 1960. Publisher: Igaku Shoin.

[162] H. Ha, "Axonal bifurcation in the dorsal root ganglion of the cat: A light and electron microscopic study," *Journal of Comparative Neurology*, vol. 140, no. 2, pp. 227–240, 1970. _eprint: https://onlinelibrary.wiley.com/doi/pdf/10.1002/cne.901400206.

[163] J. L. Gaines, K. E. Finn, J. P. Slopsema, L. A. Heyboer, and K. H. Polasek, "A model of motor and sensory axon activation in the median nerve using surface electrical stimulation," *Journal of Computational Neuroscience*, vol. 45, no. 1, pp. 29–43, 2018.

[164] J. Howells, L. Trevillion, H. Bostock, and D. Burke, "The voltage dependence of Ih in human myelinated axons," *The Journal of Physiology*, vol. 590, no. 7, pp. 1625–1640, 2012. _eprint: https://physoc.onlinelibrary.wiley.com/doi/pdf/10.1113/jphysiol.2011.225573.

[165] C. L. Kolarcik, C. A. Castro, A. Lesniak, A. J. Demetris, L. E. Fisher, R. A. Gaunt, D. J. Weber, and X. T. Cui, "Host tissue response to floating microelectrode arrays chronically implanted in the feline spinal nerve," *Journal of Neural Engineering*, vol. 17, p. 046012, July 2020.

[166] A. F. Huxley and R. Stämpfli, "Direct determination of membrane resting potential and action potential in single myelinated nerve fibres," *The Journal of Physiology*, vol. 112, pp. 476–495, Feb. 1951.

[167] A. A. Harper and S. N. Lawson, "Electrical properties of rat dorsal root ganglion neurones with different peripheral nerve conduction velocities.," *The Journal of Physiology*, vol. 359, no. 1, pp. 47–63, 1985. _eprint: https://physoc.onlinelibrary.wiley.com/doi/pdf/10.1113/jphysiol.1985.sp015574.

[168] L. Djouhri, L. Bleazard, and S. N. Lawson, "Association of somatic action potential shape with sensory receptive properties in guinea-pig dorsal root ganglion neurones," *The Journal of Physiology*, vol. 513, no. 3, pp. 857–872, 1998. _eprint: https://physoc.onlinelibrary.wiley.com/doi/pdf/10.1111/j.1469-7793.1998.857ba.x.

[169] A. Weerasuriya and A. P. Mizisin, "The Blood-Nerve Barrier: Structure and Functional Significance," in *The Blood-Brain and Other Neural Barriers: Reviews and Protocols* (S. Nag, ed.), Methods in Molecular Biology, pp. 149–173, Totowa, NJ: Humana Press, 2011.

[170] U. Wijk and I. Carlsson, "Forearm amputees' views of prosthesis use and sensory feedback," *Journal of Hand Therapy*, vol. 28, no. 3, pp. 269–278, 2015.

[171] G. Lundborg, B. Rosen, K. Lindstrom, and S. Lindberg, "Artificial Sensibility Based on the Use of Piezoresistive Sensors," *Journal of Hand Surgery*, vol. 23, no. 5, pp. 620–626, 1998.

[172] C. Pylatiuk, S. Schulz, and L. Döderlein, "Results of an Internet survey of myoelectric prosthetic hand users," *Prosthetics and Orthotics International*, vol. 31, no. 4, pp. 362–370, 2007.

[173] J. T. Belter, J. L. Segil, A. M. Dollar, and R. F. Weir, "Mechanical design and performance specifications of anthropomorphic prosthetic hands: a review.," *Journal of rehabilitation research and development*, vol. 50, no. 5, pp. 599–618, 2013.

[174] S. L. Carey, D. J. Lura, M. J. Highsmith, CP, and FAAOP, "Differences in myoelectric and body-powered upper-limb prostheses: Systematic literature review," *Journal of Rehabilitation Research and Development*, vol. 52, no. 3, pp. 247–262, 2015.

[175] B. Peerdeman, D. Boere, H. Witteveen, R. Huis in 't Veld, H. Hermens, S. Stramigioli, H. Rietman, P. Veltink, and S. Misra, "Myoelectric forearm prostheses: State of the art from a user-centered perspective," *The Journal of Rehabilitation Research and Development*, vol. 48, no. 6, p. 719, 2011.

[176] M. E. Huang, C. E. Levy, and J. B. Webster, "Acquired limb deficiencies. 3. Prosthetic components, prescriptions, and indications," *Archives of Physical Medicine and Rehabilitation*, vol. 82, no. 3, pp. S17–S24, 2001.

[177] G. Stark and M. LeBlanc, "Overview of body-powered upper extremity prostheses," *Functional restoration of adults and children with upper extremity amputation. New York: Demos Medical Publishing, Inc*, pp. 175–186, 2004.

[178] J. E. Uellendahl, "Upper extremity myoelectric prosthetics," *Physical medicine and rehabilitation clinics of North America*, vol. 11, no. 3, pp. 639–52, 2000.

[179] T. W. Williams III, "Progress on stabilizing and controlling powered upper-limb prostheses," *The Journal of Rehabilitation Research and Development*, vol. 48, no. 6, pp. ix–xix, 2011.

[180] C. Cipriani, M. Controzzi, and M. C. Carrozza, "The SmartHand transradial prosthesis," *Journal of NeuroEngineering and Rehabilitation*, vol. 8, no. 1, p. 29, 2011.

[181] B. N. Perry, C. W. Moran, R. S. Armiger, P. F. Pasquina, J. W. Vandersea, and J. W. Tsao, "Initial Clinical Evaluation of the Modular Prosthetic Limb," *Frontiers in Neurology*, vol. 9, p. 153, 2018.

[182] A. Saudabayev and H. A. Varol, "Sensors for Robotic Hands: A Survey of State of the Art," *IEEE Access*, vol. 3, pp. 1765–1782, 2015.

[183] M. Capogrosso, N. Wenger, S. Raspopovic, P. Musienko, J. Beauparlant, L. Bassi Luciani, G. Courtine, and S. Micera, "A Computational Model for Epidural Electrical Stimulation of Spinal Sensorimotor Circuits," *Journal of Neuroscience*, vol. 33, no. 49, pp. 19326–19340, 2013.

[184] E. Heming, A. Sanden, and Z. H. T. Kiss, "Designing a somatosensory neural prosthesis: Percepts evoked by different patterns of thalamic stimulation," *Journal of Neural Engineering*, vol. 7, no. 6, 2010.

[185] F. A. Lenz, M. Seike, R. T. Richardson, Y. C. Lin, F. H. Baker, I. Khoja, C. J. Jaeger, and R. H. Gracely, "Thermal and pain sensations evoked by microstimulation in the area of human ventrocaudal nucleus.," *Journal of neurophysiology*, vol. 70, no. 1, pp. 200–12, 1993.

[186] P. Agarwal and S. Sahu, "Determination of hand and palm area as a ratio of body surface area in Indian population," *Indian Journal of Plastic Surgery : Official Publication of the Association of Plastic Surgeons of India*, vol. 43, no. 1, pp. 49–53, 2010.

[187] I. Ilayperuma, G. Nanayakkara, and N. Palahepitiya, "Prediction of personal stature based on the hand length," *Galle Medical Journal*, vol. 14, no. 1, p. 15, 2009.

[188] E. Kono, M. Tada, M. Kouchi, Y. Endo, Y. Tomizawa, T. Matsuo, and S. Nomura, "Ergonomic evaluation of a mechanical anastomotic stapler used by Japanese surgeons," *Surgery Today*, vol. 44, no. 6, pp. 1040–1047, 2014.

[189] J. T. Martin and D. H. Nguyen, "Anthropometric analysis of homosexuals and heterosexuals: implications for early hormone exposure," *Hormones and Behavior*, vol. 45, no. 1, pp. 31–39, 2004.

[190] J. Rhodes, C. Clay, and M. Phillips, "The surface area of the hand and the palm for estimating percentage of total body surface area: results of a meta-analysis," *The British Journal of Dermatology*, vol. 169, no. 1, pp. 76–84, 2013.

[191] U. Zafar, Shafiq-Ur-Rahman, N. Hamid, J. Ahsan, and N. Zafar, "Correlation between height and hand size, and predicting height on the basis of age, gender and hand size," *Journal of Medical Sciences (Peshawar)*, vol. 25, no. 4, pp. 425–428, 2017.

[192] M. R. Leek, "Adaptive procedures in psychophysical research," *Perception & Psychophysics*, vol. 63, no. 8, pp. 1279–1292, 2001.

[193] H. Levitt, "Transformed Up-Down Methods in Psychoacoustics," *The Journal of the Acoustical Society of America*, vol. 49, no. 2B, pp. 467–477, 1971.

[194] M. A. García-Pérez, "Forced-choice staircases with fixed step sizes: Asymptotic and small-sample properties," *Vision Research*, vol. 38, no. 12, pp. 1861–1881, 1998.

[195] F. A. A. Kingdom and N. Prins, *Psychophysics : a practical introduction*. Elsevier Academic Press, 2 ed., 2016.

[196] W. Ellermeier, W. Westphal, and M. Heidenfelder, "On the "absoluteness" of category and magnitude scales of pain," *Perception & Psychophysics*, vol. 49, no. 2, pp. 159–166, 1991.

[197] S. S. Stevens, *Psychophysics*. Routledge, 1 ed., 1986.

[198] S. S. Stevens, "The Direct Estimation of Sensory Magnitudes: Loudness," *The American Journal of Psychology*, vol. 69, no. 1, p. 1, 1956.

[199] R. T. Verrillo, A. J. Fraioli, and R. L. Smith, "Sensation magnitude of vibrotactile stimuli," *Perception & Psychophysics*, vol. 6, no. 6, pp. 366–372, 1969.

[200] O. Foerster, "The dermatomes in man," *Brain*, 1933.

[201] M. Lee, R. McPhee, and M. Stringer, "An evidence-based approach to human dermatomes," *Clinical Anatomy*, vol. 21, no. 5, pp. 363–373, 2008.

[202] T. Cameron, "Safety and efficacy of spinal cord stimulation for the treatment of chronic pain: a 20-year literature review," *J Neurosurg*, vol. 100, no. 3 Suppl Spine, pp. 254–267, 2004.

[203] N. A. Mekhail, M. Mathews, F. Nageeb, M. Guirguis, M. N. Mekhail, and J. Cheng, "Retrospective Review of 707 Cases of Spinal Cord Stimulation: Indications and Complications," *Pain Practice*, vol. 11, no. 2, pp. 148–153, 2011.

[204] Y. E. Mironer, C. Brown, J. R. Satterthwaite, M. Cohen, L. M. Tonder, and S. Grumman, "A New Technique of "Midline Anchoring" in Spinal Cord Stimulation Dramatically Reduces Lead Migration," *Neuromodulation: Technology at the Neural Interface*, vol. 7, no. 1, pp. 32–37, 2004.

[205] J. S. Schofield, C. E. Shell, D. T. Beckler, Z. C. Thumser, and P. D. Marasco, "Long-Term Home-Use of Sensory-Motor-Integrated Bidirectional Bionic Prosthetic Arms Promotes Functional, Perceptual, and Cognitive Changes," *Frontiers in Neuroscience*, vol. 14, Feb. 2020.

[206] C. H. Alleyne, C. M. Cawley, D. L. Barrow, and G. D. Bonner, "Microsurgical anatomy of the dorsal cervical nerve roots and the cervical dorsal root ganglion/ventral root complexes," *Surgical Neurology*, vol. 50, no. 3, pp. 213–218, 1998.

[207] A. Karatas, S. Caglar, A. Savas, A. Elhan, and A. Erdogan, "Microsurgical anatomy of the dorsal cervical rootlets and dorsal root entry zones," *Acta Neurochirurgica*, vol. 147, no. 2, pp. 195–199, 2005.

[208] N. M. Tanaka, P. Fujimoto, Yoshinori MD, H. S. M. An, P. Ikuta, Yoshikazu MD, and P. Yasuda, Mineo MD, "The Anatomic Relation Among the Nerve Roots, Intervertebral Foramina, and Intervertebral Discs of the Cervical Spine," *Spine*, vol. 25, no. 3, pp. 286–291, 2000.

[209] S. F. Lempka, C. C. McIntyre, K. L. Kilgore, and A. G. Machado, "Computational analysis of kilohertz frequency spinal cord stimulation for chronic pain management.," *Anesthesiology*, 2015.

[210] G. Ekman, "Weber's Law and Related Functions," *The Journal of Psychology*, vol. 47, no. 2, pp. 343–352, 1959.

[211] N. Greiner, B. Barra, G. Schiavone, N. James, F. Fallegger, S. Borgognon, S. Lacour, J. Bloch, G. Courtine, and M. Capogrosso, "Recruitment of Upper-Limb Motoneurons with Epidural Electrical Stimulation of the Primate Cervical Spinal Cord," *bioRxiv*, p. 2020.02.17.952796, Feb. 2020. Publisher: Cold Spring Harbor Laboratory Section: New Results.

[212] I. Strauss, G. Valle, F. Artoni, E. D'Anna, G. Granata, R. D. Iorio, D. Guiraud, T. Stieglitz, P. M. Rossini, S. Raspopovic, F. M. Petrini, and S. Micera, "Characterization of multi-channel intraneural stimulation in transradial amputees," *Scientific Reports*, vol. 9, no. 1, pp. 1–11, 2019.

[213] E. Okorokova, Q. He, and S. J. Bensmaia, "Biomimetic encoding model for restoring touch in bionic hands through a nerve interface," *Journal of Neural Engineering*, 2018.

[214] M. J. Catley, A. Tabor, B. M. Wand, and G. L. Moseley, "Assessing tactile acuity in rheumatology and musculoskeletal medicine-How reliable are two-point discrimination tests at the neck, hand, back and foot?," *Rheumatology (United Kingdom)*, vol. 52, no. 8, pp. 1454–1461, 2013.

[215] J. C. Craig and K. B. Lyle, "A comparison of tactile spatial sensitivity on the palm and fingerpad," *Perception & Psychophysics*, vol. 63, no. 2, pp. 337–347, 2001.

[216] M. Solomonow, J. Lyman, and A. Freedy, "Electrotactile two-point discrimination as a function of frequency, body site, laterality, and stimulation codes," *Annals of Biomedical Engineering*, vol. 5, no. 1, pp. 47–60, 1977.

[217] J. Tong, O. Mao, and D. Goldreich, "Two-Point Orientation Discrimination Versus the Traditional Two-Point Test for Tactile Spatial Acuity Assessment," *Frontiers in Human Neuroscience*, vol. 7, no. September, pp. 1–11, 2013.

[218] J. Gonzalez, H. Soma, M. Sekine, and W. Yu, "Psycho-physiological assessment of a prosthetic hand sensory feedback system based on an auditory display: a preliminary study," *Journal of NeuroEngineering and Rehabilitation*, vol. 9, p. 33, June 2012.

[219] M. Schiefer, D. Tan, S. M. Sidek, and D. J. Tyler, "Sensory feedback by peripheral nerve stimulation improves task performance in individuals with upper limb loss using a myoelectric prosthesis," *Journal of Neural Engineering*, vol. 13, p. 016001, Feb. 2016.

[220] F. Clemente, G. Valle, M. Controzzi, I. Strauss, F. Iberite, T. Stieglitz, G. Granata, P. M. Rossini, F. Petrini, S. Micera, and C. Cipriani, "Intraneural sensory feedback restores grip force control and motor coordination while using a prosthetic hand," *Journal of Neural Engineering*, vol. 16, no. 2, p. 026034, 2019.

[221] L. Zollo, G. D. Pino, A. L. Ciancio, F. Ranieri, F. Cordella, C. Gentile, E. Noce, R. A. Romeo, A. D. Bellingegni, G. Vadalà, S. Miccinilli, A. Mioli, L. Diaz-Balzani, M. Bravi, K.-P. Hoffmann, A. Schneider, L. Denaro, A. Davalli, E. Gruppioni, R. Sac-

chetti, S. Castellano, V. D. Lazzaro, S. Sterzi, V. Denaro, and E. Guglielmelli, "Restoring tactile sensations via neural interfaces for real-time force-and-slippage closed-loop control of bionic hands," *Science Robotics*, vol. 4, Feb. 2019. Publisher: Science Robotics Section: Research Article.

[222] M. A. Schiefer, E. L. Graczyk, S. M. Sidik, D. W. Tan, and D. J. Tyler, "Artificial tactile and proprioceptive feedback improves performance and confidence on object identification tasks," *PLoS ONE*, vol. 13, Dec. 2018.

[223] C. M. Oddo, S. Raspopovic, F. Artoni, A. Mazzoni, G. Spigler, F. Petrini, F. Giambattistelli, F. Vecchio, F. Miraglia, L. Zollo, G. Di Pino, D. Camboni, M. C. Carrozza, E. Guglielmelli, P. M. Rossini, U. Faraguna, and S. Micera, "Intraneural stimulation elicits discrimination of textural features by artificial fingertip in intact and amputee humans," *eLife*, vol. 5, p. e09148, Mar. 2016. Publisher: eLife Sciences Publications, Ltd.

[224] A. Mazzoni, C. M. Oddo, G. Valle, D. Camboni, I. Strauss, M. Barbaro, G. Barabino, R. Puddu, C. Carboni, L. Bisoni, J. Carpaneto, F. Vecchio, F. M. Petrini, S. Romeni, T. Czimmermann, L. Massari, R. di Iorio, F. Miraglia, G. Granata, D. Pani, T. Stieglitz, L. Raffo, P. M. Rossini, and S. Micera, "Morphological Neural Computation Restores Discrimination of Naturalistic Textures in Trans-radial Amputees," *Scientific Reports*, vol. 10, p. 527, Jan. 2020. Number: 1 Publisher: Nature Publishing Group.

[225] L. Resnik, S. L. Klinger, and K. Etter, "The DEKA Arm: its features, functionality, and evolution during the Veterans Affairs Study to optimize the DEKA Arm," *Prosthetics and Orthotics International*, vol. 38, pp. 492–504, Dec. 2014.

[226] L. Resnik, F. Acluche, and M. Borgia, "The DEKA hand: A multifunction prosthetic terminal device-patterns of grip usage at home," *Prosthetics and Orthotics International*, vol. 42, pp. 446–454, Aug. 2018.

[227] E. Todorov, T. Erez, and Y. Tassa, "MuJoCo: A physics engine for model-based control," in *2012 IEEE/RSJ International Conference on Intelligent Robots and Systems*, pp. 5026–5033, Oct. 2012. ISSN: 2153-0866.

[228] V. Kumar and E. Todorov, "MuJoCo HAPTIX: A virtual reality system for hand manipulation," in *2015 IEEE-RAS 15th International Conference on Humanoid Robots (Humanoids)*, pp. 657–663, Nov. 2015.

[229] A. Nanivadekar, S. Chandrasekaran, R. A. Gaunt, and L. E. Fisher, "RNEL PerceptMapper," May 2020.

[230] J. N. Campbell and R. A. Meyer, "Mechanisms of Neuropathic Pain," *Neuron*, vol. 52, pp. 77–92, Oct. 2006.

[231] X. Navarro, M. Vivó, and A. Valero-Cabré, "Neural plasticity after peripheral nerve injury and regeneration," *Progress in Neurobiology*, vol. 82, pp. 163–201, July 2007.

[232] A. Latremoliere and C. J. Woolf, "Central Sensitization: A Generator of Pain Hypersensitivity by Central Neural Plasticity," *The journal of pain : official journal of the American Pain Society*, vol. 10, pp. 895–926, Sept. 2009.

[233] K. A. Raichle, M. A. Hanley, I. Molton, N. J. Kadel, K. Campbell, E. Phelps, D. Ehde, and D. G. Smith, "Prosthesis use in persons with lower- and upper-limb amputation," *Journal of rehabilitation research and development*, vol. 45, no. 7, pp. 961–972, 2008.

[234] H. Charkhkar, B. P. Christie, and R. J. Triolo, "Sensory neuroprosthesis improves postural stability during Sensory Organization Test in lower-limb amputees," *Scientific Reports*, vol. 10, p. 6984, Apr. 2020. Number: 1 Publisher: Nature Publishing Group.

[235] B. P. Christie, H. Charkhkar, C. E. Shell, C. J. Burant, D. J. Tyler, and R. J. Triolo, "Ambulatory searching task reveals importance of somatosensation for lower-limb amputees," *Scientific Reports*, vol. 10, June 2020.

[236] E. Hsu and S. P. Cohen, "Postamputation pain: epidemiology, mechanisms, and treatment," *Journal of Pain Research*, vol. 6, pp. 121–136, Feb. 2013.

[237] R. W. Davis, "Phantom sensation, phantom pain, and stump pain," *Archives of Physical Medicine and Rehabilitation*, vol. 74, pp. 79–91, Jan. 1993.

[238] T. S. Jensen, B. Krebs, J. Nielsen, and P. Rasmussen, "Immediate and long-term phantom limb pain in amputees: incidence, clinical characteristics and relationship to pre-amputation limb pain," *Pain*, vol. 21, pp. 267–278, Mar. 1985.

[239] A. Karl, W. Mühlnickel, R. Kurth, and H. Flor, "Neuroelectric source imaging of steady-state movement-related cortical potentials in human upper extremity amputees with and without phantom limb pain," *Pain*, vol. 110, pp. 90–102, July 2004.

[240] H. Flor, C. Denke, M. Schaefer, and S. Grüsser, "Effect of sensory discrimination training on cortical reorganisation and phantom limb pain," *Lancet (London, England)*, vol. 357, pp. 1763–1764, June 2001.

[241] C. Dietrich, S. Nehrdich, S. Seifert, K. R. Blume, W. H. R. Miltner, G. O. Hofmann, and T. Weiss, "Leg Prosthesis With Somatosensory Feedback Reduces Phantom Limb Pain and Increases Functionality," *Frontiers in Neurology*, vol. 9, Apr. 2018.

[242] G. Cruccu, T. Z. Aziz, L. Garcia-Larrea, P. Hansson, T. S. Jensen, J.-P. Lefaucheur, B. A. Simpson, and R. S. Taylor, "EFNS guidelines on neurostimulation therapy for neuropathic pain," *European Journal of Neurology*, vol. 14, pp. 952–970, Sept. 2007.

[243] X. Fuchs, H. Flor, and R. Bekrater-Bodmann, "Psychological Factors Associated with Phantom Limb Pain: A Review of Recent Findings," *Pain Research & Management*, vol. 2018, June 2018.

[244] O. Ulger, S. Topuz, K. Bayramlar, G. Sener, and F. Erbahçeci, "Effectiveness of phantom exercises for phantom limb pain: a pilot study," *Journal of Rehabilitation Medicine*, vol. 41, pp. 582–584, June 2009.

[245] J. Katz and R. Melzack, "Pain 'memories' in phantom limbs: review and clinical observations," *Pain*, vol. 43, pp. 319–336, Dec. 1990.

[246] V. C. Anderson-Barnes, C. McAuliffe, K. M. Swanberg, and J. W. Tsao, "Phantom limb pain–a phenomenon of proprioceptive memory?," *Medical Hypotheses*, vol. 73, pp. 555–558, Oct. 2009.

[247] K. L. Collins, H. G. Russell, P. J. Schumacher, K. E. Robinson-Freeman, E. C. O'Conor, K. D. Gibney, O. Yambem, R. W. Dykes, R. S. Waters, and J. W. Tsao, "A review of current theories and treatments for phantom limb pain," *The Journal of Clinical Investigation*, vol. 128, no. 6, pp. 2168–2176, 2018.

[248] E. O. Johnson, G. C. Babis, K. C. Soultanis, and P. N. Soucacos, "Functional neuroanatomy of proprioception," *Journal of Surgical Orthopaedic Advances*, vol. 17, no. 3, pp. 159–164, 2008.

[249] G. Macefield, S. C. Gandevia, and D. Burke, "Perceptual responses to microstimulation of single afferents innervating joints, muscles and skin of the human hand.," *The Journal of Physiology*, vol. 429, pp. 113–129, Oct. 1990.

[250] D. F. Collins and A. Prochazka, "Movement illusions evoked by ensemble cutaneous input from the dorsum of the human hand," *The Journal of Physiology*, vol. 496 (Pt 3), pp. 857–871, Nov. 1996.

[251] J.-M. Aimonetti, V. Hospod, J.-P. Roll, and E. Ribot-Ciscar, "Cutaneous afferents provide a neuronal population vector that encodes the orientation of human ankle movements," *The Journal of Physiology*, vol. 580, pp. 649–658, Apr. 2007.

[252] D. Burke, S. C. Gandevia, and G. Macefield, "Responses to passive movement of receptors in joint, skin and muscle of the human hand," *The Journal of Physiology*, vol. 402, pp. 347–361, Aug. 1988.

[253] B. B. Edin, "Quantitative Analyses of Dynamic Strain Sensitivity in Human Skin Mechanoreceptors," *Journal of Neurophysiology*, vol. 92, pp. 3233–3243, Dec. 2004. Publisher: American Physiological Society.

[254] S. C. Gandevia, "Illusory movements produced by electrical stimulation of low-threshold muscle afferents from the hand," *Brain: A Journal of Neurology*, vol. 108 (Pt 4), pp. 965–981, Dec. 1985.

[255] P. J. Cordo, "Kinesthetic control of a multijoint movement sequence," *Journal of Neurophysiology*, vol. 63, pp. 161–172, Jan. 1990.

[256] S. C. Gandevia, "Kinesthesia: Roles for Afferent Signals and Motor Commands," in *Comprehensive Physiology*, pp. 128–172, American Cancer Society, 2011. _eprint: https://onlinelibrary.wiley.com/doi/pdf/10.1002/cphy.cp120104.

[257] C. Thyrion and J.-P. Roll, "Perceptual Integration of Illusory and Imagined Kinesthetic Images," *Journal of Neuroscience*, vol. 29, pp. 8483–8492, July 2009. Publisher: Society for Neuroscience Section: Articles.

[258] U. Proske and S. C. Gandevia, "The kinaesthetic senses," *The Journal of Physiology*, vol. 587, no. 17, pp. 4139–4146, 2009. _eprint: https://physoc.onlinelibrary.wiley.com/doi/pdf/10.1113/jphysiol.2009.175372.

[259] P. L. Newland, H. Aonuma, M. Sato, and T. Nagayama, "Presynaptic inhibition of exteroceptive afferents by proprioceptive afferents in the terminal abdominal ganglion of the crayfish," *Journal of Neurophysiology*, vol. 76, pp. 1047–1058, Aug. 1996.

[260] K. Nakashima, J. C. Rothwell, B. L. Day, P. D. Thompson, and C. D. Marsden, "Cutaneous effects on presynaptic inhibition of flexor Ia afferents in the human forearm.," *The Journal of Physiology*, vol. 426, pp. 369–380, July 1990.

[261] K. Seki, S. I. Perlmutter, and E. E. Fetz, "Sensory input to primate spinal cord is presynaptically inhibited during voluntary movement," *Nature Neuroscience*, vol. 6, pp. 1309–1316, Dec. 2003. Number: 12 Publisher: Nature Publishing Group.

[262] J. M. Aimonetti, A. Schmied, J.-P. Vedel, and S. Pagni, "Ia presynaptic inhibition in human wrist extensor muscles: Effects of motor task and cutaneous afferent activity," *Journal of Physiology-Paris*, vol. 93, pp. 395–401, Sept. 1999.

[263] J.-M. Aimonetti, J.-P. Vedel, A. Schmied, and S. Pagni, "Mechanical cutaneous stimulation alters Ia presynaptic inhibition in human wrist extensor muscles: a single motor unit study," *The Journal of Physiology*, vol. 522, pp. 137–145, Jan. 2000.

[264] J. F. Iles, "Evidence for cutaneous and corticospinal modulation of presynaptic inhibition of Ia afferents from the human lower limb.," *The Journal of Physiology*, vol. 491, pp. 197–207, Feb. 1996.

[265] L. E. Osborn, K. Ding, M. A. Hays, R. Bose, M. M. Iskarous, A. Dragomir, Z. Tayeb, G. M. Lévay, C. L. Hunt, G. Cheng, R. S. Armiger, A. Bezerianos, M. S. Fifer, and N. V. Thakor, "Sensory stimulation enhances phantom limb perception and movement decoding," *Journal of Neural Engineering*, vol. 17, p. 056006, Oct. 2020. Publisher: IOP Publishing.